University of Bath

PHD

Electrochemical detection of microRNAs for cancer diagnosis

Ustuner, Serife

Award date:
2020

Awarding institution:
University of Bath

Link to publication

Alternative formats

If you require this document in an alternative format, please contact:
openaccess@bath.ac.uk

Electrochemical detection of microRNAs for cancer diagnosis

Şerife Üstüner

A thesis submitted for the degree of Doctor of Philosophy

University of Bath

Department of Electronic & Electrical Engineering

November 2019

Acknowledgements

From the bottom of my heart, I would like to say thank you to Dr. Pedro Estrela who has always been there throughout these years. My gratitude is beyond words for his precious guidance since my undergraduate degree. I feel very lucky to undertake this journey under his supervision, as he has not only provided me with his academic guidance but contributed a lot on my personal growth with his continuous support.

I also would like to thank to my co-supervisors Prof. Chris Frost and Prof. Mark Lindsay for their valuable contributions on this project.

I extend my sincerest thanks to EPSRC Centre for Doctoral Training in Sustainable Chemical Technologies for funding this project and also for providing me with the fundamental training to take outreach actions in order to engage youth in science.

I would like to also thank to some individuals that deserve special acknowledgement for their encouragement, advice and patience during my research: Dr. Pawan Jolly, Dr. Sean Goggins, Dr. Sunil Arya, Dr. Marina Batistuti, Prof. Marcelo Mulato and Sensors Lab Group in USP (Brazil), Dr. David Tatsui Atique Sawazaki, Dr. Despina Moschou, Dr. Sinead Cabezas-Hayes, Dr. Siva Sivaraya and CSCT Cohort'15.

I would like to also mention all my friends for the shared beautiful moments and for their support: Dr. Jean-Philippe Walhin, Joshua Rainbow, Jay Patel, Pavel Zhurauski, Jules Hammond, Caleb Wong, Alex Beasley, Uros Zupancic, Shu Jiang, Jahnavi Jha, Panos Koulountzios, George Rossides, Stefan Chindea, Bora Agit.

Lastly, I would like to express my immense gratitude to my parents who have stood by me at all times. Words remain insufficient to describe their constant encouragement on making me aware of my own strengths and transforming me into a better version of myself.

If this thesis becomes successful, the results of this endeavour is dedicated in the memory of my dear friend *Ilter Kirmizi*.

List of publications

- Gaiji, H., Jolly, P., **Ustuner, S.,** Goggins, S., Abderrabba, M., Frost, C. & Estrela, P., 2017, A peptide nucleic acid (PNA)-DNA ferrocenyl intercalator for electrochemical sensing. *Electroanalysis*, 29(3), 917-922

- Jolly, P., Batistuti, M., **Ustuner, S.,** Mulato, M., Arya, S. & Estrela, P., 2017, Nucleic acid–based aptasensors for cancer diagnostics-An insight into immobilisation strategies, *Next generation point-of-care biomedical sensors technologies for cancer diagnosis.* Chandra, P., Nee, Y. & Singh, S. (eds.). Singapore: Springer, 205-231

- **Ustuner, S.,** Lindsay, M. & Estrela, P., 2020, Simple fishing and pre-concentration of microRNA with LNA-modified magnetic beads for electrochemical detection, *Biosensors and Bioelectronics* (Under preparation)

Abstract

Cancer continues to grow globally, exerting serious financial and emotional strain on individuals, families, associations and health systems. Early detection is crucial in order to control the spread of the disease and improve chances of survival. Despite the significant intellectual and financial efforts worldwide, there are currently no blood-based biomarkers that are suitable for the non-invasive early detection of cancer. MicroRNAs/miRNAs are a family of non-protein-coding small RNAs which regulate the expression of nearly one third of all human genes. Over the past decade, significant evidence has emerged showing that miRNAs and modulation of their levels in human body are involved in the pathogenesis of cancer at its early stages.

The main consideration when selecting methods of detection for miRNAs is the requirement for high-sensitivity and selectivity due to their low concentrations in blood. This thesis investigates a new method of electrochemical detection which is distinctive due to its sensitivity together with its simple, rapid and reliable design. The first experimental study investigates the role of artificial oligonucleotide probes for selective recognition of miRNAs. Upon using Peptide Nucleic Acid (PNA) probes, highly-sensitive and direct electrochemical detection of a pancreatic cancer-specific miRNA has been achieved with no additional labelling steps. The second study examines the adoption of magnetic beads for separation of target miRNAs from complex solutions (e.g. blood). This strategy addresses the major problem of non-specific interactions that arises upon direct subjection of sensor surfaces to complex solutions. The final study concentrates on the use of redox active self-assembled monolayers (SAMs) on electrode surface for direct capacitive-based detection of miRNAs. Such methodology eliminates the need for pre-doping of the measurement's solution or labelling of target and is highly desirable characteristic for a point-of-care device to be used for the analysis of clinical samples.

Together, this thesis aims to serve as a potential guidance for overcoming the shortcomings of the current miRNA sensing, add value to the development of oligonucleotide-based biosensors for detection of circulating miRNA and hopefully enable the early detection of cancer state.

Table of Contents

Contents

List of Figures

List of Tables

Nomenclature

A	Area
c	Concentration
C	Capacitance
C_d	Electrochemical Double Layer Capacitance
C_H	Compact Layer Capacitance
C_D	Diffusion Layer Capaciatnce
C^*	Complex Capacitance
d	Distance
D	Diffusion constant
DO	Diffusion coefficient
E	Potential
e	Electron charge
V	Electrode potential
f	Frequency
F	Faraday constant
q	Charge
i	Current
i_p	Anodic/Cathodic Peak Current
I	Ionic strength
I_a	Adsorption effect
I_c	Capacitive Current
I_f	Faradaic Current
I_o	Amplitude of Current
J	Flux
j	Imaginary number
k	Rate constant
B	Boltzmann constant
K_d	Dissociation constant
n	Number of electrons transferred
N_A	Avogadro number

Q	Charge
Rct	Charge transfer resistance
SD_{blank}	Standard deviation of blank
t	Time
T	Temperature
V	Voltage
V_o	Amplitude of Voltage
W	Warburg impedance element
x	Direction
Yo	Magnitude of the CPE admittance at $\omega=1\ rad/s$
z	Ion valence
z_i	signed number of units of electronic charge on an ion i
Z	Impedance
Z_o	Amplitude of impedance
Z_{CPE}	Constant phase element impedance
α	Anodic transfer coefficient
Γ	Amount of species adsorbed
ε	Dielectric constant of medium
ε_0	Permittivity of free space
ε_r	Relative permittivity
η	Overpotential
n_i^0	Bulk concentration of each ion
θ	Phase
κ	Debye inverse length
λ	Conductance
λ_D	Debye length
σ	Charge density
ϕ	Electrostatic potential
υ	Scan rate
ω	Angular frequency

List of abbreviations

AuNP	Gold nanoparticle
AFP	Alpha Fetoprotein
BSA	Bovine Serum Albumin
CE	Counter electrode
CPE	Constant phase element CV Cyclic voltammetry
CA-125	Cancer antigen 125
CRC	Colorectal cancer
DL	Double layer
DNA	Deoxyribonucleic acid
DPV	Differential pulse voltammetry
EDC	1-ethyl-3-(3-dimethylaminopropyl)carbodiimide
EIS	Electrochemical impedance spectroscopy
ELISA	Enzyme-linked immunosorbent assay
FET	Field effect transistor
HER2	Human epidermal growth factor receptor 2
HSA	Human serum albumin
IHP	Inner helmholtz plane
LNA	Locked nucleic acid
LOB	Limit of blank
LOD	Limit of detection
LOC	Lab-on-a-chip
LOQ	Limit of quantitation
MCH	6-mercapto-1-hexanol
MRI	Magnetic resonance imaging
miRNA	MicroRNA
OED	Oxford English Dictionary
OHP	Outer helmholtz plane
PB	Phosphate buffer

PBS	Phosphate buffer saline
PET	Positron emission tomography
PNA	Peptide nucleic acid
PSA	Prostate specific antigen
PoC	Point of care
RIU	Refractive index unit
RNA	Ribonucleic acid
SAM	Self assembled monolayer
SWV	Square wave voltammetry
SPR	Surface plasmon resonance
TSH	Thyroid-stimulating hormone
RE	Reference electrode
UV	Ultra violet
WE	Working electrode

Chapter 1 Introduction

The core objective of this thesis is to develop oligonucleotide hybridisation-based detection of circulating microRNAs (miRNAs) that are cancer-specific. Prior to the fabrication of such a platform it is crucial to understand the issues related to the current procedures for cancer diagnosis, and the diagnostic potential of extracellular miRNAs and their origin. Hence, this chapter is an introduction to the problems of cancer, the current tests and procedures for cancer diagnosis, and the broad range of studies in the literature which have identified serum (and plasma) miRNAs as candidate biomarkers for early detection of a range of cancers. Finally, the chapter will introduce electrochemical biosensors and the hybridisation-based recognition of miRNAs by oligonucleotide functionalised capture probes, which will form the foundation of this doctoral thesis.

1. 1 What is cancer?

Cancer is a disease state caused by uncontrolled cell division leading to the growth of abnormal tissue (Herrera et al. 2008; Burgio & Migliore 2015). The genetic basis of cancer was first introduced by the German zoologist Theodor Boveri who suggested that the mutations of the chromosomes in cell nucleus could result in cell generation with unlimited growth potential that could be transferred onto its descendants (Holland & Cleveland 2009; Burgio & Migliore 2015). If the spread is not controlled, it can lead to death. There are various external factors that can initiate cancer such as tobacco use, being overweight, radiation exposure, physical or chemical insults or pathogenic microorganisms (Blot et al. 1988; Grant 2002; Key et al. 2002; Burgio & Migliore 2015). The internal factors include inherited genetics, immune conditions and hormones. Cancer has been referred to as a genetic disease and despite the introduction other models (Soto & Sonnenschein 2014), the somatic mutation theory (SMT) remains the dominant model of carcinogenesis (Blagosklonny 2005). According to SMT, carcinogenesis is a multistep process that includes initiation, promotion and progression, and is characterised by an accumulation of genetic and cytogenetic

alterations (Kinzler & Vogelstein 1996) resulting in malignancy (Klein 1981; Rowley 1998).
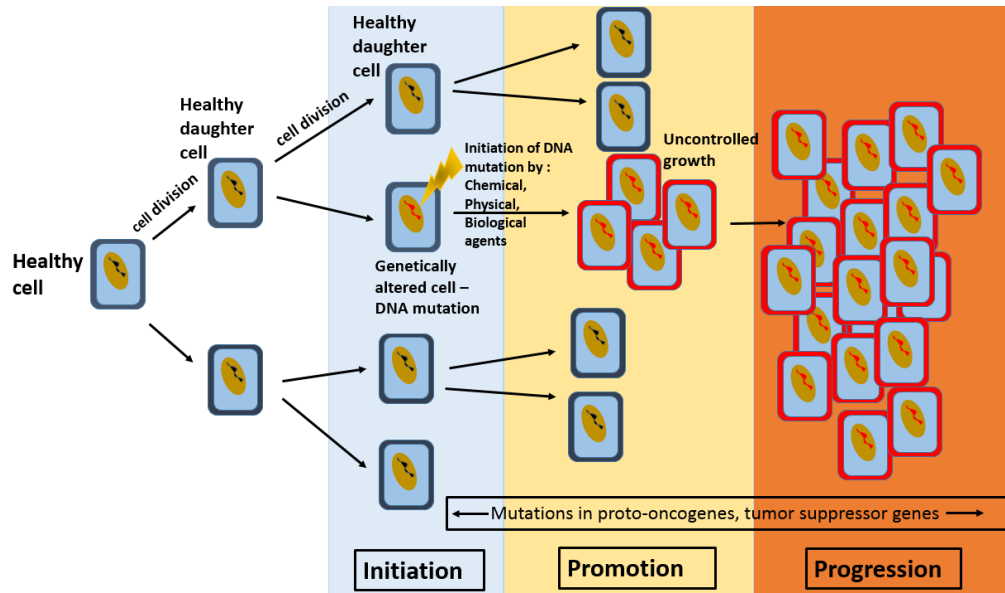
Figure 1. 1 Schematic for somatic mutation theory of cancer (Burgio & Migliore 2015)

1. 2 Cancer: A global burden

Every year, more than 14 million people develop cancer with the majority living in low- and middle- income countries (Ferlay et al. 2014; World Health Organization 2019; Cancer Research UK 2019b). The number of deaths in the low/middle class regions due to cancer exceeds the number of deaths due to HIV/AIDS, tuberculosis, and malaria all combined. Breast cancer is estimated to be the most frequently diagnosed amongst all cancer diseases in the US (Figure 1.2), with 268,600 new cases expected in 2019. This number is to be followed by prostate cancer, with an estimated 174,650 new cases in 2019. The reported figures are also similar in UK, with cancer being the leading cause of death above heart disease and dementia (Department of Public Health England 2017). In 2014, there were 55,379 reported cases of breast cancer in UK and the incident rate is expected to rise by 27% (up to 70,670 cases) by 2035 (Cancer Research UK 2019a). Prostate cancer had the second highest occurrence, with 47,343 new cases in 2014 (Cancer Research UK 2019a). As the figures suggest,

cancer continues to grow globally and exerts significant emotional and financial strain on individuals, families, communities, and health systems. As described by *WHO Cancer control: knowledge into action series,* one of the core components of cancer control is the early detection module (World Health Organization 2017). Patients diagnosed at an early stage are more likely to survive cancer (John & Broggio 2019). This is partly because patients have different treatment options when diagnosed in an early stage of cancer, compared to those diagnosed at a later stage. Hence, there is a need for the general population to understand the crucial role of early diagnosis, as many patients miss out on curative treatment because of their late diagnosis. At the same time, researchers should further explore the development of non-invasive approaches for the earliest possible identification of cancer.

	Estimated new cases			Estimated deaths		
Female	Breast	268,600	30%	Lung & bronchus	66,020	23%
	Lung & bronchus	111,710	13%	Breast	41,760	15%
	Colon & rectum	67,100	7%	Colon & rectum	23,380	8%
	Uterine corpus	61,880	7%	Pancreas	21,950	8%
	Melanoma of the skin	39,260	5%	Ovary	13,980	5%
	Thyroid	37,810	4%	Uterine corpus	12,160	4%
	Non-Hodgkin lymphoma	33,110	4%	Liver & intrahepatic bile duct	10,180	4%
	Kidney & renal pelvis	29,700	3%	Leukemia	9,690	3%
	Pancreas	26,830	3%	Non-Hodgkin lymphoma	8,460	3%
	Leukemia	25,860	3%	Brain & other nervous system	7,850	3%
	All sites	891,480		All sites	285,210	
Male	Prostate	174,650	20%	Lung & bronchus	76,650	24%
	Lung & bronchus	116,440	13%	Prostate	31,620	10%
	Colon & rectum	78,500	9%	Colon & rectum	27,640	9%
	Urinary Bladder	61,700	7%	Pancreas	23,800	7%
	Melanoma of the skin	57,220	7%	Liver & intrahepatic bile duct	21,600	7%
	Kidney & renal pelvis	44,120	5%	Leukemia	13,150	4%
	Non-Hodgkin lymphoma	41,090	5%	Esophagus	13,020	4%
	Oral cavity & pharynx	38,140	4%	Urinary Bladder	12,870	4%
	Leukemia	35,920	4%	Non-Hodgkin lymphoma	11,510	4%
	Pancreas	29,940	3%	Brain & other nervous system	9,910	3%
	All sites	870,970		All sites	321,670	

Figure 1. 2 New cases of cancer and deaths – Estimates for 2019, sourcing from American Cancer Society, Inc. Surveillance Research (American Cancer Society 2019)

1. 3 Current diagnosis of cancer: Tests and procedures

Diagnosing cancer usually follows the same few steps. A person displays a symptom, or screening results might suggest cancer. Then the doctor has to find out if the abnormality is due to cancer or some other cause. There are various types of tests the

doctor can order for accurate diagnosis, these are: blood tests, imaging procedures, and biopsies (Kok et al. 2004; Saslow et al. 2007; Fass 2008; Ciatto et al. 2012).

Blood tests are important tools, as high or low levels of certain cancer biomarkers within the bloodstream can be a sign of the disease. A few examples of these biomarkers are: alpha fetoprotein (AFP) in the screening for hepatocellular cancer (Ellis & Angeles 1988; Daniele et al. 2004), cancer antigen 125 (CA-125) for ovarian cancer (Bell et al. 1998; Jacobs et al. 1999), human epidermal growth factor receptor 2 (HER2) for the identification of women with breast cancer, and prostate specific antigen (PSA) for the screening of prostate cancer (Duffy 2013). Although widely used, the efficacy of PSA screening in reducing prostate cancer mortality remains to be shown (Duffy 2007).

However, due to the limited sensitivity and specificity of available markers, these tests cannot be solely used for the accurate diagnosis of cancer (Duffy 2001; Duffy 2007). Markers are observed to be elevated only in a proportion of patients (at highest 70-80%) with a particular tumour/cancer type and are rarely elevated in the serum of patients who experience early or primary stages of cancer (Duffy 2001). Apart from PSA, which is mainly prostate specific, none of the other clinical markers are organ specific.

Currently, the main uses for cancer biomarkers are prevention, aiding the diagnosis, and making predictions on the likely response to a given therapy (Duffy 2001). Therefore, there is still a requirement for combining lab tests with other clinical methods such as imaging of the suspected internal organs (Khalkhali et al. 1994; Fass 2008). Some imaging methods that are currently used include MRI scans, Mammography, X-rays, PET scans, and Ultrasound screening (Duffy 2001; Fass 2008).

Although imaging tests are quite helpful in detecting masses and areas of abnormality, they may not differentiate cancerous cells from non-cancerous cells. As a result, the majority of patients are asked to undergo a biopsy in order to collect cells for histological analysis. A biopsy is the procedure of removing a piece of tissue or cells from a target site in the body for further investigation in the laboratory. The procedure

varies depending on the region of abnormality observed in the patient. For instance, bone marrow biopsies (Contreras et al. 1972; Brunning et al. 1975) are carried out by a doctor collecting a sample of bone marrow out of the back of the hipbone, with the aid of a needle. All of the needle biopsies collect tissues from internal organs by inserting needles/tubes through an orifice or by making a small incision in the skin (Reid et al. 2000; Mohamad A Eloubeidi. et al. 2003). Such an endoscopic biopsy requires the use of an endoscope (flexible tube) with a light on the end in order to visualise structures inside the body. However, such procedures are uncomfortable experiences for the patients and there is a preference for non-invasive or minimally invasive tests that also make the early stage diagnosis of cancer possible (Ferracin et al. 2011). Hence, the detection of cell-free (circulating) biomarkers in plasma or serum could serve as a 'liquid biopsy' which would be extremely useful in various diagnostic applications, and eliminate the need for tumour tissue biopsies (Schwarzenbach et al. 2011). Such a technique would allow one to take repeated blood samples and continuously monitor the changes in the cell-free biomarkers during the natural course of the disease, and its treatment.

1.4 microRNAs: Candidate biomarkers for cancer diagnosis

Being first discovered in *C. elegans* in 1993 and soon after in all living organisms (Ferracin et al. 2011), microRNAs (miRNAs) are a class of non-coding RNA molecules, which are between 19-24 nucleotides in length, (Ambros 2004; Bartel 2004; Iorio & Croce 2011), which regulate the expression of nearly one third of all human genes by targeting their 3' untranslated region (UTR) (He et al. 2015). At the time of this study, thousands of miRNAs have been identified (~total of 38,589) within animals, plants, and viruses. The current version of miRBase (release 22) holds information on about 2,656 mature miRNAs in the human genome (http://mirbase.org/; Release 22.1: October 2018). Within the context of cancer disease development and progression, epigenetic alterations are considered one of the key drivers. Epigenetic alterations are shown to take place far more frequently than genetic mutations, and often appear in the early stages of tumorigenesis (Kaiser 2010;

Schwarzenbach et al. 2011). The term "epigenetic" refers to all heritable changes in gene expression, but excludes the alterations in a DNA sequence. To date, miRNAs remain the most common epigenetic alteration in circulation, a property which makes it of great interest in the search for diagnostic and prognostic biomarkers. Moreover, miRNA is shown to be quite stable in blood due to its packaging into exosomes which protect it from degradation, while other circulating nucleic acids, such as DNA, are cleared from circulation rapidly. The other types of epigenetic alterations involve aberrant DNA methylation, histone modifications, and dysregulated expression of non-coding RNAs. In the case of DNA methylation, the main drawback is the significant volume of serum/plasma that is required to obtain appropriate amounts of DNA in order to detect the process of methylation (Schwarzenbach et al. 2011). In this section we will primarily be looking into miRNAs which are shown to have great potential as cancer biomarkers in circulating blood.

The initial evidence of miRNA as cancer biomarkers was accidental: in search for the tumour suppressor gene involved in chronic lymphocytic leukemia (CLL), Calin and colleagues (Calin et al. 2002) found that the smallest common area of deletion encoded two miRNAs: miR-15a and miR-16-1. The work suggested the roles of these two miRNAs as tumour suppressor genes in CLL. This was followed by studies in 2005, stating that each miRNA when it targets several mRNAs, can directly or indirectly regulate the expression of thousands of proteins (Lim et al. 2005), suggesting that the regulation of a single miRNA can in turn lead to substantial biological consequences. Although the major mechanism of miRNA leads to down-regulation of target genes, it was reported that in some cases miRNA acts by activating translation (Vasudevan et al. 2007), or even modulating transcription (Ferracin et al. 2011). In 2011, more tumour suppressor microRNAs were discovered, such as the let-7 family which is down-regulated in the case of cancer disease that leads to the upregulation of specific proto-oncogenes (Ferracin et al. 2011) (Figure 1.3).
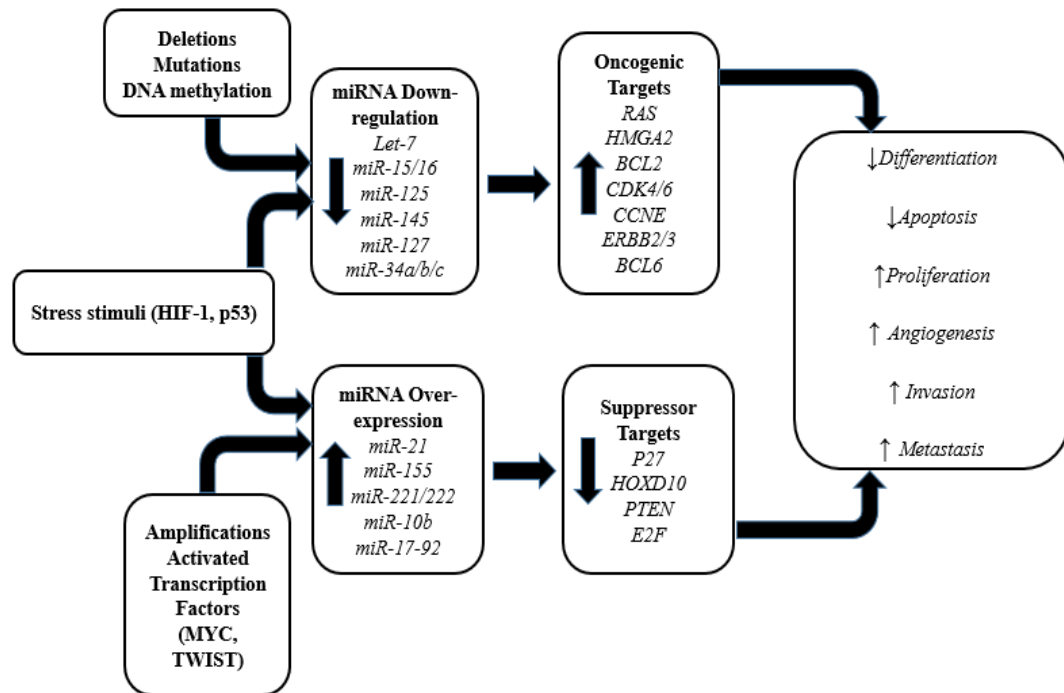
Figure 1. 3 Family of miRNAs acting as tumour repressors or oncogenes. Genetic (deletion, point mutations, amplification) or epigenetic (DNA methylation) changes, various stress stimuli or abnormal transcription factor expressions may lead to deregulation of miRNAs in cancer cells. This variation in miRNA levels can in turn affect the levels of target genes. As a result, cells may undergo various situations representing hallmarks of cancer (no differentiation, undergoing apoptosis, increased proliferation and invasion, etc.) (Ferracin et al. 2011).

MiRNAs are a particular area of interest for oncology research since their discovery and following evidence suggest that they are involved in the pathogenesis of cancer, in most cases by controlling the translation of oncogenes and tumour suppressors (Calin & Croce 2006; Esquela-kerscher & Slack 2006; Cho 2010).

A Web search (Figure 1.4) reveals the breakthrough of disease specific miRNAs, first in 2002, which was followed by their detection studies in 2003. The number of publications indicates the limitation of the detection studies, although proved to be candidate biomarkers of various diseases.

Together with their crucial role in gene regulation, in 2008 the levels of miRNAs in circulating blood were discovered to show fluctuations in cancer state (Lawrie et al. 2008). In the upcoming sections, we will be investigating the cancer specific circulating miRNAs in human plasma/serum for the development of non-invasive detection methodologies as the core objective of this thesis.
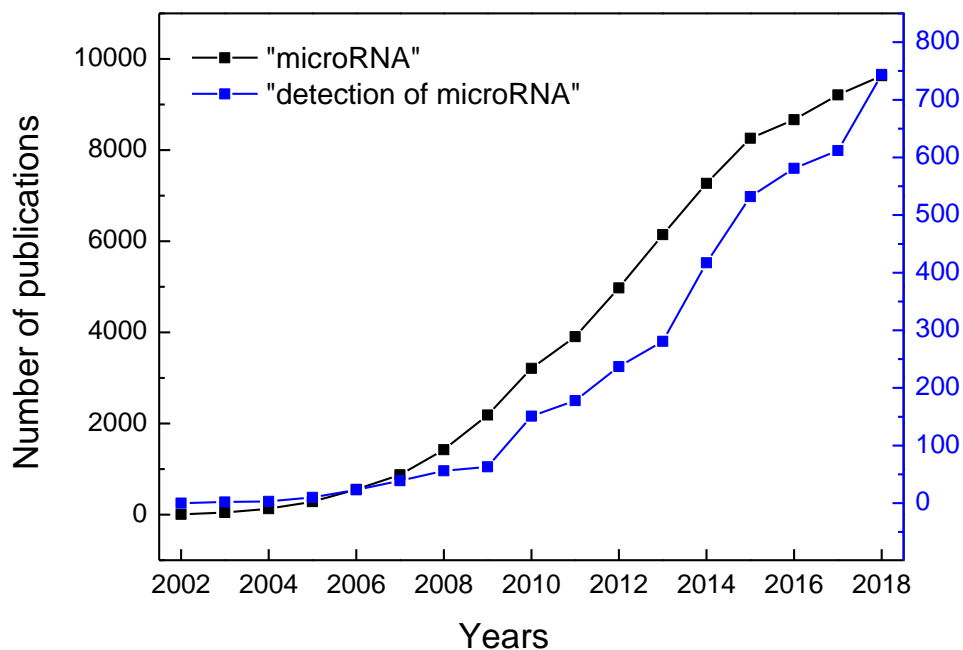
Figure 1. 4 Number of articles published on "microRNA" and "detection of microRNA" in the past 16 years (source: Web of Science™)

1. 5 Extracellular microRNAs for early detection of cancer

1.5. 1 Origin and diagnostic potential

It was not long ago that significant amounts of circulating miRNAs were detected in various biological fluids that include plasma, urine, saliva, tears, semen, breast milk, amniotic fluid and cerebrospinal fluid (Alton Etheridge 2013). Surprisingly, these circulating miRNAs were observed to be very stable and survive extreme conditions

where the common RNA species (e.g. mRNA, rRNA and tRNA) would fail to survive and degrade within several seconds (Chen et al. 2008; Turchinovich et al. 2011). In this section, we will outline the actual theories regarding the origin and the transport of these intracellular miRNAs to extracellular environments and the mechanisms involved in the protection of miRNAs in biological fluids.
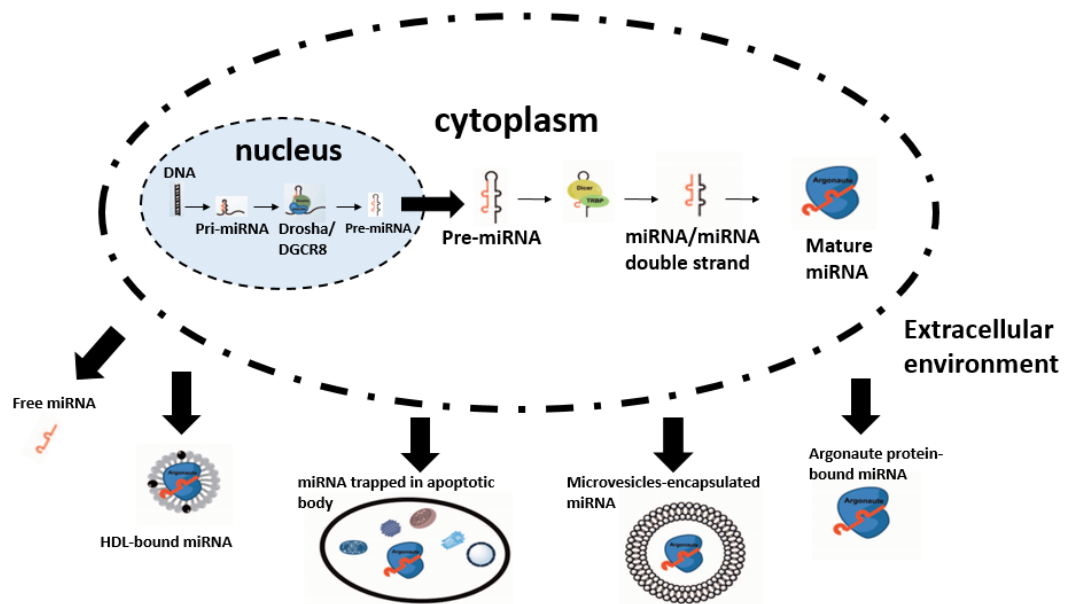
Figure 1. 5 From cell nucleus to circulating blood, the biogenesis of miRNAs. Re-created from (Turchinovich et al. 2013).

As the biogenesis model in Figure 1.5 suggests, all miRNAs are initially generated in the cell nucleus where they exist in the form of long primary miRNAs (pri-miRNAs) transcripts containing a 5'cap and a 3'polyA tail   (Lee et al. 2004). Then these are further cleaved by a microprocessor complex consisting of Drosha and DGCR8 proteins, into ~70 nucleotide (nt) hairpin precursor pre-miRNAs (Lee et al. 2003; Landthaler et al. 2004). This is in turn followed by the active transport of the pre-miRNAs into cytoplasm where they are further chopped into ~22 base pair (bp) miRNA/miRNA duplexes by the Dicer/TRBP enzyme complex (Zhang et al. 2002; Chendrimada et al. 2005). Eventually, miRNA duplexes separate leaving one of the strands associated with an Argonaute (AGO) protein (Okamura et al. 2004; Ender &

Meister 2010). Although an Argonaute family of four different proteins (AGO1, AGO2, AGO3, AGO4) were associated with mediating the translational repression of mRNA on ribosomes and mRNA decay in P-bodies, only AGO2 is capable of direct cleavage of mRNA in the cytoplasm. It is important to also note that neither pre-miRNAs nor mature miRNAs were found to be in non-protein bound forms within the cells.

On the other hand, the extracellular microRNAs are found to be in various forms such as, the in additional encapsulation of the protein-bounded form in microvesicles, HDL particles, or apoptotic bodies. Hence, these shielded forms of extracellular miRNAs protect the miRNA from RNase degradation as most reports suggest (Turchinovich et al. 2013).

The exact mechanism by which the exosomes/microvesicles are released by the cell still remains unclear, however the release is modulated by extracellular signals. Although some early studies referred to the extracellular vesicles as "garbage bags" of the cells, they are now gaining increasing recognition for intercellular communication. In this manner, they produce a pathway for the intercellular transfer of information that resembles direct cell-cell contact but acting at a distance. However, in some cases this information transfer was observed to be in favour of tumour growth, the extracellular vesicles were observed to be protective for tumour cells by clearing away molecules such as the membrane attack complex from tumour cell membranes. In a similar way, it was proposed that they educate the host environment to re-model a supportive niche for tumour growth and the spread of metastasis (Peinado et al. 2012). Also, some studies argued that miRNAs delivered by extracellular vesicles play a role in immune system regulation (Taylor et al. 2013).

With the proposal of the concept of "liquid biopsy" (Murtaza et al. 2013) the circulating miRNAs started getting more attention as good candidates for liquid biopsy, as the quantities and sequences of miRNAs convey information for diagnosis. Although circulating miRNAs were previously thought to be "garbage" from cells, it is now proposed that the "garbage" actually serves as a communication tool and should be referred to as "gold". Such that we shall provide a detection method that is based

on the mechanism of secreted miRNAs in cancer development and that "listens" to this cell-cell communication.

1.5. 2 Serum and plasma microRNAs as candidate biomarkers

Following the discovery of miRNAs as potential cancer biomarkers, various methods have been adopted for the quantification of their levels within the human body. By using techniques such as quantitative reverse transcription-polymerase chain reaction (qRT-PCR), miRNA cloning, microarray, and bead-based profiling methods, the variations of miRNA profiles can be detected in a wide spectrum of haematological malignancies and solid tumours (Lu et al. 2005; Volinia S, Calin GA, Liu CG 2006; Yanaihara et al. 2006; Cummins et al. 2006; Iorio & Croce 2011). However, there is still the requirement for non-invasive or minimal invasive methods of cancer diagnostics. One solution to this problem could be the detection of miRNA levels in the bloodstream. However, the question is: could the circulating miRNAs levels within human serum, plasma, saliva or other body fluids be related to the presence of any tumour or cancerous disease within the body?

The first suggestion was made in 2008 by Lawrie et al. who reported circulating tumour-related miRNAs as non-invasive diagnostic markers for cancer (Lawrie et al. 2008). The study compared the levels of tumour-related miR-155, miR-210 and miR-21 in serum taken from 43 healthy controls and 60 diffuse large B-cell lymphoma (DLBCL) patients. Lawrie et al. reported high serum levels of miR-21 in patients, and the levels were interestingly found to be related with the relapse-free survival of these patients. The study gave the first description of circulating miRNAs and suggested miRNAs as non-invasive biomarkers for DLBCL and possibly for other types of cancer.

Later, another study conducted by Mitchell et al. (2008) reported miRNAs to be remarkably stable in human plasma and protected from endogenous RNase activity. The same study also reported miRNAs to be entering the bloodstream from human prostate cancer xenografts and their levels could be measured readily from plasma. From distinguishing xenografted mice from controls, the concept was applied to cancer

in humans, where serum levels of miR-141 (prostate cancer specific miRNA) can distinguish prostate cancer patients from healthy controls.
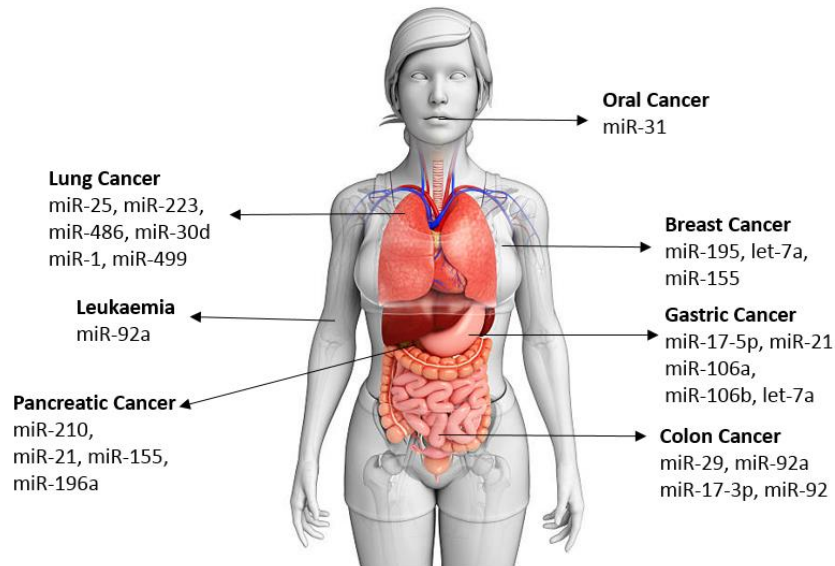
Figure 1. 6 Class of circulating miRNAs that relate with different types of cancers (Lautner & Gyurcsá 2014) (Refer to Table 1.1 for further references).

A recent study, in 2017, suggested a wide profile of miRNAs present in human plasma have significant diagnostic value for early stages of non-small cell lung cancer (NSCLC) (Zhang et al. 2017). By using reverse transcription-quantitative polymerase chain reaction, the study validated the over expression of plasma miR-145, miR-20a, miR-21 and miR-223 in 129 NSCLC patients compare to 83 healthy controls.

In 2019, Gablo et al. gave evidence that plasma miR-21, miR-210, miR-155, and miR-196a levels in blood can distinguish with high sensitivity and specificity pancreatic ductal adenocarcinoma (PDAC) patients from healthy controls (Gablo et al. 2019). Following that, in 2019, another study reported plasma miR-195 to be significantly under-expressed in patients with metastatic breast cancer, compared to healthy controls (Mcanena et al. 2019).

The most recent study, in 2020, analysed 102 breast cancer patients at diagnosis and after treatment together with 15 healthy women (Anwar et al. 2020). By using

quantitative reverse transcription polymerase chain reaction (qRT-PCR), over expression of circulating miR-155 from patients' plasma was reported. The study uncovered the potential use of circulating miR-155 as a clinical biomarker in breast cancer (Anwar et al. 2020). References to other cancer-related circulating miRNAs are displayed in Table 1.1, which presents groups of miRNAs in serum/plasma and their relation to different cancer cases. Once thought to be unstable, miRNAs proved their stability in serum/plasma such that establishing an extremely promising approach for cancer diagnosis at early stages.

Table 1. 1 List of some circulating miRNA as potential biomarkers for various cancer states

Representative miRNA	Source	Related Disease	Regulation in source	References
miR-21	Serum	Diffuse large B-cell lymphoma	Upregulated	(Go et al. 2015)
miR-141	Plasma	Prostate Cancer	Upregulated	(Li et al. 2016)
miR-145, miR-20a, miR-21, miR-223	Plasma	Non-small Cell Lung Cancer	Upregulated	(Zhang et al. 2017)
mirR-629, miR-660	Plasma	Lung Cancer	Upregulated	(Fortunato et al. 2019)
miR-141	Serum	Prostate Cancer	Upregulated	(Li et al. 2016)
miR-92, miR-17-3p	Plasma	Colorectal Cancer	Upregulated	(Wang et al. 2016)
miR-155	Serum	Breast Cancer	Upregulated	(Anwar et al. 2020)
miR-92a	Serum	Leukemia	Downregulated	(Koutova et al. 2015)
miR-21, miR-210, miR-155, miR-196a	Serum	Pancreatis ductul adeno-carcinoma	Upregulated	(Frampton et al. 2013)
miR-486, miR-30d, miR-1, miR-499	Serum	Lung Cancer	Upregulated	(Rijavec et al. 2020)
miR-29, miR-92a	Plasma	Colorectal Cancer	Upregulated	(Huang et al. 2017)
miR-195	Serum/ Plasma	Breast Cancer	Downregulated	(Mcanena et al. 2019)
miR-21, miR-155, miR-196a and miR-210	Plasma	Pancreatic Cancer	Upregulated	(Gablo et al. 2019)

1. 6 Key challenges to detection of circulating miRNA

Prior to the implementation of miRNA sensing technology for clinical applications, there are a number of technical challenges to be addressed. The most critical one is the low and undefined level of miRNA in blood to detect (Gillespie et al. 2019)**.** The literature review in previous chapter reveals the fact that the changes to specific miRNA levels in serum/plasma were defined as up- or down regulation between healthy controls and patients with disease state. There are no records stating the actual concentration of miRNA in healthy biological samples and the change of this concentration in disease state. This could be attributed to the lack of standardised protocols for separation of miRNAs, their processing and quantification. Hence, this makes it extremely difficult to carry out quantitative comparisons between the studies reported in literature due to the slightly different conditions of each study. Although, there is no reliable answer to the question of what the exact quantity of miRNA in blood is, the method of normalisation could be of extreme help for the quantification of miRNA as biomarkers. Upon defining a strict level of control (mean value of miRNAs in blood derived from healthy controls that would take into account the miRNA fluctuations influenced by diet, physical activity, etc.) more reliable analysis could be made by evaluating the variations of the miRNAs compared to the normalised levels. Other challenges are the short sequence length of miRNAs and the high sequence homology within the family of miRNAs. Hence, there is the requirement for highly specific sensors that can distinguish between miRNAs that possess single base mismatch.

1. 7 Sensors and biosensors

A sensor, in its broadest definition, is a device that detects or measures a physical property or change, and provides a resulting output/measurement in return (OED 2019). Sensors can be classified into three types: chemical, physical and biosensors. Physical sensors deal with measure of physical quantities such as weight, temperature, length, electricity, pressure, etc. A chemical sensor on the other hand, has a chemical or molecular target to measure. Chemical sensors are defined as "devices which

respond to a particular analyte in a selective way through chemical reaction and can be used for qualitative or quantitative determination of the analyte" (Sang et al. 2013).

Biosensors are considered as a sub-set of chemical sensors, however, they are most often regarded as a topic in their own right. A biosensor is a device that detects an analyte and in doing so it combines a biological component with a physiochemical detector component. The general biosensor architecture is represented in Figure 1.7 which can be divided into three main bodies (Sang et al. 2013):

1. **Bioreceptor**: The sensitive biological recognition layer that can selectively bind to analyte. This is usually achieved by functionalisation of an electrode surface with a bio-receptor molecule. The bio-receptor molecule (e.g. DNA, aptamer, antibody) acts as a capture probe that binds to a target.

2. **The transducer:** The detector element that can work in optical (Haes 2002), mass sensitive (Janshoff et al. 2000), electrochemical (Cass et al. 1984), and many other ways that can convert the signal induced by the biological interactions into a measurable signal.

3. **The signal processor**: This is the part that enhances the signal and generates an output that correlates to the amount of analyte detected.
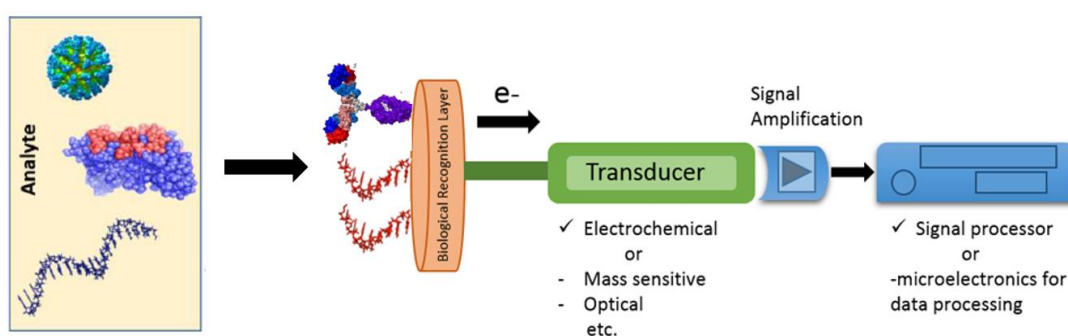
Figure 1. 7 Biosensor Architecture. Typically, the analyte is recognised by a specific biological recognition layer (bioreceptor) at the sensor interface. A transducer element converts the change in the properties of a recognition layer into quantifiable signal. The signal is further amplified and converted into readable signal by the output device (Sang et al. 2013; Jolly 2016).

A broad range of methods can be adopted for the development of biosensors and the biosensor efficiency can be assessed by important parameters listed in Table 1.2.

Table 1. 2 Parameters for biosensor performance assessment (Hammond 2017)

Parameter	Statement
Sensitivity	Ratio between the output signal and measured property
Selectivity	Capability of the biosensor to selectively distinguish the analyte in a mixture of biomolecules.
Limit of detection (LOD)	Expressed in units of concentration, LOD indicates the smallest concentration of analyte that can be reliably distinguished by the sensor from a sample without the analyte.
Dynamic range	Range between the minimum and maximum levels of detection.
Reliability	Functioning correctly with predictable performance at specified conditions.
Size/Miniaturisation	The sensor must have applicable size for transport, point-of-care use and storage.
Ease of use	Ease of operation leads to dramatic reduction on the risk of user error
Sample preparation	Minimum requirement for sample preparation reduces cost, sample loss, time and experimental difficulty
Cost	Crucial factor for the viability of the product

An example of a commonly used electrochemical set up comprises of a cell with a three-electrode configuration, which are the working electrode (WE), reference electrode (RE) and a counter electrode (CE), placed in an electrochemical solution. The WE is the recognition interface which is functionalised with a biological probe that specifically binds to the target molecules. Voltage potentials are set between the WE and the RE and the current flow is monitored between the WE and the CE. The

main benefit of introducing the RE is for stabilizing the voltage between the WE and the RE. Hence, such a configuration allows the establishment of the potential of the WE against the RE without compromising the RE stability by passing a current through it (Wang 2006).
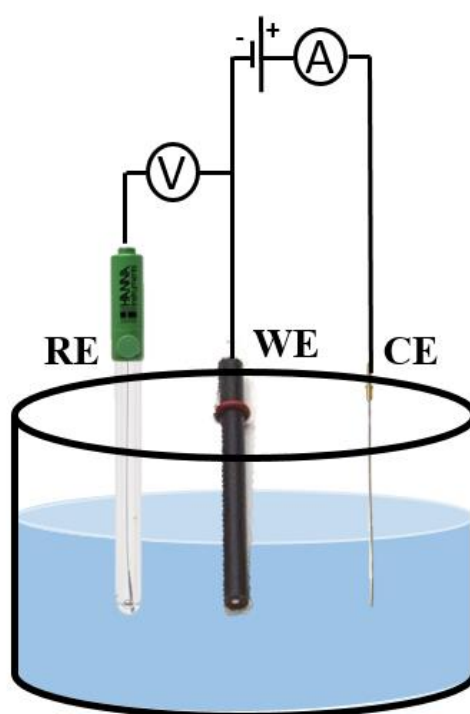
Figure 1. 8 Electrochemical cell in three-electrode configuration. RE, WE and CE refers to reference electrode, working electrode and counter electrode respectively.

1.7. 1 The ideal biosensor for microRNA sensing

Before the definition of the ideal miRNA biosensor, a clear definition is required for its use. The requirements of a biosensor for point-of-care use varies significantly from laboratory use. There are many compelling laboratory methods that already exist for miRNA detection. Quantitative reverse transcription PCR (RT-qPCR) is known as the gold standard (Gillespie et al. 2019), together with other powerful techniques such as northern blotting and next generation sequencing. PCR-based technologies are well established with their ability to detect sequences of various lengths, and any new technology must therefore possess significant advantages in order to compete with current technology.

On the other hand, for point-of-care use, an optimal biosensor should be easily usable by someone who has minimal training, require no sample preparation, have a long shelf life, be easy to store, and fit for diagnostic purposes. The most crucial requirement is the validation of the fabricated miRNA biosensor with clinical samples, which reflects the actual ability to transfer the biosensor into a technology that is usable within the field. In this thesis, the main focus will be given on the development of a point-of-care device for miRNA sensing.

1. 8 Hybridisation based recognition of miRNA

Molecular recognition is commonly adopted in electrochemical detection and the molecular recognition of miRNA is most generally achieved by adopting deoxyribonucleic acid (DNA) oligonucleotide or synthetic mimics of DNA, and the recognition is achieved through complementary Watson-Crick base-pairing. The chemical structure of an oligonucleotide is composed of phosphodiester (phosphate group) linkage between its bases and the backbone is made up of alternating phosphate and sugar (ribose in RNA and deoxyribose in DNA) residues (Rothenberg et al. 1989). However, the unmodified/natural DNA has several limitations that prevent their use in medical applications. Their phosphate group that forms the bridge between bases is a substrate for DNases and is usually cleaved before even reaching the target, they also lack target specificity. Moreover, DNA is not able to enter cells rapidly due to its large

and highly charged nature (Pierre Murat et al). Hence, the studies were targeted on solving these issues and synthetic analogues of DNA were developed where the phosphate backbone was subjected to a variety of chemical modifications. Synthetic oligonucleotide analogues represent a valuable alternative to standard DNA or RNA (Bala & Gorski 2016).

Such DNA mimics offer the opportunity for rebuilding the specificity and affinity of hybridisation with natural DNA and RNA. The modifications can enhance the desired signal against a background of competing interactions which is of a strong interest for medical applications (Levicky et. al). In this section we will be introducing selective probes that include locked nucleic acids (LNAs), peptide nucleic acids (PNA), morpholinos (MOs) and hexitol nucleic acids (HNA) for the electrochemical detection of oligonucleotides.
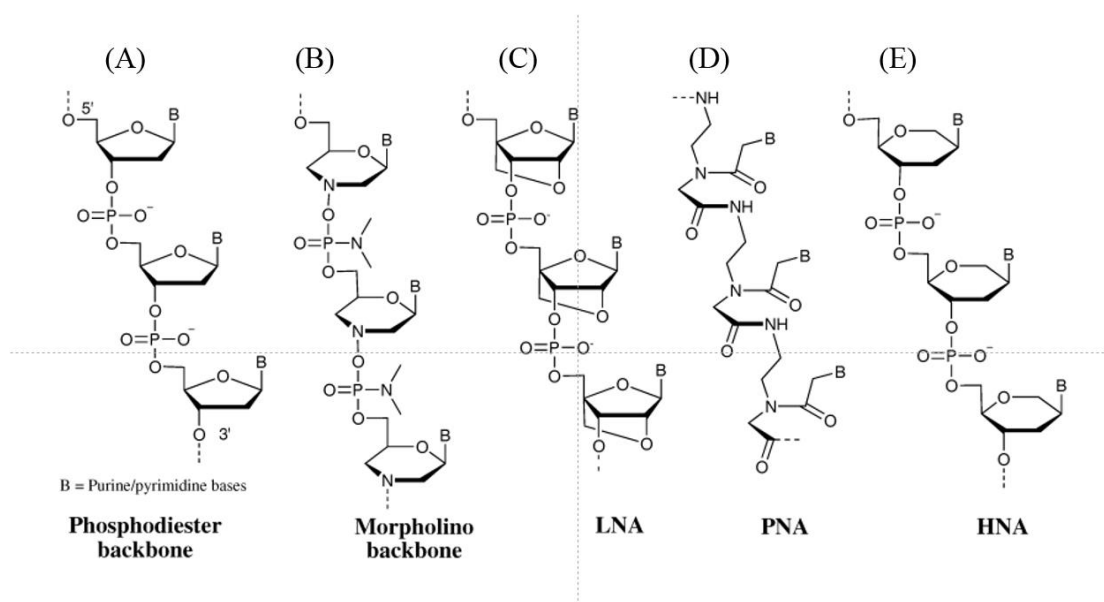
Figure 1. 9 Structures of natural and modified oligonucleotide backbones: (A) natural phosphodiester, DNA; (B) morpholino; (C) locked nucleic acid (LNAs); (D) peptide nucleic acids (PNAs); and (F) hexitol nucleic acids (HNAs) (Pierre Murat et. al).

1.8. 1 Locked nucleic acids (LNA)

One nucleic acid analogue that is known for displaying extraordinary hybridisation affinity towards complementary DNA and RNA is locked nucleic acid (LNA). Several reports have revealed LNA as promising tool for the development of oligonucleotide-based detection particularly for the recognition of RNA (Petersen & Wengel 2003; Kaur et al. 2006; Natsume et al. 2007b; Natsume et al. 2007a). The melting temperatures (T_m) of LNA-RNA and LNA-DNA hybrids are respectively 2–10˚ C and 1–8˚ C higher than those of DNA–RNA and DNA–DNA (Natsume et al. 2007a). The enhanced affinity is a result of the modified chemical structure of LNA, in which the furanose ring of the ribose sugar is chemically locked by the introduction of a methylene linkage between O_2 and C4′ (Laschi et al. 2009). Hence, the resulting covalent bridge ends up to be an effective lock of the ribose in the N-type (3-endo) conformation that is dominant in A-form DNA and RNA. The improved affinity results from the conformation that enhances base stacking and phosphate backbone pre-organisation. These properties make LNA well suited for miRNA detection and analysis for cancer diagnostics. Hence, LNA probes were successfully applied for the optimisation of miRNA northern blot analysis, allowing sensitive and highly specific detection (Valoczi et al. 2004; Varallyay et al. 2007). A sensitive microarray platform for genome-wide profiling of mature miRNAs (miChip) was developed by utilising LNA modified capture probes (Castoldi et al. 2006). Moreover, LNA-probes were successfully applied for in situ detection of miRNA accumulation in developing animal embryos and in tissue sections (Wienholds et al. 2005; Silahtaroglu et al. 2007; Obernosterer et al. 2007; Sempere et al. 2007).

1.8. 2 Peptide nucleic acids (PNA)

Peptide Nucleic Acid is another class of DNA mimic which comes with neutral charge and a high affinity for hybridisation with single strand DNA (Egholm et al. 1992; Wang 1998; Nelson et al. 2000). Being first invented by a group of researchers from the University of Copenhagen in 1991 (Nielsen et al. 1991) their charge neutrality was achieved by replacing the negatively charged specific backbone phosphate groups of DNA by a polyamide backbone. This model of protein-induced bending for neutrality

of DNA, has also been tested by several later studies in 1997/98 (Strauss-Soukup et al. 1997; Strauss-soukup & Maher 1998), where strategically placed polyamide backbones could induce bends of 3–4° per base pair in DNA. Such that the charge-neutralisation-induced DNA bending provides significant contribution to the binding energetics of protein recognition processes (Strauss-soukup & Maher 1998; Okonogi et al. 2002). The higher binding energetics is a result of the lack of electrostatic repulsion present in the hybridisation of PNA: DNA compared to DNA: DNA or DNA: RNA. In addition, PNA displays excellent stability (chemical, biochemical, thermal) when used as probes, making them ideal capture tools.

Providing a shift from a completely neutral platform to a negatively charged one upon hybridisation, PNA became an ideal candidate for electrochemical detection assays. These studies that use the surface charge variations of hybrid assays as their detection methodology, produced excellent results when adopting PNA as the capture probes for DNA recognition; e.g. field effect transistors (FET) (Aoki et al. 2000), electrochemical impedance spectroscopy (EIS) (Keighley et al. 2008), nanopore sensors (Jagerszki et al. 2007; Ali et al. 2010), and channel sensors (Aoki et al. 2000). It was not long ago that the same strategy was adopted by *Jolly et al.* (Jolly et al. 2016) for the development of a sensitive electrochemical detection platform for miRNA detection where fM detection limits were achieved.
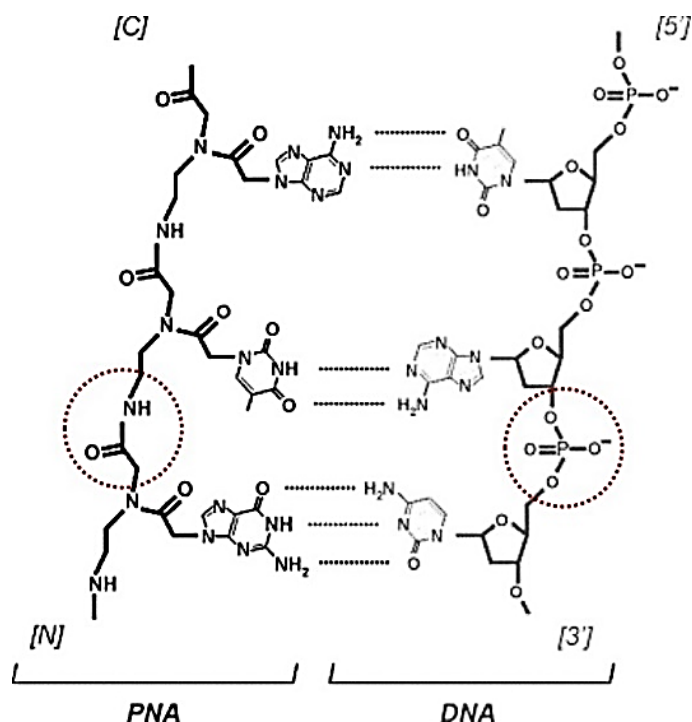
Figure 1. 10 Chemical structure model of PNA (sequence N-GTA-C) hybridised in antiparallel orientation with its complementary DNA (sequence 5-TAC-3) (Nielsen et al. 1991) .

1.8. 3 Morpholinos (MOs)

First discovered in 1985, morpholinos are another a class of synthetic nucleic acid mimics with an uncharged nature (Summerton & Weller 1993; Summerton et al. 1997). Such a property is anticipated to strongly affect the hybridisation rules that construct their emerging applications based on solid-phase hybridisation for diagnostic applications (Tercero et al. 2009; Gao & Ting 2009; Wang & Smirnov 2009; Zhang et al. 2010). The subunit of a morpholino comprises of a nucleic acid base, a morpholino ring, and a non-ionic phosphorodiamidate intersubunit linkage. In contrast to PNA that is also neutrally charged, Morpholino comes with a flexibility in length synthesis. The reduced constraint on sequence length provides essential flexibility for applications in gene expression or pathogenic identification which adopt lengths of up to 70 nt (Hughes et al. 2001; Bodrossy & Sessitsch 2004). Additional properties that make it excel include; stability, nuclease-resistance, long-term activity, efficacy, water

solubility, low toxicity, and exquisite specificity in comparison to PNA and DNA (Zhang et al. 2010). In 2009 *Tercero et al.* reported the construction of Morpholino monolayers on a gold surface and the hybridisation of Morpholino with DNA on the surface (Tercero et al. 2009). The same year, *Gao & Ting* adopted a Morpholino oligomer as a capture probe and in combination with a redox polymer for the ultrasensitive detection of DNA achieving a detection limit of 1 pM (Gao & Ting 2009). Recently, in 2017, one study demonstrated a phosphorodiamidate morpholino oligos (PMO)-functionalised nanochannel biosensor for the label-free detection of miRNAs (Zhang et al. 2010; Liao et al. 2017). The nanochannel-based biosensor attained a reliable and low limit detection in PBS followed by a 10 fM limit of detection in serum. Hence, it is expected that such a new methodology will benefit miRNA detection in clinical diagnosis.

1.8. 4 Hexitol nucleic acids (HNA)

When compared to DNA, the chemical structure of hexitol nucleic acid (HNA) is modified by inserting an extra methylene group in the backbone between C1′ and O4′ of the â-D-2′-deoxyribose unit (Declercq et al. 2002). Hence, HNAs end up forming quite stable self-complementary duplexes as well as stable duplexes with their natural components (Hendrix et al. 1997). The resulting duplexes have the nucleic acid A structure with complementary DNA or RNA oligomers and the experiments investigating the melting temperatures and the gel shift analysis revealed the following order of duplex stability: HNA-HNA > HNA-RNA > HNA-DNA (Kozlov et al. 1999). The study of HNA duplex structure offers new insights into how sugar modifications can lead to the stabilisation of duplex structures, and provides valuable information for the design of various backbone modifications for innovative properties. The interest in such properties arises especially because of the capability to induce selective inhibition of gene expression for diagnostic applications. Furthermore, the promising structural modification of HNAs makes them an interesting tool for nucleic acid diagnostics. The enhanced hybridisation properties with DNA and RNA targets makes it worthwhile to investigate their use more meticulously. Moreover, such properties make them an exciting tool for the development of innovative methodologies for high mismatch

discrimination within the field of electrochemical detection of target DNA and RNA (Abramov et al. 2008).

1. 9 Electrochemical sensing methodologies for microRNAs

As of now, the most common methods of miRNA detection have been via; cloning, northern blotting, microarray or qRT-PCR, and next-generation sequencing (Chen et al. 2005; Lautner & Gyurcsџnyi 2014; Lee et al. 2010). However, most of these methods come with drawbacks, such as having either low throughput, low sensitivity of detection, or requiring considerable time and effort for sample handling and detection protocols (Lautner & Gyurcsá 2014).

Electrochemical detection is considered to be a cost-effective alternative to today's well-established methods due to their high sensitivity and adoption of simple instrumentation that is applicable to microfabrication technology (Zayats et al. 2002; Ruan et al. 2002; Yang et al. 2004; Xu et al. 2005). A typical electrochemical biosensor consists of an electrode surface immobilized with short-single stranded nucleotides, that are complementary to the target, and electroactive hybridisation indicators. The performance of the electrochemical biosensors is dependent on the hybridisation efficiency between the probe and the complementary target sequence (Hamidi-asl et al. 2013). The novel approach of electrochemical detection platforms for miRNA only started in 2009 (source: Web of Science™) and has showed an increasing trend in publications since the first breakthrough. All of the electrochemical miRNA detection studies presented in the literature rely on hybridisation.

Owing to their cost effectiveness, very high sensitivity and proven compatibility with point-of care devices, electrochemical detection presents a clear niche for miRNA detection (Hamidi-asl et al. 2013; Lautner & Gyurcsџnyi 2014; Jolly et al. 2015; Jolly et al. 2016). The following sections, will introduce some methodologies that are adopted in electrochemical detection for enhancement of nucleic acid (e.g. miRNA) detection.

1.9. 1 Electroactive intercalators

Intercalators are molecules that selectively insert themselves into base pairs of double-stranded oligonucleotides (Gillespie et al. 2019). This property of intercalators is utilised in electrochemical detection for the recognition of hybridised duplexes and as an amplification step after the capture of the target oligonucleotide (Gaiji et al. 2017). The hybridised duplex (Figure 1.11) is monitored by an electroactive intercalator that can be easily reduced/oxidised on the surface. Some examples of intercalators that were used for miRNA sensing are: oracet blue, methylene blue and toluidine blue (Li et al. 2015; Azimzadeh et al. 2016; Rafiee-Pour et al. 2016; Guo et al. 2018a; Tian et al. 2018a). On the other hand, our study of the literature reports on the adoption of a naphthalene diimide intercalator bearing ferrocene moieties (FND) for the recognition of DNA (Figure 1.11). The electrochemical signal of the ferrocene molecules tagged on the FND intercalator were utilised to monitor the DNA recognition after selective binding of the intercalator with the PNA-DNA duplex (Gaiji et al. 2017). Differential pulse voltammetry was adopted to evaluate the oxidation potential of the FND intercalator related to its interaction with a complementary PNA-DNA hybrid. The oxidation peaks of the ferrocene, demonstrated a good linear dependence on DNA concentration in the range 1 fM to 100 nM of target DNA, with a low detection limit of 11.68 fM. The selectivity of the response was approved by an investigation with a non-complementary DNA sequence, which indicated the selective response of the FND intercalator to the target PNA-DNA duplex. Similar methodology can be adapted for its use in electrochemical detection of other nucleic acids such as RNA/miRNA.
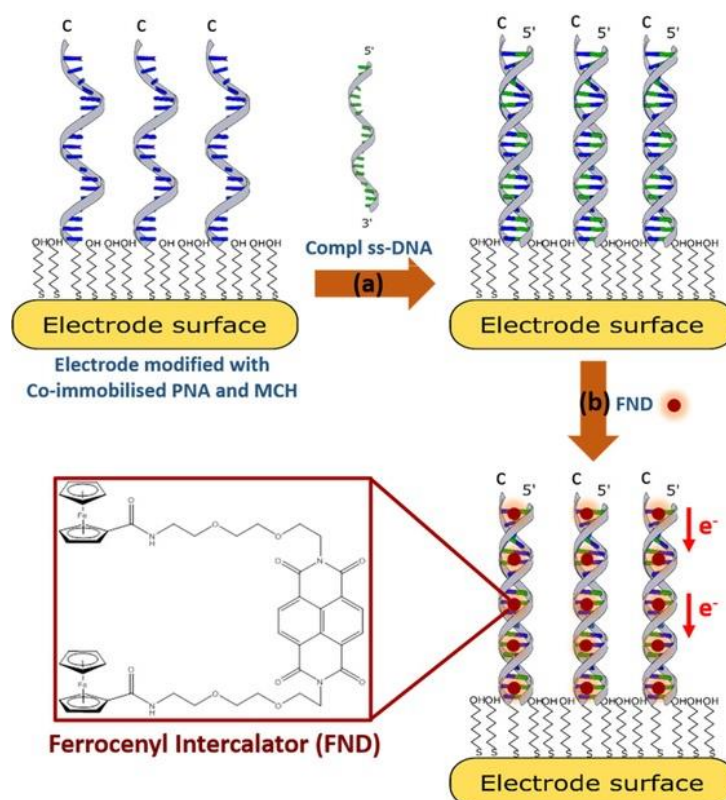
Figure 1. 11 Schematic representation of the Fc-tagged intercalator based biosensor for detection of DNA by using PNA-probe. (a) Steps for PNA-DNA hybridisation (b) FND binding with PNA-DNA duplex (Gaiji et al. 2017).

1.9. 2 Redox Labelling

The concept of redox labelling a target sequence prior to detection has been an alternative approach in electrochemical detection of miRNA. Such methodology is carried out in a couple steps and requires the labelling of miRNA prior to analysis. In a representative study, miRNA was initially labelled with the electroactive complex of osmium(VI) and 2,2′-bipyridine (Os(VI)bipy) which specifically attaches to the ribose at the 3′-end of the miRNA (Bartosik et al. 2014). This was then followed by the hybridisation of the labelled miRNA target with a DNA capture probe that is complementary to target. The detection of miRNA was then carried out at hanging mercury drop electrode at the femtomole level (fM, 10^{-15} M) as a result of the electrocatalytic nature of the peak from the electroactive complex (Os(VI)bipy)

(Bartosik et al. 2014). However, such methodologies come with a significant drawback of the requirement for sample preparation that is not ideal for point-of-care applications.

1.9. 3 Modifications with nanoparticles

Metal nanoparticles possess unique physiochemical properties depending on their size and material, easy and simple functionalisation, conductance and a high surface to volume ratio (Jolly et al. 2017). All noble metals, heavy metals, iron and metal oxides such as titanium dioxide are examples for metal nanoparticles. Gold nanoparticles (AuNPs) are the highlighted examples as they are the most extensively studied nanomaterial, and led to the development of numerous methods for molecular diagnostics, imaging, drug delivery and therapeutics because of their unique properties (Doria et al. 2012). Although there are many applications for nanoparticles, their use in electrochemical sensing can be classified into a couple of categories based on their mode of action: expanding the electrode surface area, binding to biological probes for signal enhancement and acting to raise the concentration of the analyte (Jolly et al. 2017).

Expanding the surface area is an effective method to increase the amount of probes immobilised. For example, AuNPs can be immobilised on different carbon-based matrices such as a carbon nanotube, graphene or graphene oxide; gold surfaces or others polymers (Sardar et al. 2009). This raises the amount of probes immobilised, especially thiol molecules which have a high affinity to bind with AuNPs. Due to increased amount of probe, the amount of biomolecules anchored are raised resulting in an amplification of signal. Furthermore, AuNPs or other metal NPs can be used to mediate reactions amplifying the signal. For instance, capture probes can be initially immobilised on a substrate and then AuNPs modified with target probes are introduced for specific recognition, resulting in signal amplification (Jolly et al. 2016).

On the other hand, magnetic micro- and nanoparticles are other frequently used nano-particles in order to pre-concentrate target miRNAs from a sample (Li et al. 2015; Azimzadeh et al. 2016; Rafiee-Pour et al. 2016; Guo et al. 2018a; Tian et al. 2018a; Wang et al. 2013a; Zhu et al. 2014; Bartosik et al. 2014; Zhang et al. 2016; Koo et al.

2016; Islam et al. 2018; Boriachek et al. 2018). Magnetic beads are particles that are under the control of a magnetic field (Yáñez-sedeño et al. 2016; Gómez-pastora et al. 2017). They are released into a biological sample, where time is allowed for hybridisation with target miRNA and then the beads are separated by the use of a magnet. Then the target miRNA is removed from the surface of magnetic beads either by heating or utilizing a magnetic electrode in order to concentrate magnetic beads at the surface. Hence, magnetic beads offer a valuable and effective method for sample preparation and separation of miRNA from complex samples.

1.9. 4 Enzyme-based detection

Electrochemical biosensors that are based on enzymes, are the oldest and most established biosensors following their commercialisation after the first glucose test in PoC format. For the case of miRNA detection, enzymes are employed as an amplification step via a sandwich sensor design. Recently, several studies reported the adoption of an enzymatic reaction for the recognition of a hybridisation event between the probe and miRNA targets. A representative study in literature initially immobilized a capture probe 1 on a gold electrode through Au—S (Gold-thiol) interaction (Mandli et al. 2017). In the presence of target miRNA, the capture probe 1 hybridised with part of the target. The second part of the target, on the other hand, hybridised with a biotinylated capture probe 2. This was followed by the immobilisation of a streptavidin-conjugated enzyme (such as alkaline phosphate) on the biotinylated capture probe 2 via biotin-streptavidin interaction (Mandli et al. 2017). The miRNA detection was achieved through monitoring the variations in α-naphtol oxidation signals, as the enzyme (SA-ALP, streptavidin-conjugated alkaline phosphatase) catalyses the electro-inactive α-naphtyl phosphate to an electro-active α-naphtol (Mandli et al. 2017). Under the optimal detection conditions, the fabricated biosensor performed selective and sensitive detection with a detection limit of 100 pM. There are many other similar studies that adopt various types of enzymes such as horseradish peroxide (HRP), alkaline phosphatase and glucose oxidase (Gao 2012; Bettazzi et al. 2013; Campuzano et al. 2014).
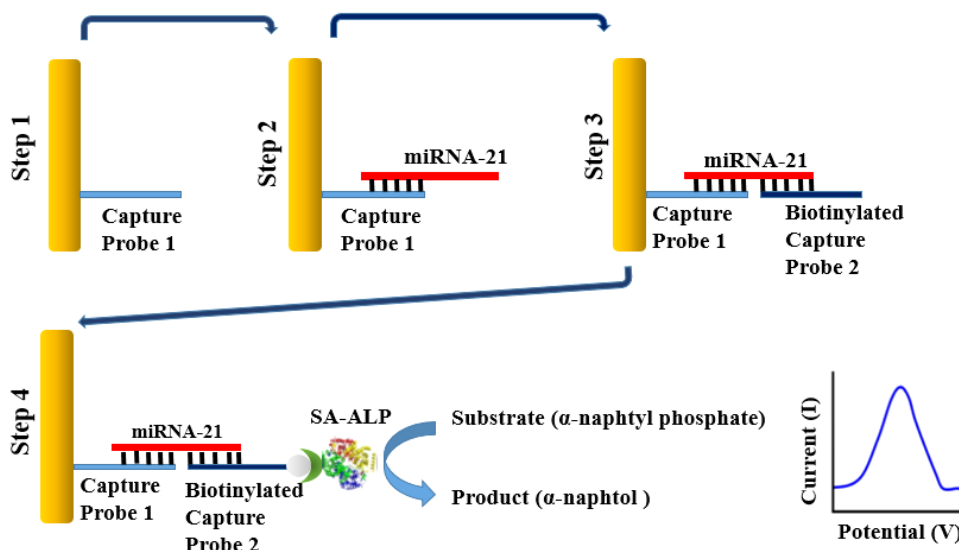
Figure 1. 12 Principle of the enzyme-based electrochemical biosensor for miRNA detection. Re-created from (Mandli et al. 2017).

1.9. 5 Electrocatalytic oxidation of guanine

The label-free electrochemical detection of miRNA (or DNA) hybridisation based on a guanine moiety oxidation signal of the probe (or target) in electrochemical sensors, seems to be simple, faster, and more applicable in comparison to other methods (Hamidi-asl et al. 2013). In the most commonly adopted label free oligonucleotide biosensors, there is no guanine base in the probe sequence, they are replaced by several cytosines. Hence, the electrochemical signal is enhanced during hybridisation with targets containing several guanine bases (Raoof et al. 2011). An inventive electrochemical approach was reported in 2009 for the early detection of miRNAs, it presented an electrochemical detection based on guanine oxidation which is a consequent of the hybrid formation between the miRNA and its inosine substitute capture probe (Lusi et al. 2009). Differential pulse voltammetry was adopted for generating an electrical signal for the oxidation of guanine during the hybrid formation on the surface of the electrode. Such a method is label free and does not require labelling of miRNA with any substances. However, the sensitivity of the assay was poor with a detection limit of 0.1 pmol.

Table 1. 3 Summary of electrochemical detection techniques for miRNA detection

Detection technique	Limit of detection (M)	Biological sample	References
Intercalator			
DPV	1.5×10^{-17}	Spiked in plasma	(Guo et al. 2018b)
DPV	3.3×10^{-17}	Serum	(Tian et al. 2018b)
DPV	8.4×10^{-14}	-	(Rafiee-Pou et al. 2016)
Redox Labelling			
SWV	1×10^{-17}	50% diluted blood	(Tavallaie et al. 2018)
DPV	6.7×10^{-17}	RNA extracted from exosomes	(Zhang et al. 2018)
CV	5×10^{-16}	-	(Mohammadniaei et al. 2017)
DPV	10^{-15}	-	(Bartosik et al. 2013)
Modification with nanoparticles			
DPV	3.7×10^{-16}	-	(Jolly et al. 2016)
DPV	1.92×10^{-15}	Cell lysates	(Wang et al. 2017)
Enzyme-based			
CV & CA	2.2×10^{-19}	Spiked saliva	(Wang et al. 2013b)
DPV	10^{-15}	-	(Mandli et al. 2017)
CV	0.4×10^{-15}	-	(Campuzano et al. 2014)
Guanine oxidation			
DPV	10^{-12}	-	(Li et al. 2014)
DPV	6.82×10^{-10}	-	(Raoof et al. 2011)
DPV	7.27×10^{-12}	-	(Eksin & Erdem 2018)

With the current technology, many novel electrochemical detection methodologies are developed upon exploiting exciting molecular mechanisms as listed in Table 1.3. Most of these techniques are quite sensitive, however they incorporate different ideas in order to achieve low limits of detection. This adds up in the number of experimental steps required and it becomes more challenging to justify the advantage of each step. On the other hand, some of these methods require pre-labelling of target sequence that is not applicable for clinical use and point-of-care applications. Creating a simple electrochemical biosensing design which yields an ultrasensitive and direct detection of miRNA still remains a challenge.

1. 10 General overview of the project

This particular thesis is based on a project entitled "Electrochemical detection of microRNAs for cancer diagnosis". The principal aspect of the current work is to study circulating miRNAs as cancer biomarkers, then investigate the design and immobilisation techniques of oligonucleotide-based capture probes for the development of direct electrochemical detection platforms. The study draws attention to the availability of a broad range of miRNAs in circulating blood as cancer biomarkers. Particular attention is given to miR-21-5p throughout our study, which is a pancreatic cancer specific circulating miRNA. In parallel, this thesis investigates the efficient separation of miRNA from biological samples and the design of redox active self-assembled monolayers that offer label-free detection.

The following points will be highlighted with this thesis:

1. In Chapter 3, use of electrochemical impedance spectroscopy for the development of highly sensitive and direct detection platforms for miRNA, which requires no additional amplification steps, is investigated. Chapter 3 also investigates the adoption of Peptide Nucleic Acids as capture probes for improved affinity (and specificity) to target miRNA and the crucial role of surface chemistry optimisation for highly sensitive and direct (label-free) detection.

2. Chapter 4 presents a new method for efficient separation/fishing of target miRNA from complex solutions prior to detection. Such a strategy is crucial for pre-concentration of the target, hence for further amplification of the detection that is presented previously in Chapter 3.

3. In Chapter 5, redox active self-assembled monolayers and their adoption in design of oligonucleotide-based detection probes for label-free detection is investigated. Such a methodology comes with a major advantage of eliminating the need for doping of the measurement solution that is required for the measurements presented in previous chapters. Hence, the final results chapter investigates further improvement of the methodologies presented in chapters 3 & 4.

All in all, a highly-sensitive and direct electrochemical detection of miRNA is presented in Chapter 3. This is followed by a new method that is demonstrated in Chapter 4 in order to overcome the difficulty of direct detection of miRNA from serum. Hence, Chapter 4 looks into further improving the direct electrochemical detection presented in Chapter 3. Finally, in Chapter 5 a redox active self- assembled monolayer is investigated for label-free and capacitive based detection. If successfully implemented, such biosensor eliminates the need for doping of the measurement solution used within Chapters 3 &5 hence, simplifying the detection further.

References

Abramov, M. et al., 2008. HNA and ANA high-affinity arrays for detections of DNA and RNA single-base mismatches. *Biosensors and Bioelectronics*, 23, pp.1728–1732.

Ali, M., Neumann, R. & Ensinger, W., 2010. Sequence-specific recognition of DNA oligomer using peptide nucleic acid (PNA)-modified synthetic ion channels: PNA/DNA hybridization in nanoconfined environment. *American Chemical Society Nano*, 4(12), pp.7267–7274.

Ambros, V., 2004. The functions of animal microRNAs. *Nature*, 431, pp.350–355.

American Cancer Society, 2019. Cancer Facts & Figures 2019. , pp.9–10. Available at: https://www.cancer.org/ [Accessed November 5, 2019].

Anwar, S.L. et al., 2020. Dynamic changes of circulating mir-155 expression and the potential application as a non-invasive biomarker in breast cancer. *Asian Pacific Journal of Cancer Prevention*, 21, pp.491–497.

Aoki, H., Buhlmann, P. & Umezawa, Y., 2000. Electrochemical detection of a one-base mismatch in an oligonucleotide using ion-channel sensors with self-assembled PNA monolayers. *Electroanalysis*, 12(16), pp.1272–1276.

Azimzadeh, M. et al., 2016. An electrochemical nanobiosensor for plasma miRNA-155 , based on graphene oxide and gold nanorod , for early detection of breast cancer. *Biosensors and Bioelectronics*, 77, pp.99–106.

Bala, A. & Gorski, Ł., 2016. Application of nucleic acid analogues as receptor layers for biosensors. *Analytcial Methods*, 8, pp.236–244.

Bartel, D.P., 2004. MicroRNAs : genomics , biogenesis , mechanism , and function genomics : the miRNA genes. *Cell Press*, 116, pp.281–297.

Bartosik, M. et al., 2014. Magnetic bead-based hybridization assay for electrochemical detection of microRNA. *Analytica Chimica Acta*, 813, pp.35–40.

Bartosik, M. et al., 2013. Os (VI) bipy-based electrochemical assay for detection of specific microRNAs as potential cancer biomarkers. *Electrochemistry Communications*, 33, pp.55–58.

Bell, R., Petticrew, M. & Sheldon, T., 1998. The performance of screening tests for ovarian cancer : results of a systematic review. *British Journal of Obstetrics and Gynaecology*, 105, pp.1136–1147.

Bettazzi, F. et al., 2013. Electrochemical detection of miRNA-222 by use of a magnetic bead-based bioassay. *Analytical and Bioanalytical Chemistry*, 405(2-3), pp.1025–1034.

Blagosklonny, M. V., 2005. Molecular theory of cancer. *Cancer Biology and Therapy*, 4(6), pp.621–627.

Blot, W.J. et al., 1988. Smoking and drinking in relation to oral and pharyngeal cancer. *Cancer Research*, 48, pp.3282–3287.

Bodrossy, L. & Sessitsch, A., 2004. Oligonucleotide microarrays in microbial diagnostics. *Current Opinion in Microbiology*, 7, pp.245–254.

Boriachek, K. et al., 2018. An amplification-free electrochemical detection of exosomal miRNA-21 in serum samples. *Analyst*, 143, pp.1662–1669.

Brunning, R.D. et al., 1975. Bilateral trephine bone marrow biopsies in lymphoma and other neoplastic diseases. *Annals of Internal Medicine*, 82(3), pp.365–366.

Burgio, E. & Migliore, L., 2015. Towards a systemic paradigm in carcinogenesis :

linking epigenetics and genetics. *Molecular Biology Reports*, 42, pp.777–790.

Calin, G.A. et al., 2002. Frequent deletions and down-regulation of micro- RNA genes miR15 and miR16 at 13q14 in chronic lymphocytic leukemia. *Proceedings of the National Academy of Sciences*, 99(24), pp.15524–15529.

Calin, G.A. & Croce, C.M., 2006. MicroRNA signatures in human cancers. *Nature Reviews*, 6, pp.857–866.

Campuzano, S. et al., 2014. Magnetobiosensors based on viral protein p19 for microRNA determination in cancer cells and tissues. *Angewandte Chemie International Edition*, 53, pp.6168–6171.

Cancer Research UK, 2019a. Cancer in the UK 2019. , pp.3–4. Available at: https://www.cancerresearchuk.org [Accessed November 4, 2019].

Cancer Research UK, 2019b. Cancer Research Data and Statistics - Worldwide cancer statistics. Available at: https://www.cancerresearchuk.org [Accessed August 4, 2019].

Cass, A.E.G. et al., 1984. Ferrocene-mediated enzyme electrode for amperometric determination of glucose. *Analytical Chemistry*, 56(4), pp.667–671.

Castoldi, M. et al., 2006. A sensitive array for microRNA expression profiling (miChip) based on locked nucleic acids (LNA). *The RNA Journal*, 12(5), pp.913–920.

Chen, C. et al., 2005. Real-time quantification of microRNAs by stem – loop RT – PCR. *Nucleic Acids Research*, 33(20), pp.1–9.

Chen, X. et al., 2008. Characterization of microRNAs in serum : a novel class of biomarkers for diagnosis of cancer and other diseases. *Cell Research*, 18, pp.997–1006.

Chendrimada, T.P. et al., 2005. TRBP recruits the Dicer complex to Ago2 for microRNA processing and gene silencing. *Nature*, 436(7051), pp.740–744.

Cho, W.C.S., 2010. MicroRNAs: potential biomarkers for cancer diagnosis, prognosis and targets for therapy. *The International Journal of Biochemistry & Cell Biology*, 42(8), pp.1273–81.

Ciatto, S. et al., 2012. Prostate-cancer mortality at 11 years of follow-up. *The New England Journal of Medicine*, 366(11), pp.981–990.

Contreras, E., Ellis, L.D. & Lee, R.E., 1972. Value of the bone marrow biopsy in the diagnosis of metastatic carcinoma. *Cancer*, 29(3), pp.778–783.

Cummins, J.M. et al., 2006. The colorectal microRNAome. *Proceedings of the National Academy of Sciences of the USA*, 103, pp.3687–92.

Daniele, B., Bencivenga, A. & Megna, A.S., 2004. α -fetoprotein and ultrasonography screening for hepatocellular carcinoma. *American Gastroenterological Association*, 127(5), pp.108–112.

Declercq, R. et al., 2002. Crystal structure of double helical hexitol nucleic acids. *Journal of the American Chemical Society*, 124(6), pp.928–933.

Department of Public Health England, 2017. Major causes of death and how they have changed. In *Health profile for England: 2017*. Available at: www.gov.uk [Accessed August 4, 2019].

Doria, G. et al., 2012. Noble Metal Nanoparticles for Biosensing Applications. *Sensors*, 12, pp.1657–1687.

Duffy, M.J., 2001. Clinical uses of tumor markers : a critical review. *Critical Reviews in Clinical Laboratory Sciences*, 38(3), pp.225–262.

Duffy, M.J., 2007. Role of tumor markers in patients with solid cancers : A critical

review. *European Journal of Internal Medicine*, 18, pp.175–184.

Duffy, M.J., 2013. Tumor markers in clinical practice : a review focusing on common solid cancers. *Medical Principles and Practice*, 22, pp.4–11.

Egholm, M. et al., 1992. Peptide nucleic acids (PNA). Oligonucleotide analogues with an achiral peptide backbone. *Journal of the American Chemical Society*, 114(5), pp.1895–1897.

Eksin, E. & Erdem, A., 2018. Electrochemical detection of microRNAs by graphene oxide modi fi ed disposable graphite electrodes. *Journal of Electroanalytical Chemistry*, 810, pp.232–238.

Ellis, J.C. & Angeles, L., 1988. Screening for hepatocellular carcinoma. Review and perspective. *The Western Journal of Medicine*, 149(2), pp.183–187.

Ender, C. & Meister, G., 2010. Argonaute proteins at a glance. *Journal of Cell Science*, 123, pp.1819–1823.

Esquela-kerscher, A. & Slack, F.J., 2006. Oncomirs – microRNAs with a role in cancer. *Nature Reviews Cancer*, 6(4), pp.259–269.

Fass, L., 2008. Imaging and cancer : A review. *Molecular Oncology*, 2, pp.115–152.

Ferlay, J. et al., 2014. Cancer incidence and mortality worldwide: Sources, methods and major patterns in GLOBOCAN 2012. *Internal Journal of Cancer*, 136(5), pp.359–386.

Ferracin, M., Calin, G.A. & Negrini, M., 2011. MicroRNAs in cancer (an overview). In W. C. S. Cho, ed. *MicroRNAs in Cancer Translational Research*. Springer, Dordrecht, pp. 1–73.

Fortunato, O. et al., 2019. Exo-miRNAs as a New Tool for Liquid Biopsy in Lung Cancer. *Cancers*, 11(888).

Frampton, A.E. et al., 2013. Circulating peripheral blood mononuclear cells exhibit altered miRNA expression patterns in pancreatic cancer. *Expert Review of Molecular Diagnostics*, 13(5).

Gablo, N.A. et al., 2019. Cell-free microRNAs as non-invasive diagnostic and prognostic bio-markers in pancreatic cancer. *Current Genomics*, 20, pp.569–580.

Gaiji, H. et al., 2017. A peptide nucleic acid (PNA) -DNA ferrocenyl intercalator for electrochemical sensing. *Electroanalysis*, 29, pp.917–922.

Gao, Z., 2012. A highly sensitive electrochemical assay for microRNA expression profiling. *Analyst*, 137, pp.1674–1679.

Gao, Z. & Ting, B.P., 2009. A DNA biosensor based on a morpholino oligomer coated indium-tin oxide electrode and a cationic redox polymer. *Analyst*, 134, pp.952–957.

Gillespie, P., Ladame, S. & O'Hare, D., 2019. Molecular methods in electrochemical microRNA detection. *Analyst*, 144, pp.114–129.

Go, H. et al., 2015. MicroRNA-21 plays an oncogenic role by targeting FOXO1 and activating the PI3K / AKT pathway in diffuse large B-cell lymphoma. *Oncotarget*, 6(17).

Gómez-pastora, J. et al., 2017. Analysis of separators for magnetic beads recovery : From large systems to multifunctional microdevices. *Separation and Purification Technology*, 172, pp.16–31.

Grant, W.B., 2002. An estimate of premature cancer mortality in the U.S. due to inadequate doses of solar ultraviolet-B radiation. *Cancer*, 94(6), pp.1867–1875.

Guo, J. et al., 2018a. An electrochemical biosensor for microRNA-196a detection

based on cyclic enzymatic signal amplification and template-free DNA extension reaction with the adsorption of methylene blue. *Biosensors and Bioelectronics*, 105, pp.103–108.

Guo, J. et al., 2018b. An electrochemical biosensor for microRNA-196a detection based on cyclic enzymatic signal amplification and template-free DNA extension reaction with the adsorption of methylene blue. *Biosensors and Bioelectronics*, 105, pp.103–108. Available at: https://doi.org/10.1016/j.bios.2018.01.036.

Hamidi-asl, E. et al., 2013. A review on the electrochemical biosensors for determination of microRNAs. *Talanta*, 115, pp.74–83.

Hammond, J.L., 2017. *Micro- and nanogap based biosensors (Published doctoral dissertation)*. University of Bath.

He, Y. et al., 2015. Current state of circulating microRNAs as cancer biomarkers. *Clinical Chemistry*, 61(9), pp.1138–1155.

Hendrix, C. et al., 1997. 1',5'-Anhydrohexitol oligonucleotides: synthesis, base pairing and recognition by regular oligodeoxyribonucleotides and oligoribonucleotides. *Chemistry A European Journal*, 3(1), pp.110–120.

Herrera, L.A. et al., 2008. The epigenetic origin of aneuploidy. *Current Genomics*, 9, pp.43–50.

Holland, A.J. & Cleveland, D.W., 2009. Boveri revisited: Chromosomal instability, aneuploidy and tumorigenesis. *Nature Reviews Molecular Cell Biology*, 10(7), pp.478–487.

Huang, Q. et al., 2017. Circulating MicroRNAs in Colorectal Cancer. *Journal of Molecular and Genetic Medicine*, 11(3), pp.1–6.

Hughes, T.R. et al., 2001. Expression profiling using microarrays fabricated by an ink-jet oligonucleotide synthesizer. *Nature Biotechnology*, 19, pp.342–347.

Iorio, M. V & Croce, C.M., 2011. MicroRNA dysregulation in cancer : diagnostics , monitoring and therapeutics . A comprehensive review. *EMBO Molecular Medicine*, 4, pp.143–159.

Islam, N. et al., 2018. Gold-loaded nanoporous ferric oxide nanocubes for electrocatalytic detection of microRNA at attomolar level. *Biosensors and Bioelectronics*, 101, pp.275–281.

Jacobs, I.J. et al., 1999. Screening for ovarian cancer : a pilot randomised controlled trial. *The Lancet*, 353, pp.1207–1210.

Jagerszki, G. et al., 2007. Hybridization-modulated ion fluxes through peptide-nucleic-acid- functionalized gold nanotubes . A New approach to quantitative label-free DNA analysis. *Nano Letters*, 7(6), pp.1609–1612.

Janshoff, A., Galla, H. & Steinem, C., 2000. Piezoelectric mass-sensing devices as biosensors - an alternative to optical biosensors? *Angewandte Chemie International Edition*, 39, pp.4004–4032.

John, S. & Broggio, J., 2019. *Cancer survival in England : national estimates for patients followed up to 2017*, Available at: https://www.ons.gov.uk/.

Jolly, P. et al., 2015. A simple and highly sensitive electrochemical platform for detection of microRNAs. *Institute of Electrical and Electronics Engineers Sensors*, pp.803–806.

Jolly, P. et al., 2016. Highly sensitive dual mode electrochemical platform for microRNA detection. *Scientific Reports*, 6(36719), pp.1–9.

Jolly, P. et al., 2017. Nucleic acid-based aptasensors for cancer diagnostics: an

insight into immobilisation strategies. In P. Chandra, Y. N. Tan, & S. P. Singh, eds. *Next Generation Point-of-care Biomedical Sensors Technologies for Cancer Diagnosis*. pp. 205–231.

Jolly, P., 2016. *Oligonucleotide-based biosensors for the detection of prostate cancer biomarkers (Published doctoral dissertation)*. University of Bath , UK.

Kaiser, J., 2010. Keeping Tabs on Tumor DNA. *Science*, 327, p.1074.

Kaur, H. et al., 2006. Thermodynamic , counterion , and hydration effects for the incorporation of locked nucleic acid nucleotides into DNA duplexes. *Biochemistry*, 45, pp.7347–7355.

Keighley, S.D. et al., 2008. Optimization of label-free DNA detection with electrochemical impedance spectroscopy using PNA probes. *Biosensors and Bioelectronics*, 24, pp.906–911.

Key, T.J. et al., 2002. The effect of diet on risk of cancer. *The Lancet*, 360, pp.861–868.

Khalkhali, I., Mena, I. & Diggles, L., 1994. Review of imaging techniques for the diagnosis of breast cancer: a new role of prone scintimammography using technetium-99m sestamibi. *European Journal of Nuclear Medicine*, 21(4), pp.357–362.

Kinzler, K.W. & Vogelstein, B., 1996. Lessons from hereditary colorectal cancer. *Cell*, 87, pp.159–170.

Klein, G., 1981. The role of gene dosage and genetic transpositions in carcinogenesis. *Nature*, 294, pp.313–318.

Kok, T. et al., 2004. Efficacy of MRI and mammography for breast-cancer screening in women with a familial or genetic predisposition. *The New England Journal of Medicine*, 351(5), pp.427–437.

Koo, K.M. et al., 2016. Poly(A) extensions of miRNAs for amplification-free electrochemical detection on screen-printed gold electrodes. *Analytical Chemistry*, 88, pp.2000–2005.

Koutova, L. et al., 2015. The impact of standard chemotherapy on miRNA signature in plasma in AML patients. *Leukemia Research*, 39(12), pp.1389–1395.

Kozlov, I.A. et al., 1999. Nonenzymatic synthesis of RNA and DNA oligomers on hexitol nucleic acid templates : the importance of the A Structure. *Journal of the American Chemical Society*, 121(12), pp.2653–2656.

Landthaler, M., Yalcin, A. & Tuschl, T., 2004. The human DiGeorge syndrome critical region gene 8 and its D. melanogaster homolog are required for miRNA biogenesis. *Current Biology*, 14, pp.2162–2167.

Laschi, S. et al., 2009. Enzyme-amplified electrochemical hybridization assay based on PNA , LNA and DNA probe-modified micro-magnetic beads. *Bioelectrochemistry*, 76(1-2), pp.214–220.

Lautner, G. & Gyurcsµnyi, R.E., 2014. Electrochemical Detection of miRNAs. *Electroanalysis*, 26, pp.1224–1235.

Lautner, G. & Gyurcsá, R.E., 2014. Electrochemical detection of miRNAs. *Electroanalysis*, 26, pp.1224–1235.

Lawrie, C.H. et al., 2008. Detection of elevated levels of tumour-associated microRNAs in serum of patients with diffuse large B-cell lymphoma. *British Journal of Haematology*, 141, pp.672–675.

Lee, L.W. et al., 2010. Complexity of the microRNA repertoire revealed by next-generation sequencing. *RNA*, 16(11), pp.2170–2180.

Lee, Y. et al., 2004. MicroRNA genes are transcribed by RNA polymerase II. *Tje European Molecular Biology Organization Journal*, 23, pp.4051–4060.

Lee, Y. et al., 2003. The nuclear RNase III Drosha initiates microRNA processing. *Nature*, 425, pp.415–419.

Li, F. et al., 2014. Carbon nanotube-based label-free electrochemical biosensor for sensitive detection of miRNA-24. *Biosensors and Bioelectronics*, 54, pp.158–164.

Li, F. et al., 2015. Carbon nanotube-polyamidoamine dendrimer hybrid-modified electrodes for highly sensitive electrochemical detection of microRNA24. *Analytcial Chemistry*, 87, pp.4806–4813.

Li, Z. et al., 2016. Exosomal microRNA-141 is upregulated in the serum of prostate cancer patients. *OncoTargets and Therapy*, 9, pp.139–148.

Liao, T. et al., 2017. Ultrasensitive detection of microRNAs with morpholino-functionalized nanochannel biosensor. *Analytical Chemistry*, 89, pp.5511–5518.

Lim, L.P. et al., 2005. Microarray analysis shows that some microRNAs downregulate large numbers of target mRNAs. *Nature*, 435, pp.769–772.

Lu, J. et al., 2005. MicroRNA expression profiles classify human cancers. *Nature*, 435, pp.834–838.

Lusi, E.A. et al., 2009. Innovative electrochemical approach for an early detection of microRNAs. *Analytical Chemistry*, 81(7), pp.2819–2822.

Mandli, J., Mohammadi, H. & Amine, A., 2017. Electrochemical DNA sandwich biosensor based on enzyme amplified microRNA-21 detection and gold nanoparticles. *Bioelectrochemistry*, 116, pp.17–23.

Mcanena, P. et al., 2019. Circulating microRNAs miR-331 and miR- 195 differentiate local luminal a from metastatic breast cancer. *BMC Cancer*, 19(436), pp.1–10.

Mitchell, P.S. et al., 2008. Circulating microRNAs as stable blood-based markers for cancer detection. *Proceedings of the National Academy of Sciences USA*, 105(30), pp.10513–10518.

Mohamad A Eloubeidi., V.K.C. et al., 2003. Endoscopic ultrasound–guided fine needle aspiration biopsy of patients with suspected pancreatic cancer: diagnostic accuracy and acute and 30-day complications. *The American Journal of Gastroenterology*, 98(12), pp.2663–2668.

Mohammadniaei, M. et al., 2017. Electrochemical nucleic acid detection based on parallel structural dsDNA / recombinant azurin hybrid. *Biosensors and Bioelectronics*, 98, pp.292–298.

Murtaza, M. et al., 2013. Non-invasive analysis of acquired resistance to cancer therapy by sequencing of plasma DNA. *Nature*, 497, pp.108–112.

Natsume, T. et al., 2007a. Effect of base mismatch on the electronic properties of DNA – DNA and LNA – DNA double strands : Density-functional theoretical calculations. *Chemical Physics Letters*, 446, pp.151–158.

Natsume, T. et al., 2007b. Hybridization energies of double strands composed of DNA , RNA , PNA and LNA. *Chemical Physics Letters*, 434, pp.133–138.

Nelson, K.E., Levy, M. & Miller, S.L., 2000. Peptide nucleic acids rather than RNA may have been the first genetic molecule. *Proceedings of the National Academy of Sciences of the United States of America*, 97(8), pp.3868–3871.

Nielsen, P.E. et al., 1991. Sequence-Selective Recognition of DNA by Strand Displacement with a Thymine-Substituted Polyamide. *Science*, 254, pp.1497–

1501.

Obernosterer, G., Martinez, J. & Alenius, M., 2007. Locked nucleic acid-based in situ detection of microRNAs in mouse tissue sections. *Nature Protocols*, 2(6), pp.1508–1514.

OED, 2019. Sensor. *Oxford University Press*. Available at: https://www.oed.com/view/Entry/176005 [Accessed October 22, 2019].

Okamura, K. et al., 2004. Distinct roles for Argonaute proteins in small RNA-directed RNA cleavage pathways. *Genes & Development*, 18(14), pp.1655–1666.

Okonogi, T.M. et al., 2002. Phosphate backbone neutralization increases duplex DNA flexibility : A model for protein binding. *Proceedings of the National Academy of Sciences*, 99(7), pp.4156–4160.

Peinado, H. et al., 2012. Melanoma exosomes educate bone marrow progenitor cells toward a pro-metastatic phenotype through MET. *Nature Medicine*, 18(6), pp.883–891.

Petersen, M. & Wengel, J., 2003. LNA : a versatile tool for therapeutics and genomics. *Trends in Biotechnology*, 21(2), pp.74–81.

Rafiee-Pou, H.-A., Behpour, M. & Keshavarz, M., 2016. A novel label-free electrochemical miRNA biosensor using methylene blue as redox indicator : application to breast cancer biomarker. *Biosensors and Bioelectronics*, 77, pp.202–207.

Rafiee-Pour, H.-A., Behpour, M. & Keshavarz, M., 2016. Biosensors and Bioelectronics A novel label-free electrochemical miRNA biosensor using methylene blue as redox indicator : application to breast cancer biomarker. *Biosensors and Bioelectronics*, 77, pp.202–207.

Raoof, J.B. et al., 2011. Preparation of an electrochemical PNA biosensor for detection of target DNA sequence and single nucleotide mutation on p53 tumor suppressor gene corresponding oligonucleotide. *Sensors & Actuators B: Chemical*, 157, pp.195–201. Available at: http://dx.doi.org/10.1016/j.snb.2011.03.049.

Reid, B.J. et al., 2000. Optimizing endoscopic biopsy detection of early cancers in Barrett's high-grade dysplasia. *The American Journal of Gastroenterology*, 95(11), pp.3089–3096.

Rijavec, E. et al., 2020. Liquid biopsy in non-small cell lung cancer : highlights and challenges. *Cancers*, 12(17), pp.1–17.

Rothenberg, M. et al., 1989. Oligodeoxynucleotides as anti-sense inhibitors of gene expression: therapeutic implications. *Journal of the National Cancer Institute*, 81(20), pp.1539–1544.

Rowley, J.D., 1998. The critical role of chromosome translocations in human leukemias. *Annual Review of Genetics*, 32, pp.495–519.

Ruan, C., Yang, L. & Li, Y., 2002. Immunobiosensor chips for detection of escherichia coli O157 : H7 using electrochemical impedance spectroscopy. *Analytical Chemistry*, 74(18), pp.4814–4820.

Sang, S., Zhang, W. & Zhao, Y., 2013. Review on the design art of biosensors. In T. Rinken, ed. *State of the Art in Biosensors - General Aspects*. IntechOpen, pp. 90–105.

Sardar, R. et al., 2009. Gold nanoparticles : past , present , and future. *Langmuir*, 25(24), pp.13840–13851.

Saslow, D. et al., 2007. American cancer society guidelines for breast screening with MRI as an adjunct to mammography. *CA: A New Cancer Journal for Clinicians*, 57(2), pp.75–89.

Schwarzenbach, H., Hoon, D.S.B. & Pantel, K., 2011. Cell-free nucleic acids as biomarkers in cancer patients. *Nature Reviews Cancer*, 11(6), pp.426–37.

Sempere, L.F. et al., 2007. Altered microRNA expression confined to specific epithelial cell subpopulations in breast cancer. *Cancer Research*, 67(24), pp.11612–11621.

Silahtaroglu, A.N. et al., 2007. Detection of microRNAs in frozen tissue sections by fluorescence in situ hybridization using locked nucleic acid probes and tyramide signal amplification. *Nature Protocols*, 2(10), pp.2520–2528.

Soto, A.M. & Sonnenschein, C., 2014. One hundred years of somatic mutation theory of carcinogenesis: Is it time to switch? *BioEssays*, 36(1), pp.118–120.

Strauss-Soukup, J.K. et al., 1997. Effects of Neutralization Pattern and Stereochemistry on DNA Bending by Methylphosphonate Substitutions. *Biochemistry*, 36(29), pp.8692–8698.

Strauss-soukup, J.K. & Maher, L.J., 1998. Electrostatic effects in DNA bending by GCN4 mutants. *Biochemistry*, 37, pp.1060–1066.

Summerton, J. et al., 1997. Morpholino and phosphorothioate antisense oligomers compared in cell-free and in-cell systems. *Antisense and Nucleic Acid Drug Development*, 7, pp.63–70.

Summerton, J.E. & Weller, D.D., 1993. Uncharged morpolino-based polymers having phosphorous containing chiral intersubunit linkages.

Tavallaie, R. et al., 2018. Nucleic acid hybridization on an electrically reconfigurable network of gold-coated magnetic nanoparticles enables microRNA detection in blood. *Nature Nanotechnology*, 13(November).

Tercero, N. et al., 2009. Morpholino monolayers: preparation and label-free DNA analysis by surface hybridization. *Journal of the American Chemical Society*, 131(13), pp.4953–4961.

Tian, L. et al., 2018a. Gold nanoparticles superlattices assembly for electrochemical biosensor detection of microRNA-21. *Biosensors and Bioelectronics*, 99, pp.564–570.

Tian, L. et al., 2018b. Gold nanoparticles superlattices assembly for electrochemical biosensor detection of microRNA-21. *Biosensors and Bioelectronics*, 99, pp.564–570.

Turchinovich, A. et al., 2011. Characterization of extracellular circulating microRNA. , 39(16), pp.7223–7233.

Turchinovich, A. et al., 2013. Circulating miRNAs : cell – cell communication function ? *Frontiers in Genetics*, 4(119), pp.1–10.

Valoczi, A. et al., 2004. Sensitive and specific detection of microRNAs by northern blot analysis using LNA-modified oligonucleotide probes. *Nucleic AcidS Reseacrh*, 32(22).

Varallyay, E., Burgyan, J. & Havelda, Z., 2007. Detection of microRNAs by Northern blot analyses using LNA probes using LNA probes. *Methods*, 43, pp.140–145.

Vasudevan, S., Tong, Y. & Steitz, J.A., 2007. Switching from repression to activation: microRNAs can upregulate translation. *Science*, 318, pp.1931–4.

Volinia S, Calin GA, Liu CG, et al., 2006. A microRNA expression signature of

human solid tumors defines cancer gene targets. *Proceedings of the National Academy of Sciences*, 103, pp.2257–61.

Wang, J., 1998. DNA biosensors based on peptide nucleic acid (PNA) recognition. *Biosensors & Bioelectronics*, 13, pp.757–762.

Wang, J., 2006. Electrochemical biosensors: towards point-of-care cancer diagnostics. *Biosensors and Bioelectronics*, 21(10), pp.1887–1892.

Wang, X. et al., 2016. Screening miRNAs for early diagnosis of colorectal cancer by small RNA deep sequencing and evaluation in a Chinese patient population. *OncoTargets and Therapy*, 9, pp.1159–1166.

Wang, X. & Smirnov, S., 2009. Label-Free DNA Sensor Based on Surface Charge Modulated Ionic Conductance. *American Chemical Society Nano*, 3(4), pp.1004–1010.

Wang, Y. et al., 2017. Integrated amplified aptasensor with in-situ precise preparation of copper nanoclusters for ultrasensitive electrochemical detection of microRNA 21. *Biosensors and Bioelectronics*, 98, pp.386–391.

Wang, Z. et al., 2013a. A novel electrically magnetic-controllable electrochemical biosensor for the ultra sensitive and specific detection of attomolar level oral cancer-related microRNA. *Biosensors and Bioelectronics*, 45, pp.108–113.

Wang, Z. et al., 2013b. A novel electrically magnetic-controllable electrochemical biosensor for the ultra sensitive and specific detection of attomolar level oral cancer-related microRNA. *Biosensors and Bioelectronics*, 45, pp.108–113.

Wienholds, E. et al., 2005. MicroRNA Expression in Zebrafish Embryonic Development. *Science*, 309, pp.310–312.

World Health Organization, 2019. Cancer Key Facts. Available at: https://www.who.int/cancer/resources/keyfacts/en/ [Accessed August 4, 2019].

World Health Organization, 2017. Guide to cancer early diagnosis. Available at: http://www.who.int/cancer/publications/cancer_early_diagnosis/en/ [Accessed September 20, 2017].

Xu, D. et al., 2005. Label-Free Electrochemical Detection for Aptamer-Based Array Electrodes. *Analytical Chemistry*, 77(16), pp.5107–5113.

Yanaihara, N. et al., 2006. Unique microRNA molecular profiles in lung cancer diagnosis and prognosis. *Cancer Cell*, 9, pp.189–198.

Yáñez-sedeño, P., Campuzano, S. & Pingarrón, J.M., 2016. Magnetic particles coupled to disposable screen printed transducers for electrochemical biosensing. *Sensors*, 16, pp.1–32.

Yang, L. et al., 2004. Interdigitated microelectrode (IME) impedance sensor for the detection of viable Salmonella typhimurium. *Biosensors and Bioelectronics*, 19, pp.1139–1147.

Zayats, M. et al., 2002. Probing antigen-antibody binding processes by impedance measurements on ion-sensitive field-effect transistor devices and complementary surface plasmon resonance analyses: development of cholera toxin sensors. *Analytical Chemistry*, 78(18), pp.4763–73.

Zhang, G. et al., 2010. Morpholino-functionalized silicon nanowire biosensor for sequence-specific label-free detection of DNA. *Biosensors and Bioelectronics*, 25, pp.2447–2453.

Zhang, H. et al., 2002. Human Dicer preferentially cleaves dsRNAs at their termini without a requirement for ATP. *European Molecular Biology Organization*, 21(21), pp.5875–5885.

Zhang, H. et al., 2017. Plasma miR-145 , miR-20a , miR-21 and miR-223 as novel biomarkers for screening early-stage non-small cell lung cancer. *Oncology Letters*, 13, pp.669–676.

Zhang, J. et al., 2018. A ratiometric electrochemical biosensor for the exosomal microRNAs detection based on bipedal DNA walkers propelled by locked nucleic acid modi fi ed toehold mediate strand displacement reaction. *Biosensors and Bioelectronics*, 102(October 2017), pp.33–40.

Zhang, J. et al., 2016. An immobilization-free electrochemical impedance biosensor based on duplex-specific nuclease assisted target recycling for amplified detection of microRNA. *Biosensors and Bioelectronics*, 75, pp.452–457.

Zhu, W. et al., 2014. A label-free and PCR-free electrochemical assay for multiplexed microRNA pro fi les by ligase chain reaction coupling with quantum dots barcodes. *Biosensors and Bioelectronisc*, 53, pp.414–419.

Page | 44

Chapter 2 Principles and Methods

This chapter provides an insight into the immobilisation of oligonucleotide based probes on the electrode surface, and particular attention is given to the self-assembled monolayers that are extensively adopted in our experimental work. In addition, this chapter presents the technical details behind electrochemical techniques, with a focus to the ones adopted in our experimental studies (Cyclic Voltammetry, Electrochemical Impedance Spectroscopy and Differential Pulse Voltammetry). Part of the work presented in this chapter is published in Jolly et al. (Jolly et al. 2017) where the main contributions to the study were made in the analysis of different strategies available for immobilisation of bio-recognition probes on the electrode surface, and the adoption of metal nanomaterials for the enhancement of detection.

2. 1 Methods of immobilisation

One of the key factors to account for in order to construct a successful biosensor is the design of the surface chemistry. The success of the fabricated biosensor highly depends on the surface engineering that is the initial step of the fabrication process. The design of the surface chemistry requires a decision being made on an oligonucleotide-based probe that is specific to the target, hence resulting in high-affinity binding. This is followed by the immobilisation of this probe on the electrode surface. An appropriate control of the immobilisation of the probe is crucial for establishing a good sensitivity, selectivity, and stability of the biosensor (Campuzano et al. 2006). Immobilisation methodologies can be classified into four groups: physical adsorption, covalent binding, affinity, and entrapment. An insight into the advantages and drawbacks of these techniques are provided in Table 2.1. There have been many reported studies on the utilisation of different electrode surfaces for immobilisation, such as graphene, glassy carbon, carbon nanotubes, gold nanoparticles etc. However, the work in this thesis adopts a gold electrode surface for the fabrication of the biosensor.

2.1. 1 Self-assembled monolayer

A broad range of methods have been reported for the immobilisation of oligonucleotide-based probes, depending on the electrode surface and application. However, the most commonly reported techniques specifically for gold electrode surfaces are self-assembled monolayers (SAM), due to their highly controlled density and thicknesses on the transducer surface (Hong et al. 1999). The key condition to take into consideration for the immobilisation of oligonucleotide-based probes on a gold electrode surface is to have an optimum density (Keighley et al. 2008). Thiols, sulphides and disulphides have demonstrated a very high affinity for gold by forming a covalent bond between the sulphur and gold atoms, making alkane thiol-based SAMs very popular (Bain & Whitesides 1989; Bain et al. 1989; Love et al. 2005).

Table 2. 1 Methods of immobilisation and their characteristics

Immobilisation Strategy	Type of interaction	Advantages	Drawbacks	References
Physical	Non-covalent interactions such as Van der Waals, hydrophobic, electrostatic interactions.	The simplest method of all, that is rapid and low cost.	High risk of random orientation of probe and instability (affected by conditions like change in ionic strength of buffer, pH or other reagents)	(Du et al. 2012) (Madaboosi et al. 2015)
Covalent e.g. self-assembled monolayer (SAM)	Probe is attached to the electrode surface by chemical bonding.	Bonds can only be broken under extreme conditions which ensures good stability, well-ordered layer, high degree of control and thickness of electrode surface, high sensitivity and uniform orientation.	Requires pre-modification of the probe and linker molecules, the process can be slow, irreversible and expensive.	(Li et al. 2012) (Zhu et al. 2013)
Affinity	Specific tendency to combine, such as between streptavidin/avidin and biotin	Appreciable orientation ensuring high functionalisation through specificity and well controlled	Expensive due to employing biomolecule linkers	(Ma et al. 2013) (Zhang et al. 2013)
Entrapment (Encapsulation)	Involves trapping of probes within a polymer like pyrrole, chitosan, dopamine, acrylamide etc.	Results in high entrapment of probes, high thermal stability, stability against nucleases, no covalent modification needed, well controlled polymer growth	Could result into leaching of probes and reduced binding efficiency.	(Prabhakar et al. 2007) (Jolly, Tamboli, et al. 2016)

When sulphur comes in close contact with gold, the following reaction takes place:

$$RSH + Au \leftrightarrow RS - Au + H^+ + e^-$$

The reaction is spontaneous leading to 80%-90% coverage in the first few minutes. However, the formation of a well organised layer takes up to 12-16 hours (Schreiber 2000). The formation of well-organised SAMs is not only dependent on factors such as the presence of contaminants, and surface quality (roughness and purity), but also on the length of alkanethiols (Finklea 1996). The better kinetics for longer alkyl thiols could be attributed to amplified van der Waals interactions (Darling et al. 2002). The maximum density of alkane thiol on a gold surface was defined to be 4.64×10^{14} molecules/cm^2, with a gap of 4.99 Å between two adjacent molecules (Love et al. 2005).
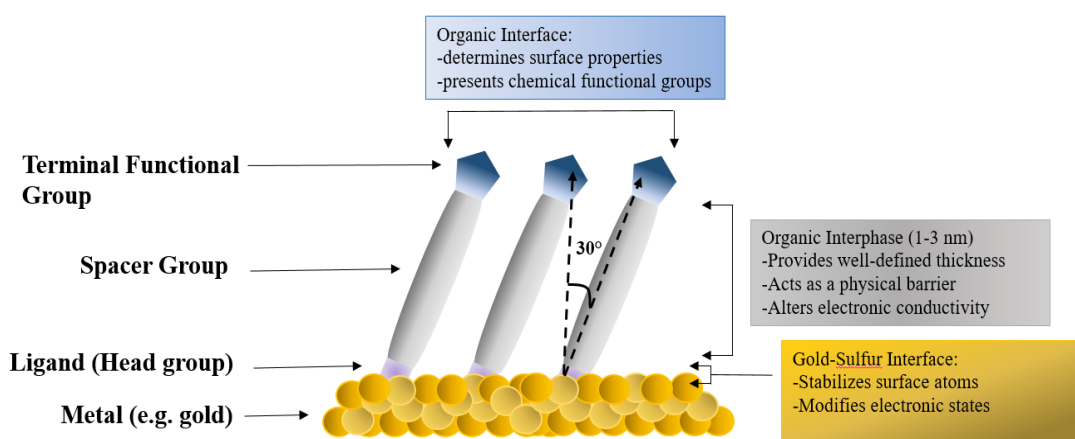
Figure 2. 1 Schematic representation of SAM formation on gold electrode surface. Re-created from *Love et al. 2005*.

The formation of a well-organised SAM undergoes two main steps. There is spontaneous assembly within the first couple minutes. Initially, alkane thiols lie flat on the gold electrode surface through physical adsorption, this is referred to as the 'lying-down' phase (Camillone et al. 1994). This is followed by a chemisorption process where a crystalline or a semi-crystalline structure is formed due to van der

Waals forces resulting in lateral movement until a tilt angle of about 30° between the hydrocarbon chains is achieved (Love et al. 2005). The ability of thiols to move laterally along the gold surface leads to the formation of well-ordered layering, and the healing of defects (Ulman 1996). In such a process, the properties of the SAM are highly affected by the terminal groups of the alkanethiol that define the SAM's interactions with biological molecules. For instance, a carboxylate group can be used to covalently bind an antibody by using ethyl (dimethylaminopropyl) carbodimiide (EDC) and N-hydroxysuccinimide (NHS) activation step (Fischer 2010; Sam et al. 2010).
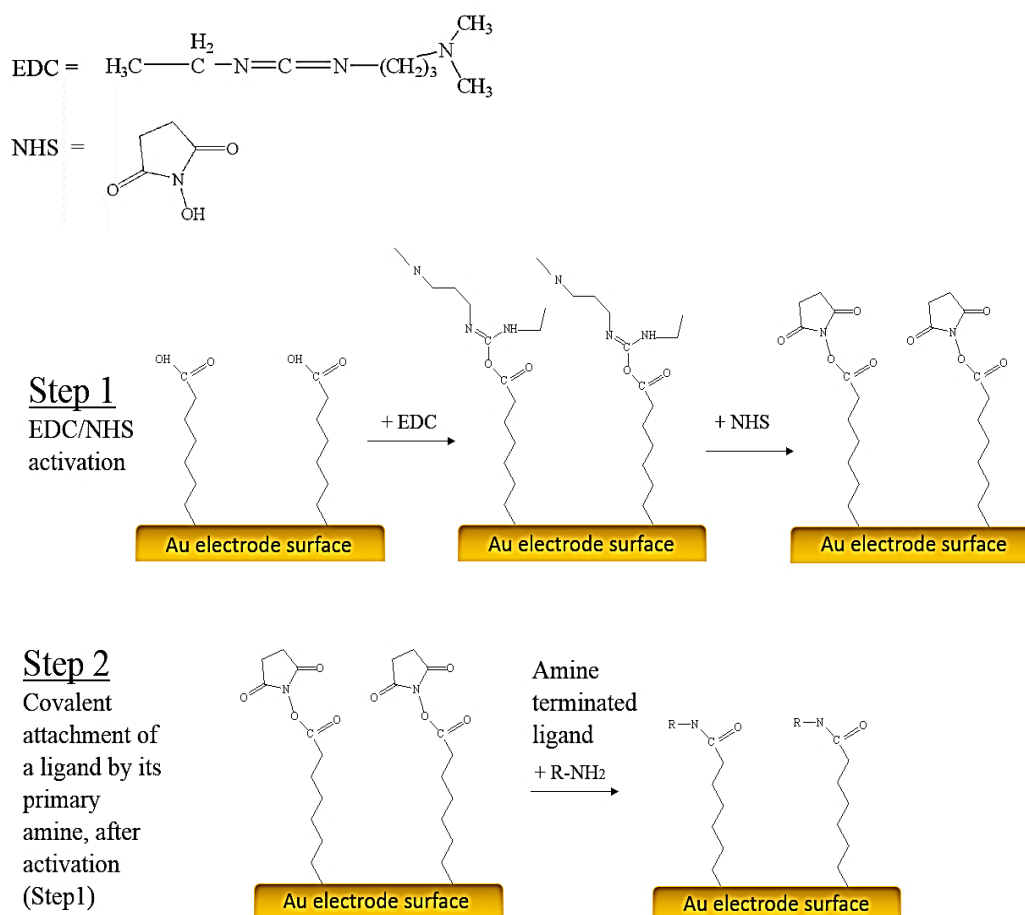
Figure 2. 2 The chemical reaction scheme for the coupling of a ligand to the surface of a gold electrode. At the first step (Step 1), the terminal carboxyl group of the SAM that is immobilised on gold electrode surface is activated by EDC/NHS. This is

followed by the covalent attachment of the ligand by its primary amine, NH_2 (Step 2). In this scheme R stands for oligonucleotides or aptamers (Sam et al. 2010).

SAMs allow researchers to engineer novel and controlled biosensor designs as a result of offering the opportunity of having diverse functional terminal groups. SAMs have been adopted to immobilise various molecules from DNA aptamers (Jolly, Formisano, et al. 2019), peptides (Laurent et al. 2008), biological enzymes (Fang et al. 2003) to metals such as gold nanoparticles (Bertok et al. 2013), copper (Nishizawa et al. 1997) etc.) and more. Furthermore, in Chapter 5 we will discuss the adoption of a ferrocene tagged SAM on the gold substrate to fabricate biosensors. The modification of SAM layers have resulted in the establishment of such mixed SAMs (composed of a redox layer with an antibody receptive component) which offers direct capacitive analysis of target recognition (Santos et al. 2015). The effect of DNA probe density on hybridisation efficiency by using co-immobilised binary SAMs on gold electrodes was demonstrated in 2008 (Keighley et al. 2008a). Moreover, in 2010 studies (Wu et al. 2010) reported a ternary SAM on screen printed gold electrodes as a potential antifouling SAM for amperometric detection of oligonucleotides. Careful selection of the spacer molecules within a SAM would lead to the desired hydrophobicity or hydrophilicity as well as significant chemical reactivity. Therefore, such an approach could block non-specific binding and enhance the electrochemical signals (Herne & Tarlov 1997).

2. 2 Electrochemical techniques

2.2. 1 Electrode-solution interface

Before describing electrochemical set ups and measurements it is crucial to understand what happens at the electrode/solution interface. Two types of processes are observed at the electrode surface, one in which charges (electrons) are transferred across the metal-solution interface (Faradaic process), and the other one where there is no transfer of charges but charge is progressively stored in the metal-solution interface (non-Faradaic process) (Bard & Faulkner 1980). The processes of oxidation and reduction, which are electron transfer based reactions, take place at charge-transfer electrodes.

Since these reactions are controlled by Faraday's law (the amount of chemical reaction caused by the flow of current is proportional to the amount of electricity passed), they are called Faradaic processes. Under some conditions, the charge transfer reactions are thermodynamically or kinetically unfavourable at a range of potentials. However, there will still be adsorption and desorption processes and these are called non-Faradaic processes.

For an ideal polarised electrode, no charge transfer across the metal-solution interface would take place regardless of the potential applied by an outside source of voltage. As a result, it is characterised by an absence of net current between the electrode surface and the electrolyte (Bard & Faulkner 1980). Since, no charge can pass across the interface when the potential is altered, the behaviour of the electrode-solution interface is comparable to that of a capacitor. A capacitor, in its most basic form, is an electrical circuit element that consists of two parallel conductive (metal) plates which are separated by a dielectric material. The behaviour is governed by the following equation;

$$\frac{q}{E} = C \qquad\qquad\qquad \textbf{Equation 2. 1}$$

Where q is the charge on the capacitor (in coulombs, C), E is the potential across the capacitor (in volts, V) and C is the capacitance (in farads, F). The capacitors ability to store charge, q, between its metal plates is proportional to the applied voltage E, for a known capacitance in Farads. A current, referred as charging current, will flow during this charging process. The interface of the electrode and solution has been presented experimentally to behave like a capacitor (Bard & Faulkner 1980). Hence, the interfacial region can be modelled resembling a capacitor. The specific capacitance C of an electric double-layer capacitor is evaluated analogous to a plate capacitor and is describe with the equation:

$$C = \frac{\varepsilon_r \varepsilon_0\, A}{d} \qquad\qquad\qquad \textbf{Equation 2. 2}$$

Where A is the electrode surface area, d is the charge separation distance (i.e., the distance between the adsorbed ion and the electrode surface), ε_r is the dielectric constant of the electrolyte and ε_0 is the permittivity in vacuum, respectively. The charge on the metal, whether it is going to be negative or positive with respect to the solution, is dependent on the potential across the interface and the composition of the solution. At the contact interface of two different phases of electrode surface and liquid, positive and negative charges are arrayed at counter positions with an extremely short distance (e.g. atomic distance). Such charge layers are referred to as the electric double layer. Since the first introduction of the double layer model, referred to as the Helmholtz model (Helmholtz 1879) (Figure 2.3a), there has been a significant evolution of the theories in history that reflect the model of a double layer that we acknowledge today. Helmholtz, who was the first to think about charge separation at interfaces, proposed the first model of the double layer (Bard & Faulkner 1980). The model considered the ordering of positive and negative charges in a rigid fashion on the two sides of the interface and recognised no interactions stretching into solution. Such a structure is similar to a parallel-plate capacitor where the relation between the stored charge density σ and the voltage drop V between the plates is given by the following equation:

$$\sigma = \frac{\varepsilon\varepsilon_0}{d} \, V \qquad\qquad \textbf{Equation 2. 3}$$

Where ε is the dielectric constant of the medium, ε_0 is the permittivity of free space and d is the distance between the two plates. Hence, differential capacitance (C_d) is;

$$\frac{\partial\sigma}{\partial V} = C_d = \frac{\varepsilon\varepsilon_0}{d} \qquad\qquad \textbf{Equation 2. 4}$$

However, the Helmholtz model was found to encounter some principal errors. The weakness of the model is apparent in the way it predicts C_d to be constant while it is experimentally proven that C_d varies with potential and electrolyte concentration in real systems (Bard & Faulkner 1980). Variations in C_d with potential and electrolyte concentration suggest that either ε or d must depend on these variables. The Helmholtz

model also ignores interactions occurring further from the electrode than the first layer of adsorbed species. Hence a more sophisticated model was required.

It was only the beginning of the following century that a double layer model was developed by Gouy (Gouy 1910), and Chapman (Chapman 1913) independently, in which electrolyte concentration and the applied potential were considered to both affect the value of the double layer capacity. At low concentrations of electrolyte there is a relatively low density of charge carriers. As a result, it might take a significant thickness of solution in order to compile the excess charge required to counterbalance the total excess charge density on the metal electrode side. Therefore, in this new model, the Helmholtz's description was improved where the double layer would not be as compact but of a variable thickness, and the ions have freedom to move. This is described as the diffuse double layer. The highest concentration of excess charge would be closest to the electrode where at this distance electrostatic forces are most capable of conquering the thermal processes. Moving further away from the electrode the concentrations of charges would drop progressively as the electrostatic forces weaken. Hence, with such an approach Gouy and Chapman independently introduced the idea of the solution being subdivided into laminae, parallel to the electrode and with a thickness of *dx* (Bard & Faulkner 1980).
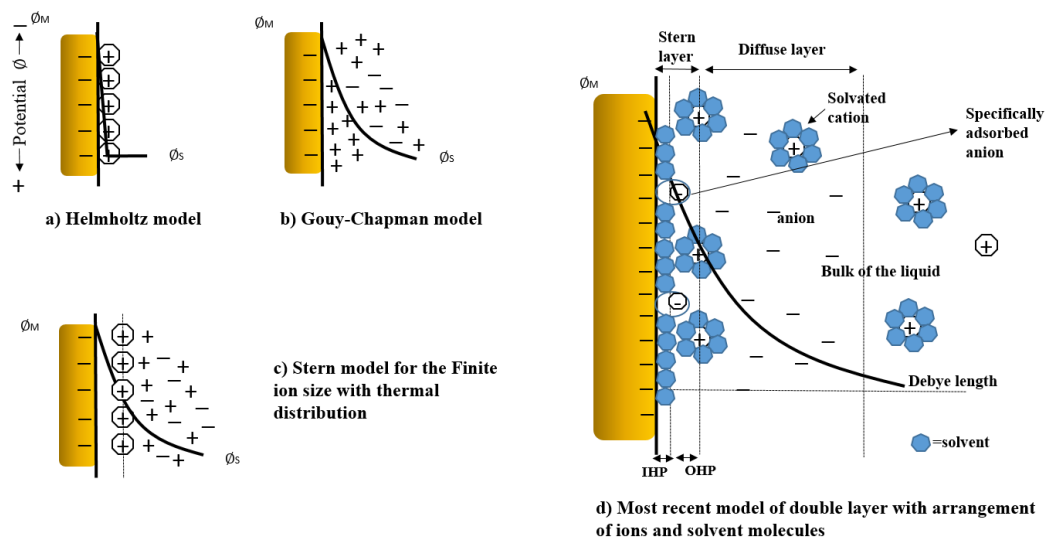
Figure 2. 3 Evolution of the models for the double layer. (a) Initial model of Helmholtz (Helmholtz 1879), (b) Gouy-chapman model (Gouy 1910; Chapman

1913), (c) Stern model (Stern 1924), (d) BDM (Bockris, Devanathan, Muller) model (Bockris et al. 1963)

All laminae are in thermal equilibrium with each other. Moving through various laminae, as the electrostatic potential (ϕ) varies, the energy level of ions of any species would vary accordingly. Therefore, the laminae can be considered as energy states with equivalent decadence and the number of concentrations of species in two laminae have a ratio that is determined by Boltzmann factor.

The population in any other lamina can be evaluated by taking a reference lamina distant from the electrode, where each ion is at its bulk concentration n_i^0 (Bard & Faulkner 1980);

$$n_i = n_i^0 \exp\left(\frac{-z_i\, e\, \phi}{kT}\right)$$ **Equation 2. 5**

where ϕ is measured with respect to the bulk solution, e represents the charge on the electron, k is the Boltzmann constant, T represents the absolute temperature, and z_i is the number of units of electronic charge on ion i.

Hence, in any lamina, the total charge per unit volume is given as;

$$\rho(x) = \sum_i n_i\, z_i\, e = \sum_i n_i^0 z_i\, e\, \exp\left(\frac{-z_i\, e\, \phi}{kT}\right)$$ **Equation 2. 6**

From electrostatics it is a known fact that $\rho(x)$ is related to the potential at distance x by the Poisson equation;

$$\rho(x) = -\varepsilon\varepsilon_0 \frac{d^2\phi}{dx^2}$$ **Equation 2. 7**

On combining equations 2.6 and 2.7 we can describe the system with the Poisson-Boltzmann equation (Bard & Faulkner 1980);

$$\frac{d^2\phi}{dx^2} = \frac{e}{\varepsilon\varepsilon_0} \sum_i n_i^0 z_i\, e\, \exp\left(\frac{-z_i\, e\, \phi}{kT}\right)$$ **Equation 2. 8**

The equation is integrated and re-arranged recognizing that at distances far from the electrode surface, $\phi = 0$ and $(d\phi/dx)=0$. For a symmetrical electrolyte the equation is specialised as;

$$\frac{d\phi}{dx} = \left(\frac{8kTn^0}{\varepsilon\varepsilon_0} \right)^{1/2} \sinh \left(\frac{z\,e\,\phi}{2kT} \right)$$

Equation 2. 9

Where n_i^0 is the number of concentration of each ion in the bulk and z is the magnitude of the charge on the ions.

Moving further away from the surface, the potential is always observed to decay. For a highly charged electrode (having high electrostatic potential ϕ) the drop is sharp as the diffuse layer is quite compact. As ϕ turns smaller, the decline becomes more gradual and takes an exponential form. Upon re-arranging the equation 2.9 in order to provide a general description for the potential profile in the diffuse layer identity, the spatial decay of potential can be characterised by κ, characteristic thickness of the diffuse layer;

$$\kappa = \left(\frac{2n^0 z^2 e^2}{\varepsilon\varepsilon_0 kT} \right)^2$$

Equation 2. 10

Where κ has dimensions of distance.

Finally, we can develop the differential capacitance as;

$$C_d = \frac{d\sigma_M}{d\phi_0} = \left(\frac{2z^2 e^2 \varepsilon\varepsilon_0 n^0}{kT} \right)^{1/2} \cosh \left(\frac{ze\phi}{2kT} \right)$$

Equation 2. 11

With the Gouy-Chapman model, the actual capacitance is usually much lower than the predicted value. The partial success of Gouy-Chapman model suggests that there are still significant failures indicating major defects.

Gouy-Chapman model predicted the ions as point charges that can approach the surface arbitrarily close. In conditions such as high polarisation, the distance

separating the metallic and solution-phase charge zones drop continuously towards zero. However, this is not the real case as ions come with finite size and it is not possible to approach the surface any closer than the ionic radius. Moreover, there is the requirement to account for a layer of solvent on the electrode surface. The restriction on the predicted capacitance is less apparent in the low electrolyte concentrations as the thickness of the diffuse layer is large compare to the thickness of inner Helmholtz plane (IHP) and outer Helmholtz planes (OHP) combined (Figure 2.3). However, as the electrolyte becomes more concentrated, the charges become more tightly compressed against the boundary at OHP. This makes the whole system similar to Helmholtz model (Helmholtz 1879) and we expect the levelling of the differential capacitance. Hence, the plane at outer Helmholtz (OHP) is a crucial factor.

Later, the new model suggested by Stern (Stern 1924) combined the two models of Helmholtz and the Gouy-Chapman by extending the considerations of these earlier models. The new model suggested that the double layer capacitance is made up of two components: The layer closest to the electrode surface that contains the solvents molecules and some other specifically adsorbed ions and molecules, is referred as the IHP. As we move further away from this region, solvated ions are present in the OHP. Beyond the inner Helmholtz plane, the ions approach to the surface due to electrostatic forces and are said to be non-specifically adsorbed. Hence, such solvated molecules stay distant to metal surface and form the outer Helmholtz plane. The molecules further away from the two regions of IHP and OHP that extends into bulk solution, lack the competency to compensate with the overall charges hence, forming the diffuse layer. Such situation is explained by Bockris, Devanathan and Muller model (Bockris et al. 1963) where the layer near the interface is predominated by solvent molecules. According to the latest expression, the differential capacitance is re-defined as the inverse;

$$\frac{1}{Cd} = \frac{X_2}{\varepsilon \varepsilon_0} + \frac{1}{\left(\frac{2z^2 e^2 \varepsilon \varepsilon_0 n^0}{kT}\right)^{1/2} \cosh(\frac{ze\phi_2}{2kT})} \qquad \textbf{Equation 2. 12}$$

Hence,

$$\frac{1}{C_d} = \frac{1}{C_H} + \frac{1}{C_D}$$

Equation 2. 13

where C_d, C_H and C_D respectively represent the capacitance of the electrochemical double layer, the capacitance of the compact layer (within the OHP) and the capacitance of the diffuse layer. The C_d is dominated by the smaller of the two capacities C_H and C_D. The thickness of the C_H is highly dependent on the ionic concentration and can reach up to 10 nm in diluted solutions (Oschatz et al. 2016).

Debye length (λ_D) is the term used to define the distance covered from the OHP to the point where the ions are affected by the electrostatic effect of the electrode surface (diffuse layer), and the limit of detection of impedimetric and potentiometric biosensors are dependent on this crucial factor (Bard & Faulkner 2001). It is well advised to work within the range of Debye length that can be defined as;

$$\lambda_D = \sqrt{\frac{\varepsilon_0 \varepsilon_r kT}{2 N_A q^2 I}}$$

Equation 2. 14

N_A is Avogadro's number, q is the electron charge and I is the ionic strength. As the Equation 2.14 suggests, the Debye length is highly dependent on the ionic concentration of the solution and can reach up to 300 nm in diluted solutions (Hammond 2017). It is a known fact that DNA/RNA molecules are negatively charged due to their phosphate groups in sugar backbone, and the length of each nucleotide is estimated as 0.34 nm (Piunno et al. 1999). For proteins, their charge is generally dependent on the pH conditions of the solution. The isoelectric point of a protein is defined as the pH at which the net charge of the protein is zero. In order to overcome the limiting factor of Debye length on the sensitivity of the sensor, researchers established alternatives to overcome such screening effect. The use of polymer chains (like PEG) on the electrode surface was introduced to provide detection of biomolecules in electrolyte solutions with higher ionic strength, that increases the effective screening length (Gao et al. 2015). A couple of other studies introduced new

strategies in order to work under high ionic strength electrolyte solutions (Jang et al. 2015; Jolly 2016)

2. 3 Electrochemical detection techniques

Depending on the mode of measurement that is performed, electrochemical sensors are classified into groups (Thévenot et al. 2001; Grieshaber et al. 2008) : amperometric, potentiometric, conductometric, impedimetric, ion charge or field effect. This section will be presenting part of these types with particular focus given on the techniques reported in the experimental study of this thesis.

2.3. 1 Amperometry

Amperometric measurements are carried out by recording the current that results from the oxidation and reduction reactions of electroactive species when a fixed potential is applied at the working electrode with respect to the reference electrode (Grieshaber et al. 2008). Faradaic currents can be either directly generated by the redox activity of the analyte at the electrode interface or of the interaction of an electroactive mediator with the biomolecule of interest (Luppa et al. 2001). The second approach is most commonly preferred and amperometry is considered as one of the most sensitive techniques in electrochemistry where the resulting current is directly correlated to the bulk concentration of electroactive species in analyte solution (Thévenot et al. 2001).

The method of amperometry is classified depending on the nature of the potential applied for the electrochemical measurements: the technique is referred as amperometry only if a constant potential is applied between reference and working electrode, whereas it is referred as voltammetry if controlled alterations on potential are made with specific waveshapes and amplitudes. As a result, different types of voltammetry can be applied by using broad applied voltage profiles but voltammetry is still considered as an amperometric method as the working principle for both is the same (Bard & Faulkner 1980; Andrade et al. 2011);

In a typical assay based on voltammetry, the current is monitored upon applying an appropriate potential wave and the resulting currents are generated by three different contributions:

> 1. Capacitive currents (I_c, Non-Faradic currents),
> 2. Faradaic currents (I_f),
> 3. Adsorption effects (I_a).

I_c and adsorption effects perform the background current which do not offer any analytical information in response to an electrochemical reaction. On the other hand, the quantification of the processes of interest by analytical species inside the electrochemical setup is provided by I_f. The accumulation of charges at the interfacial region generate the capacitive currents (I_c) at the electrochemical double layer. The capacitive currents are sensitive to the potential alterations applied at the electrode surface:

$$I_c = C_d \frac{dV}{dt}$$

Equation 2. 15

where C_d is the capacitance of the electrochemical double layer and V is the applied potential at the electrode surface. Therefore, the faster the potential change then the higher the capacitive current will be. In order to minimise the capacitive current, it is always suggested to have reasonable low scan rates as I_c increases linearly with the scan rate.

On the other hand, the Faradaic current (I_f) is the major component that constitutes to the quantitative analysis of test molecules and its signal strength and rate is known to be influenced by a few factors:

> 1. concentration of the electroactive species (I_f is linearly proportional to concentration
> 2. mass transfer (diffusion rate) of the oxidised electroactive active species in the solution towards the electrode
> 3. charge transfer taking plane on the electrode surface after electroactive

species approach the electrode

The kinetic rate of the reaction is proportional to the current measured. Depending on the nature of the analyte analytical conditions, the current is controlled by the slowest case between mass and the electron transfer. For instance, the current flow is limited by the mass transfer, if the mass transfer of the electroactive species from the bulk is slower than the electron transfer (Bard & Faulkner 1980).

The currents due to adsorption effects, on the other hand, depend on the speed at which the potential steps are applied and defined by the following formula;

$$I_a = \frac{(nF)^2 A \Gamma_a}{4RT} \frac{dv}{dt}$$ **Equation 2. 16**

Where Γ_a refers to the amount of species adsorbed per unit area on the electrode surface. The adsorption peak presence and its shape provides information about the contamination and quality of the electrode under investigation.

2.3. 2 Cyclic voltammetry (CV)

Cyclic voltammetry is most commonly preferred as a characterisation technique for the kinetics of a reaction and the measurements are current signals that are based on the electrochemical activities of the species inside the analyte. Cyclic voltammetry is a well-established and commonly used technique for initial electrochemical studies of new systems and has proven to be quite useful for gathering information about complicated electrode reactions. The measurements are carried out by applying a varying electrode potential at the working electrode that is swept back and forward linearly with time vs. the reference electrode. The resulting flowing current is monitored with time. The voltage is measured between the reference and working electrode whereas the current is monitored between the working and counter electrode.

When a specific potential window is imposed on the molecules that are present inside the solution this can cause them to oxidise (lose electrons) or reduce (to gain electrons). Such molecules are referred as redox probes and a CV scan will show its respective

peaks. As illustrated in Figure 2.4 (a), the voltage is swept between two values at a fixed rate. The scan is reversed when the voltage reaches V_2 and the voltage is swept back to V_1. The duration of the scan must allow sufficient time for a meaningful chemical reaction to take place hence, the scan rate, $(V_2 - V_1) / (T_2 - T_1)$ is a critical factor. Varying the scan rate yields correspondingly varied results (Bard & Faulkner 2001).
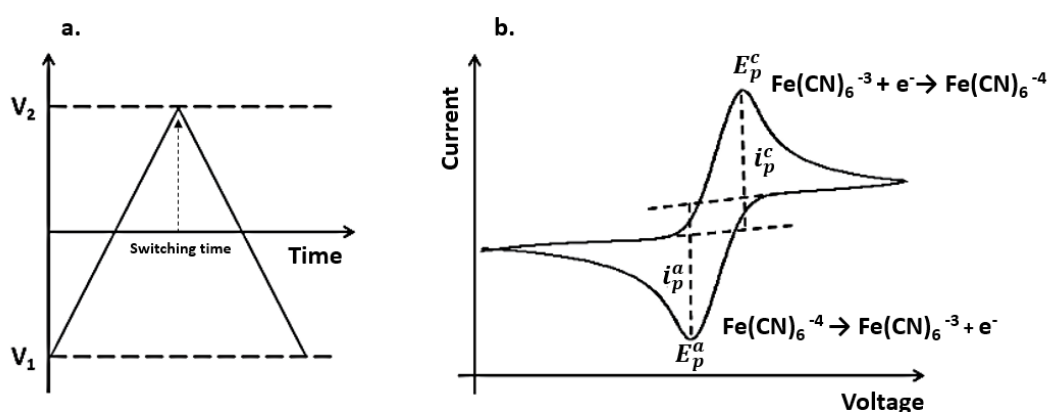
Figure 2. 4 Example cyclic voltammetry waveform (a) Cyclic voltammogram of a fully reversible redox reaction (b) E_p^c (E_p^a) and i_p^c (i_p^a) are the potential and current at cathodic and anodic peaks, respectively. Fe $(CN)_6$ $^{3-/4-}$ is adopted as an example for typical reduction and oxidation reactions of a redox molecule at cathodic and anodic peaks. The diagrams are re-created from (Andrade et al. 2011).

The resulting measurements are in turn plotted as current vs. voltage graph that is referred as voltammogram. For instance, in Figure 2.4 (b) when the voltage applied at the working electrode (WE) increases and reaches a value close to the reduction potential of the redox molecule, WE loses an electron which becomes associated with the redox molecule and the molecule in turn becomes reduced. Therefore, the transfer of electron from the electrode surface to the solution results in the appearance of a reduction peak in the voltammogram. As the voltage is reversed in order to complete the scan toward V_1, potential approaches the oxidation potential of the redox molecule. This process will result in current of opposite polarity as compared to forward scan and the second peak provides information about the reversibility of a reaction at the

given scan rate. The anodic and cathodic currents measured by the system corresponds to the sum of two components (Bard & Faulkner 1980; Andrade et al. 2011) :

1. A capacitive component, also referred as non-Faradaic process that results from re-distribution of charged and polar species at the surface of the electrode.

2. A component that results from transfer of electrons between the electrode and the redox species free in solution or immobilised at the electrode surface. This is also refereed as Faradaic process.

The Faradaic component of current is influenced by the diffusion rate of the electroactive species towards the electrode surface. For a redox species (R) with a redox potential of E^0, the Faradaic current is expressed as followed;

$$I_f = nFAD_0 \qquad\qquad\qquad \textbf{Equation 2. 17}$$

Where A is the electroactive area of the electrode (cm^2), n is the number of electrons involved in the redox transfer event (usually 1), F is the Faraday's constant ($C\ mol^{-1}$), D is the diffusion coefficient of the species reduced and oxidised (cm^2/s).

For a fully reversible system, the anodic and cathodic peak current is described by Randles-Sevčik law (Bard & Faulkner 1980):

$$i_p = 0.4436An^{3/2}\left(\frac{F^3D\upsilon}{RT}\right)^{1/2}c \qquad\qquad \textbf{Equation 2. 18}$$

Where υ is the scan rate (V/s), c is the bulk concentration of the redox species (mol/cm^3), T is the temperature (K) and R is gas constant ($J\ K^{-1}\ mol^{-1}$).

The formula is equally valid for reduction and oxidation peaks and performs linear proportionality to the concentration of the electroactive species and the square root of the scan rate, υ. The plot of i_p vs. $\upsilon^{1/2}$ is an important diagnostic tool and if the curve is linear it is reasonably safe to conclude that the electrode reaction is controlled by diffusion.

2.3. 3 Differential pulse voltammetry (DPV)

Differential Pulse Voltammetry was developed with the aim of reducing the non-Faradaic (capacitive) currents in order to achieve better sensitivity (Bard & Faulkner 1980). The potential waveform of Differential Pulse Voltammetry is composed of small pulses (with constant amplitude) that are superimposed upon a staircase wave form. The current is then evaluated by taking the difference between the currents right before and at the end of the pulse. Hence, DPV is more immune to background currents. This is because the non-Faradaic (capacitive) currents drop exponentially with time where the Faradaic current decays with $t^{-1/2}$ that results in a more sensitive system. A typical voltammogram displays the differential currents versus the applied potential and the concentration of the analyte in solution is directly proportional to the current peak height.
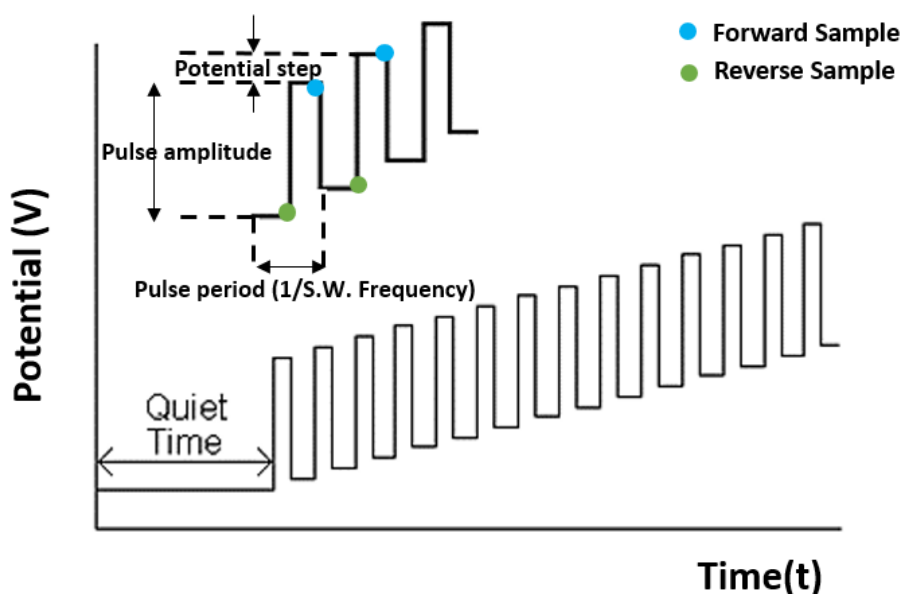
Figure 2. 5 Potential waveform for Differential Pulse Voltammetry. The potential waveform is composed of small pulses (of constant amplitude) that are superimposed upon a staircase wave form. The diagram is re-created from (Basi Electrochemistry 2020).

2.3. 4 Square wave voltammetry (SWV)

In a historical context, the square wave voltammetry originates from the Kalousek commutator (Ramaley & Krause 1969) and Barker's square-wave polarography (Barker & Jenkins 1952; Barker & Gardner 1992). The modern version of SWV that is adapted into today's digital electrochemical instruments, adopts a staircase potential ramp modified with square-shape potential pulses (Figure 2.6) (Mirceski et al. 2013). Such a methodology was developed in order to eliminate the problem of background signals due to non-faradaic (background) currents in methods such as cyclic voltammetry. Each step of the staircase ramps in square wave voltammetry (Figure 2.6) imposes two equal potential pulses that are opposite in direction but equal in height. Single potential cycle in SW consist of two of such potential pulses. For the case of a square wave voltammetry experiment, the potential cycle is applied for each step of the staircase ramp. The method provides an insight into the electrode mechanism as the electrode reaction is driven in both anodic and cathodic directions during single potential cycle. The duration of a single pulse, $t_p=t/2$, represent the critical time of the voltammetric experiment and the interpretation of the data can be carried out by also using the frequency of the potential modulation as: $f=1/t$ (Mirceski et al. 2013). The net current, i_{net}, is evaluated by taking the difference between the forward current and reverse current ($i_{for}-i_{rev}$) that is calculated at the end of each half cycle respectively. Such a subtraction further suppresses the non-Faradaic (background) current. The net current is centred on the redox potential and the peak height of net current has a linear relationship with the concentration of the electroactive species. The method offers direct detection limits as low as 10^{-8} M (Kounaves 1997). The method has couple advantages compare to others. One of them is its rejection to background currents, which becomes a problem in the case of cyclic voltammetry. In CV, both Faradaic and non-Faradaic currents are produced, and this leads to the difficulty of differentiating analytical peaks from background signal (Bard and Faulkner 1980). Square wave voltammetry was developed in order to overcome such difficulties and the voltage pulse technique results in an increase in the ratio of Faradaic current and non-Faradaic current, hence the sensitivity of measurement. Another advantage is the speed (Samuel et. al). Square wave voltammetry can be

adopted to perform an experiment much faster, at scan rates up to 1 V/sec or faster, compare to differential pulse techniques with typical scan rates of 1 to 10 mV/sec (Osteryoung & Osteryoung 1985). The areas that commonly adopt square wave voltammetry include: the study of electrode kinetics with regard to preceding, following or catalytic homogenous chemical reactions, decision of some species at trace levels and its adoption in HPLC with electrochemical detection (Kounaves 1997).
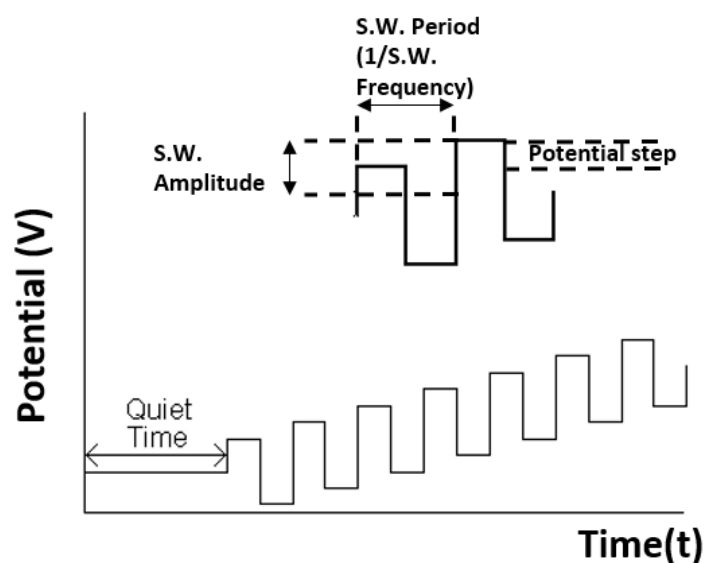
Figure 2. 6 Potential wave form for square wave voltammetry. The diagram is re-created from (Basi Electrochemistry 2020).

2.3. 5 Electrochemical impedance spectroscopy (EIS)

In Electrochemical Impedance Spectroscopy, a.c. potential (typically 5-10 mV) is adopted rather than dc signal, for stimulating the system. This is due to the richer information provided by ac signal which offers better characterisation of the system. The information is used to quantitatively identify the electrochemical reactions taking place at the sensor interface (Janata 2002; Lasia 2002; Barsoukov & Macdonald 2005; Orazem et al. 2006).

It is crucial to distinguish between two different types of EIS measurements: Faradaic (using redox markers) and non-Faradaic. Faradaic measurements employ equal concentration of a redox couple of reduced and oxidised forms inside measurement

solution. These redox markers result in Faradaic processes that leads to Faradaic currents in the system. The method monitors these currents hence evaluates the charge transfer resistance that is the electrostatic repulsion between the working electrode surface and the redox couple within the electrolyte solution. Such that the resistance of the system is a measure of how easily the redox markers can approach the electrode surface. On the other hand, for non-Faradaic measurements, the redox markers are eliminated. For such systems, the impedance of the system is dependent on the solution resistance and the charge distribution of ions in solution. The non-faradaic response is dominated mainly by the changes in double layer capacitance. In EIS, a small a.c. potential is applied to the system;

$$V(t) = V_o \sin(\omega t)$$ <div align="right">**Equation 2. 19**</div>

Where V_o is amplitude of voltage signal and ω is the angular frequency $(2\pi f)$. f is measured in Hertz. The resulting a.c. current response as a function of time is as followed;

$$I(t) = I_o \sin(\omega t - \theta)$$ <div align="right">**Equation 2. 20**</div>

Where I_o is the amplitude of current signal and θ is the system response phase shift. By adopting ohms law, the complex notation can be transferred into impedance form;

$$Z = \frac{V(t)}{I(t)} = \frac{V_0 \sin(\omega t)}{I_0 \sin(\omega t + \theta)} = Z_0 \frac{\sin(\omega t)}{\sin(\omega t + \theta)}$$ <div align="right">**Equation 2. 21**</div>

Hence, by using the following Euler's equation;

$$\exp(j\theta) = \cos\theta + j\sin\theta$$ <div align="right">**Equation 2. 22**</div>

Where j is the imaginary number. Equations 2.19 and 2.20 can be further expressed as a function of time as followed;

$$V(t) = V_o \exp(j\omega t)$$ <div align="right">**Equation 2. 23**</div>

$$I(t) = I_o \exp(j\omega t - j\theta)$$ <div align="right">**Equation 2. 24**</div>

Hence, the impedance can be expressed as a complex number by using Equations 2.22, 2.23 and 2.24 in Equation 2.25

$$Z = \frac{V(t)}{I(t)} = \frac{V_o \sin(\omega t)}{I_o \sin(\omega t + \theta)}$$

$$= Z_o \exp(j\theta) = Z_o (\cos\theta + j\sin\theta) = Z' + jZ''$$ **Equation 2. 25**

Where Z_0 is the amplitude of the impedance signal, Z' and Z'' are the real and imaginary parts of the impedance, respectively. In further explanation, the real part (Z') is the resistance of the circuit to the flow of current and Z'' is the ability of the circuit to store electrical energy. Such that these components of impedance reflect the resistive and capacitive components of the fabricated biosensor. The most common circuit that is adopted to best fit the description is Randles equivalent circuit which is composed of solution resistance R_s, the resistance to charge transfer R_{ct}, the double layer capacitance C_{dl}, and a Warburg impedance element W (Lisdat & Schäfer 2008).
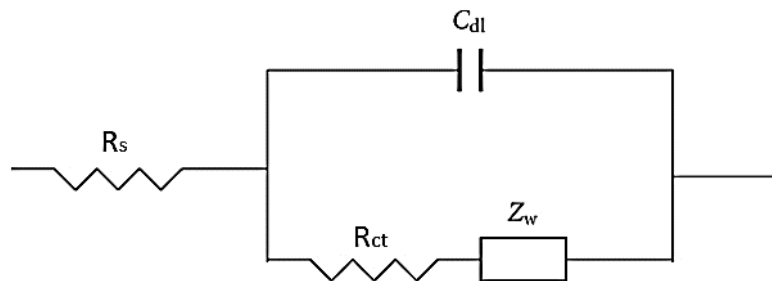
Figure 2. 7 The Randles' equivalent circuit representation for an electrode in contact with an electrolyte. The double-layer capacitance C_{dl} refers to the amount of charge stored in the double layer at the interface of electrode surface and the electrolyte. R_{ct} is the charge transfer resistance, R_s is the solution resistance and Z_W is the Warburg element (Lisdat & Schäfer 2008).

However, a slight modification was introduced on Randles equivalent circuit after several studies (Brug et al. 1984) (Hirschorn et al. 2010) have shown that replacing C_{dl}

with constant phase element (CPE), is a better representation of the distributed nature of the electrochemical double layer. The impedance of constant phase element (CPE) is now given by;

$$Z_{CPE} = Y_o(j\omega)^{-\alpha}$$ **Equation 2. 26**

Where ω is the frequency and Y_o is the magnitude of admittance where $\alpha \leq 1$.
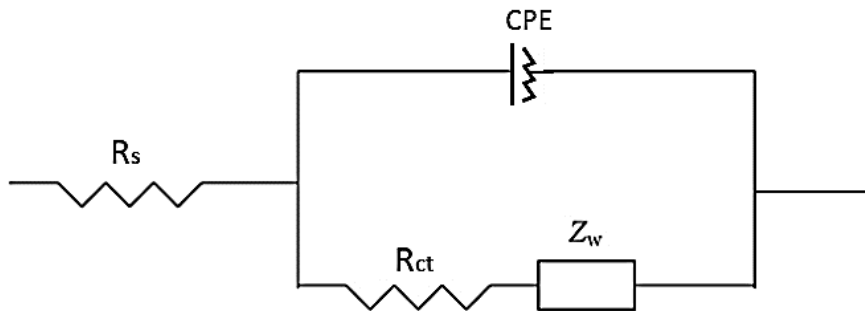
Figure 2. 8 Modified version of Randles equivalent circuit. CPE is the constant phase element, R_s is the solution resistance, R_{ct} is the charge transfer resistance and Z_w is the Warburg element.

Hence, and estimation for the replaced capacitor double layer can be done as followed;

$$C_{dl} = \frac{(Y_o R_{ct})^{1/\alpha}}{R_{ct}}$$ **Equation 2. 27**

In real EIS measurements, the Faradaic currents are affected by the diffusion processes. This factor is taken into account by the Warburg impedance, W, which is the impedance element due to diffusion of ions from bulk solution to electrode surface. This frequency dependent element only becomes predominant at lower frequencies with a phase angle of 45° in a diffusion controlled Faradaic process. Typical result from an electrochemical impedance spectroscopy is shown in Figure 2.9. The Nyquist plot given in the figure provides a way of comparing R_{ct} values, given by the diameter of the semicircle Z, calculated from each assay.
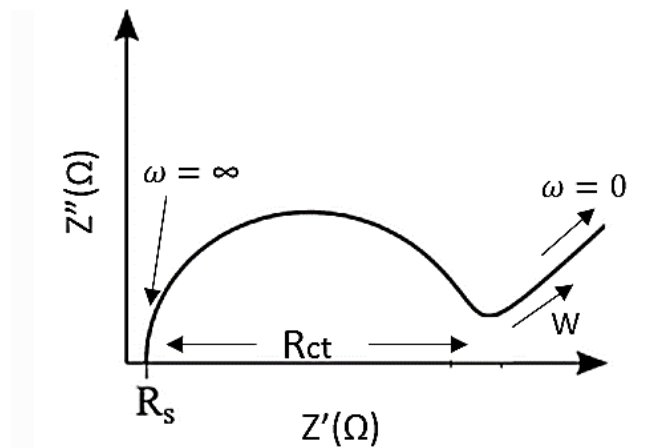
Figure 2. 9 Example Nyquist Plot of an EIS measurement (Lisdat & Schäfer 2008).

2.3.5. 1 Non-Faradaic EIS measurements

The main distinguishing factor of Faradaic and non-Faradaic impedance approaches is the absence of redox molecules. In such an approach the transduction occurs through variations in double layer capacitance (C_{dl}) rather than resistance of the system to charge flow (R_{ct}) (Daniels & Pourmand 2007; Tsouti et al. 2011). The capacitance arises as a result of immersing the electrode inside a solution and applying a certain potential. This will lead to the orientation of charged species and dipoles on the electrode interface which generate the double layer capacitance, a quantity that is physically measurable and quite sensitive to variations on the interface (Santos et al. 2014). According to literature, the common approach to evaluate capacitance is ignoring the contributions by R_{ct} and W and replacing an equivalent circuit that consists of a single resistor in series with a capacitor (Couniot et al. 2015).
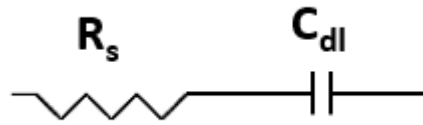
Figure 2. 10 Representative circuit for a non-faradaic measurement

As a result, the Equation 2.25 for the evaluation of impedance that was expressed earlier takes a new form;

$$Z = Z' + j\ Z'' \approx R_s^* - \ j\frac{1}{\omega C_{DL}^*}$$

$\qquad$ **Equation 2. 28**

In Equation 2.28, the real part of the capacitance can be expressed as followed;

$$C_{DL}^* = -\ \frac{1}{\omega Z''}$$

$\qquad$ **Equation 2. 29**

Second approach that is reported in literature is the evaluation of a complex capacitance (C^*) on using the impedance data (Jolly, Formisano, et al. 2015) (Jolly, Tamboli, et al. 2016);

$$C^* = -\ \frac{Z''}{\omega|Z|^2} - j\frac{Z'}{\omega|Z|^2} = C' + jC''$$

$\qquad$ **Equation 2. 30**

Hence, in such an approach the real (C') and imaginary (C'') components of capacitance are evaluated on using impedance values of Z' and Z''. This is better represented by a Cole-Cole plot that is given in Figure 2.11 where the Nyquist plot for an electroactive peptide-SAM that is immobilised on gold electrode at its half-wave potential is used to evaluate the capacitive response of the system. The diameter of the semicircle in capacitance graph gives an estimate for the capacitance of the system.
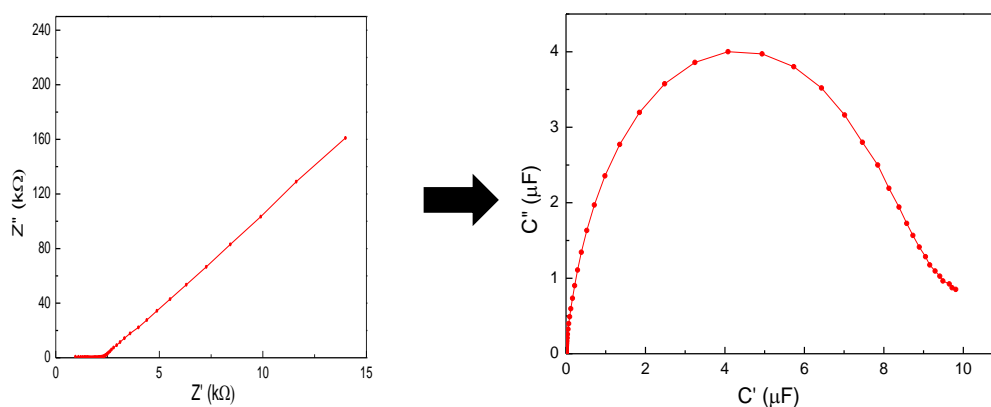
Figure 2. 11 Nyquist impedimetric plot (left) of Z" versus Z' for electroactive peptide-SAM immobilised on gold electrode surface at electrode potential corresponding to half-wave potential. The analogous capacitive response of Z" versus Z' (right).

2. 4 Other techniques

Apart from all the electrochemical techniques that were explained earlier, surface plasmon resonance and UV-spectrophotometry were adopted during the development of specific biosensor methodologies in this thesis.

2.4. 1 Surface plasmon resonance (SPR)

Since the development of the first surface plasmon based biosensor in 1983 (Prabowo et al. 2018), the use of the technique increased rapidly. There is an underlying physical explanation for the functioning of SPR (Merwe 2002; Formisano 2016). When a beam of light passes from a medium/material with a higher refractive index (e.g. glass prism) into a medium/material with lower refractive index (e.g. water) some light is reflected from the interface. The light is completely reflected only when the angle of strike of the light onto interface (angle of incidence, Θ) is bigger than the critical angle (Θ_c).
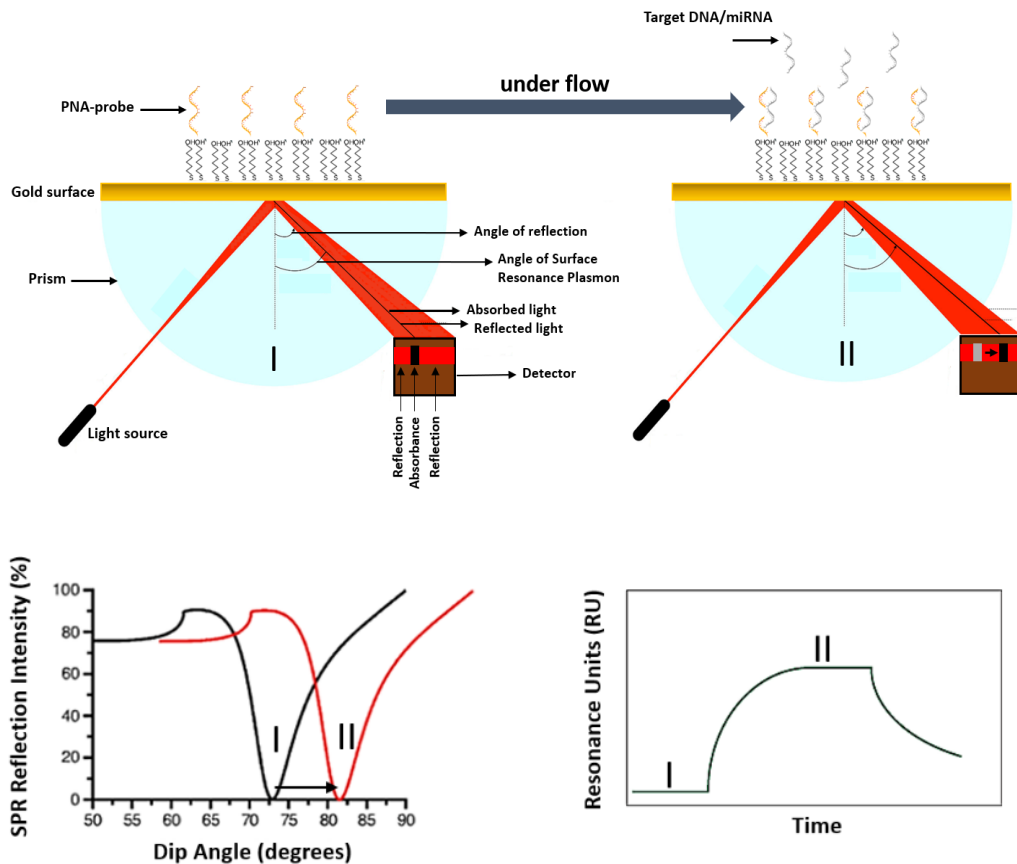
Figure 2. 12 Schematics for Surface Plasmon Resonance (SPR). A dark line in the reflected beam (on detector) results from the excitation of the surface plasmons at certain angle of light. Upon molecular binding events (DNA/miRNA binding) there is a shift of the angular positioning of this dark line and the dark line can be monitored as a dip in the SPR reflection intensity. The shift on the position of the dip represents the molecular binding event or a conformational change in the molecules near surface. The diagram is re-created from (Jolly 2016).

However, when the glass surface is covered with a thin film of a noble metal such as gold, some of the light is lost into metal and the reflection is not observed to be total. This lost is observed to be greatest at a second angle that is greater than critical angle and at which the reflected angle intensity reaches to minimum. Now this angle is

referred as the surface plasmon resonance angle Θ_{spr} that results from the oscillation of mobile electrons at the surface of the metal film (e.g. gold). When wave vector of the incident wave matches the metal plasmons (mobile electrons), it results in the resonance of the plasmons. In such a condition, the energy of the photons is transferred to plasmons. This resonance is also referred as surface plasmon resonance. As a result, the coupling of the incident wave to the oscillating electron (plasma) on the surface leads to energy loss and a drop on the intensity of reflected light. The wave that penetrates into metal (evanescent wave) decays exponentially in the perpendicular to the metal surface into the medium. The depth of the evanescent wave from the sensor surface is within 300 nm depending on the thickness of the gold film and the refractive index of the medium above the metal surface (Merwe 2002). The method of SPR excites and detects collective oscillations of surface plasmons (free electrons) via Kretschemann configuration (Figure 2.12), where light is focused onto a metal film through a glass prism and the resulting reflection is detected. The dark band line in the reflected beam (Figure 2.12, Detector) is created by the absorption of light at the certain incident angle where plasmons are set to resonate with light. The dark band line is observed as a dip in the SPR reflection intensity and a shift in the reflection of the dark band line corresponds to a molecular binding to the gold film. The molecular binding events are studied commonly by monitoring this shift versus time graphs (Szabo et al. 1995; Mcdonnell 2001; Karlsson 2004).

2.4. 2 Ultra violet (UV) spectrophotometry

Ultraviolet-visible spectroscopy is an important tool for the qualitative analysis and identification of chemicals in analytical chemistry. Its main use is considered as quantitative determination of different organic and inorganic compounds in solution (Ferree et al. 2001; Albalasmeh et al. 2013). Similar to SPR, spectroscopy is related to the interaction of light with matter. Upon absorption of light by matter, the energy content of atoms/molecules increases and UV absorption by a chemical compound will display a distinct spectrum.

UV spectrophotometer principle follows the Beer-Lambert Law that states that when a beam of monochromic light is passed through a solution with absorbing species, the

reducing rate of radiation intensity along with the thickness of the absorbing solution is proportional to the concentration of the solution and the incident rate (Swineharf 1962):

$$A = \log_{10} \frac{P_0}{P} = abc$$ **Equation 2. 31**

Where A is the absorbance, P_o refers to the intensity of light upon a sample cell, P refers to the intensity of light upon leaving the sample cell, a refers to the molar absorptivity, b refers to the length of the sample cell, c refers to the concentration of the solute.
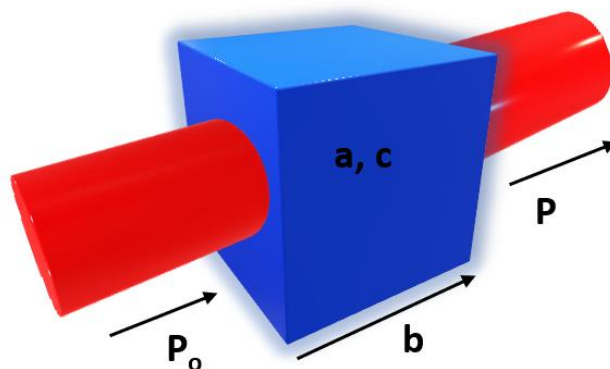
Figure 2. 13 Beer-Lambert Law. Principle of Beer-Lambert Law that relates the concentration of the sample to the passed light path length (Swineharf 1962).

The concept and principle of UV spectrophotometer has many applications and one that is most common is the identification of unknown compounds. This is normally carried out by comparing the resulting spectrum with a reference compound for observing if the spectrums coincide hence the compound is successfully identified. UV spectrophotometry in this thesis has been employed for the identification of nucleic acids and proteins inside a solution. It was used as a validation technique to confirm the existence of the nucleic acids inside the solution by comparing the wavelengths for the absorbance peaks to ones reported in literature (Tinoco et al. 1980; Aitken & Learmonth 2009).

References

Aitken, A. & Learmonth, M.P., 2009. Protein determination by UV absorption. In J. M. Walker, ed. *The Protein Protocols Handbook*. Humana Press, Totowa, NJ, pp. 3–6.

Albalasmeh, A.A., Berhe, A.A. & Ghezzehei, T.A., 2013. A new method for rapid determination of carbohydrate and total carbon concentrations using UV spectrophotometry. *Carbohydrate Polymers*, 97(2), pp.253–261.

Andrade, C.A.S. et al., 2011. Biosensors for detection of low-density lipoprotein and its modified forms. In P. A. Serra, ed. *Biosensors for Health, Environment and Biosecurity*. pp. 215–240.

Bain, C.D. et al., 1989. Formation of monolayer films by the spontaneous assembly of organic thiols from solution onto gold. *Journal of the American Chemical Society*, 111(1), pp.321–335.

Bain, C.D. & Whitesides, G.M., 1989. Formation of monolayers by the coadsorption of thiols on gold : variation in the length of the alkyl chain. *American Chemical Society*, 111(18), pp.7164–7175.

Bard, A.J. & Faulkner, L.R., 1980. *Electrochemical methods - fundamentals and applications*, John Wiley & Sons:USA.

Bard, A.J. & Faulkner, L.R., 2001. *Electrochemical methods: fundamentals and applications* 2nd Ed., John Wiley & Sons:USA.

Barker, G.C. & Gardner, A.W., 1992. Forty years of square-wave polarography. *Analyst*, 117, pp.1811–1828.

Barker, G.C. & Jenkins, I.L., 1952. Square wave polarography. *Analyst*, 77, pp.685–696.

Barsoukov, E. & Macdonald, J.R., 2005. *Impedance spectroscopy: theory, experiment, and applications* 2nd ed., John Wiley & Sons.

Basi Electrochemistry, 2020. Pulse Voltammetric Techniques. Available at: https://www.basinc.com [Accessed March 30, 2020].

Bertok, T. et al., 2013. Label-free detection of glycoproteins by the lectin biosensor down to attomolar level using gold nanoparticles. *Talanta*, 108, pp.11–18.

Bockris, J.O., Devanathan, M.A.V. & Müller, K., 1963. On the structure of charged interfaces. *Proceedings of the Royal Society of London. Series A. Mathematical and Physical Sciences*, 274(1356), pp.55–79.

Brug, G.J. et al., 1984. The analysis of electrode impedances complicated by the presence of a constant phase element. *Journal of Electroanalytical Chemistry and Interfacial Electrochemistry*, 176(1-2), pp.275–295.

Camillone, N. et al., 1994. New monolayer phases of n -alkane thiols self-assembled on Au (111): preparation , surface characterization , and imaging. *The Journal of Chemical Physics*, 101(12), pp.11031–11036.

Campuzano, S. et al., 2006. Characterization of alkanethiol-self-assembled monolayers-modified gold electrodes by electrochemical impedance spectroscopy. *Journal of Electroanalytical Chemistry*, 586, pp.112–121.

Chapman, D.L., 1913. A contribution to the theory of electrocapillarity. *Philosophical Magazine*, 25, pp.475–481.

Couniot, N. et al., 2015. Capacitive biosensing of bacterial cells : analytical model and numerical simulations. *Sensors & Actuators B: Chemical*, 211, pp.428–438.

Daniels, J.S. & Pourmand, N., 2007. Label-Free Impedance Biosensors:

Opportunities and Challenges. *Electroanalysis*, 19(12), pp.1239–1257.

Du, M. et al., 2012. Chemical Electrochemical logic aptasensor based on graphene. *Sensors & Actuators B: Chemical*, 169, pp.255–260.

Fang, A., Ng, H.T. & Li, S.F.Y., 2003. A high-performance glucose biosensor based on monomolecular layer of glucose oxidase covalently immobilised on indium-tin oxide surface. *Biosensors and Bioelectronics*, 19, pp.43–49.

Ferree, M.A. et al., 2001. Evaluation of a second derivative UV/visible spectroscopy technique for nitrate and total nitrogen analysis of wastewater samples. *Water Research*, 35(1), pp.1–6.

Fischer, M.J.E., 2010. Amine coupling through EDC/NHS: a practical approach. In N. J. de Mol & M. J. E. Fischer, eds. *Surface plasmon resonance: methods and protocols*. Humana Press, pp. 55–75.

Formisano, N., 2016. *A study on the optimisation of electrochemical impedance spectroscopy biosensors (Published doctoral dissertation)*. University of Bath.

Gao, N. et al., 2015. General strategy for biodetection in high ionic strength solutions using transistor-based nanoelectronic sensors. *Nano Letters*, 15, p.2143−2148.

Gouy, M., 1910. Sur la constitution de la charge électrique à la surface d'un électrolyte. *Journal of Theoretical and Applied Physics*, 9(1), pp.457–468.

Grieshaber, D. et al., 2008. Electrochemical Biosensors - Principles and Applications. *Sensors*, 8, pp.1400–1458.

Hammond, J.L., 2017. *Micro- and nanogap based biosensors (Published doctoral dissertation)*. University of Bath.

Helmholtz, H., 1879. Studien über electrische Grenzschichten. *Annalen der physik*, 7, p.337.

Herne, T.M. & Tarlov, M.J., 1997. Characterization of DNA Probes Immobilized on Gold Surfaces. *American Chemical Society*, 119, pp.8916–8920.

Hirschorn, B. et al., 2010. Determination of effective capacitance and film thickness from constant-phase-element parameters. *Electrochimica Acta*, 55(21), pp.6218–6227.

Hong, H.S., Kim, S.J. & Lee, K.S., 1999. Long-term oxidation characteristics of oxygen-added modified Zircaloy-4 in 360 ° C water. *Journal of Nuclear Materials*, 273, pp.177–181.

Janata, J., 2002. Electrochemical sensors and their impedances : a tutorial. *Critical Reviews in Analytical Chemistry*, 32(2), pp.109–120.

Jang, H. et al., 2015. Electrical signaling of enzyme-linked immunosorbent assays with an ion-sensitive fi eld-effect transistor. *Biosensors and Bioelectronics*, 64, pp.318–323.

Jolly, P. et al., 2016. Aptamer – MIP hybrid receptor for highly sensitive electrochemical detection of prostate specific antigen. *Biosensors and Bioelectronic*, 75, pp.188–195.

Jolly, P. et al., 2015. Chemical Label-free impedimetric aptasensor with antifouling surface chemistry : A prostate specific antigen case study. *Sensors and Actuators B : Chemical*, 209, pp.306–312.

Jolly, P. et al., 2017. Nucleic acid-based aptasensors for cancer diagnostics: an insight into immobilisation strategies. In P. Chandra, Y. N. Tan, & S. P. Singh, eds. *Next Generation Point-of-care Biomedical Sensors Technologies for Cancer Diagnosis*. pp. 205–231.

Jolly, P., 2016. *Oligonucleotide-based biosensors for the detection of prostate cancer*

biomarkers (Published doctoral dissertation). University of Bath , UK.

Jolly, P., Formisano, N. & Estrela, P., 2019. DNA aptamer-based detection of prostate cancer. *Chemical Papers*, 69(1), pp.77–89.

Karlsson, R., 2004. SPR for molecular interaction analysis : a review of emerging application areas. *Journal of Molecular Recognition*, 17, pp.151–161.

Keighley, S.D. et al., 2008. Optimization of DNA immobilization on gold electrodes for label-free detection by electrochemical impedance spectroscopy. *Biosensors and Bioelectronics*, 23, pp.1291–1297.

Kounaves, S.P., 1997. Voltammetric Techniques. In F. A. Settle, ed. *Handbook of Instrumental Techniques for Analytical Chemistry*. Prentice Hall PTR, Upper Saddle River, New Jersey, pp. 709–725.

Lasia, A., 2002. Electrochemical Impedance Spectroscopy and its Applications. In B. E. Conway, J. Bockris, & R. E. White, eds. *Modern Aspects of Electrochemistry*. Springer US, pp. 143–248.

Laurent, N. et al., 2008. Enzymatic glycosylation of peptide arrays on gold surfaces. *ChemBioChem*, 9, pp.883–887.

Li, Y. et al., 2012. Simple and sensitive aptasensor based on quantum dot-coated silica nanospheres and the gold screen-printed electrode. *Talanta*, 99, pp.637–642.

Lisdat, F. & Schäfer, D., 2008. The use of electrochemical impedance spectroscopy for biosensing. *Analytical and Bioanalytical Chemistry*, 391, pp.1555–1567.

Love, J.C. et al., 2005. Self-assembled monolayers of thiolates on metals as a form of nanotechnology. *Chemical Reviews*, 105, pp.1103–1169.

Luppa, P.B., Sokoll, L.J. & Chan, D.W., 2001. Immunosensors — principles and applications to clinical chemistry. *Clinica Chimica Acta*, 314, pp.1–26.

Ma, W. et al., 2013. Femtogram ultrasensitive aptasensor for the detection of Ochratoxin A. *Biosensors and Bioelectronics*, 42, pp.545–549.

Madaboosi, N. et al., 2015. A microfluidic immunoassay platform for the detection of free prostate specific antigen : a systematic and quantitative approach. *Analyst*, 140, pp.4423–4433.

Mcdonnell, J.M., 2001. Surface plasmon resonance: towards an understanding of the mechanisms of biological molecular recognition. *Current Opinion in Chemical Biology*, 5, pp.572–577.

Merwe, P.A. Van Der, 2002. Surface Plasmon Resonance. In S. E. Harding & B. Z. Chowdhry, eds. *Protein-Ligand Interactions: Hydrodynamics and Calorimetry*. Oxford University Press, pp. 137–170.

Mirceski, V. et al., 2013. Square-wave voltammetry : a review on the recent progress. *Electroanalysis*, 25(11), pp.2411–2422.

Nishizawa, M., Sunagawa, T. & Yoneyama, H., 1997. Underpotential deposition of copper on gold electrodes through self-assembled monolayers of propanethiol. *Langmuir*, 13, pp.5215–5217.

Orazem, M.E., Pébère, N. & Tribollet, B., 2006. Enhanced graphical representation of electrochemical impedance data. *Journal of the Electrochemical Society*, 153(4), pp.129–136.

Oschatz, M. et al., 2016. Interactions between electrolytes and carbon-based materials — NMR studies on electrical double-layer capacitors , lithium-ion batteries , and fuel cells. In *Annual Reports on NMR Spectroscopy*. Academic Press, pp. 237–318.

Osteryoung, J.G. & Osteryoung, R.A., 1985. Square wave voltammetry. *Analytical Chemistry*, 57(1).

Prabhakar, N. et al., 2007. DNA entrapped polypyrrole – polyvinyl sulfonate film for application to electrochemical biosensor. *Analytical Biochemistry*, 366, pp.71–79.

Prabowo, B.A., Purwidyantri, A. & Liu, K.-C., 2018. Surface plasmon resonance optical sensor : a review on light source technology. *Biosensors*, 8(80), pp.1–27.

Ramaley, L. & Krause, M.S., 1969. Theory of square wave voltammetry. *Analytical Chemistry*, 41(11), pp.1362–1365.

Sam, S. et al., 2010. Semiquantitative study of the EDC/NHS activation of acid terminal groups at modified porous silicon surfaces. *Langmuir*, 26(2), pp.809–814.

Santos, A. et al., 2015. Redox-tagged peptide for capacitive diagnostic assays. *Biosensors and Bioelectronics*, 68, pp.281–287.

Santos, A., Davis, J.J. & Bueno, P.R., 2014. Fundamentals and applications of impedimetric and redox capacitive biosensors. *Journal of Analytical & Bioanalytical Techniques*, S7.

Stern, O.Z., 1924. Zur Theorie der Elektrolytischen Doppelschicht. *Zeitschrift fur Elektrochemie*, 30, pp.508–516.

Swineharf, D.F., 1962. The Beer-Lambert Law. *American Chemical Society*, 39(7), pp.333–335.

Szabo, A., Stolz, L. & Granzow, R., 1995. Surface plasmon resonance and its use in biomolecular interaction analysis (BIA). *Current Opinion in Structural Biology*, 5, pp.699–705.

Thévenot, D.R. et al., 2001. Electrochemical biosensors : recommended definitions and classification. *Analytical Letters*, 34(5), pp.635–659.

Tinoco, I., Bustamante, J. and C. & Maestre, M.F., 1980. The optical activity of nucleic acids And their aggregates. *Annual Review of Biophysics and Bioengineering*, 9, pp.107–41.

Tsouti, V. et al., 2011. Capacitive microsystems for biological sensing. *Biosensors and Bioelectronics*, 27(1), pp.1–11.

Ulman, A., 1996. Formation and structure of self-assembled monolayers. *Chemical Reviews*, 96, pp.1533–1554.

Wu, J. et al., 2010. Ternary surface monolayers for ultrasensitive (zeptomole) amperometric detection of nucleic acid hybridization without signal amplification. *Analytical Chemistry*, 82, pp.8830–8837.

Zhang, K. et al., 2013. A new strategy based on aptasensor to time-resolved fluorescence assay for adenosine deaminase activity. *Biosensors and Bioelectronics*, 41, pp.123–128.

Zhu, Y., Chandra, P. & Shim, Y., 2013. Ultrasensitive and selective electrochemical diagnosis of breast cancer based on a hydrazine − Au nanoparticle − aptamer bioconjugate. *Analytical chemistry*, 85, p.1058−1064.

Chapter 3 Direct and sensitive electrochemical detection of miR-21-5p as circulating biomarker for pancreatic cancer

In this chapter, the development of a highly sensitive electrochemical detection platform for miRNA sensing is presented. If a certain miRNA is detected in blood, it can act as a fingerprint for cancer or many other diseases. The platform was developed by the adoption of Peptide Nucleic Acids (PNA) as the capture probe on a gold electrode surface. The main focus was to inspect the role of total probe to thiol ratio on a gold electrode surface for advancing the existing limit of detection, with no additional labelling steps. Initially, a controlled fabrication strategy was adopted for the detection of target DNA which is less vulnerable to RNAse degradation compared to miRNA. Hence, after optimisation of the probe for DNA detection, the strategy can be easily adapted for miRNA detection. Electrochemical impedance spectroscopy was used to monitor the changes in charge transfer resistance on the electrode surface due to binding activities of target miRNAs. The optimisation studies presented in this chapter include: electrochemical impedance spectroscopy measurements upon designing a DNA-equivalent of the PNA-probe for the approval of the better performance of PNA-probes, detection of long target DNA, specific to the human pathogen C.difficile, by using PNA-probes, re-adjusting the design of PNA-probes for direct and sensitive detection of short miRNA sequences.

3. 1 Background

Early detection is a core module for the control of the spread of cancer and improves the chances of survival. Being discovered in *C. Elegans* in 1993 and soon after in all living organisms (Ferracin et al. 2011), microRNAs (miRNAs) are a class of 19-24 nucleotide-long non-coding RNAs (Ambros 2004; Bartel 2004; Iorio & Croce 2011) which regulate the expression of nearly one third of all human genes. It was only in the last decade that significant evidence emerged showing that miRNAs are involved in the pathogenesis of cancer (Ramaswamy et al. 2001; He et al. 2005; Lu et al. 2005) and became an area of interest for oncology research. A few examples include the up-regulation of miR-155 and miR-21, and down-regulation of miR-91 in breast cancer, the up-regulation of miR-17-3p and miR-92 in patients with colorectal cancer (CRC) (Ng et al. 2009), or the down-regulation of miR-145 in several cancer types (blood cancer, colon cancer, breast and ovarian cancer, prostate cancer) (Esquela-kerscher & Slack 2006; Akao et al. 2007; Ichimi et al. 2009; Spizzo et al. 2013; Dahiya & Morin 2010).

This study will be addressing the detection of circulating miR-21-5p, a pancreatic cancer biomarker (Wang et al. 2013; Matsuzaki & Ochiya 2017; Qu et al. 2017), as a non-invasive biomarker for the early detection of the disease. The early diagnosis of pancreatic cancer is difficult and currently no protein biomarkers in blood can be used to identify the disease in its early stages. The disease usually becomes fatal within months of diagnosis. Hence, the exploration of detection techniques for early diagnosis of the disease will greatly benefit patients with pancreatic cancer.

Most techniques are restricted to central laboratories, some of these being powerful but complex. There is still the need for portable, simple and sensitive techniques to quantify levels of miRNAs inexpensively. Therefore, this study adopts electrochemical approaches for the development of a point-of-care detection. Electrochemical biosensors come with various advantages, such as specificity, portability, and low cost (Wang 2006). Previous studies have shown that miRNA detection down to femtomolar (fM, 10^{-5} M) levels could be achieved by adopting amplification steps such as use of nanoparticles (Jolly et al. 2016; Peng & Gao 2011)

and enzymes (Ren et al. 2013). However, such steps lack simplicity and this work focuses on eliminating any additional steps, and achieving low limits of detection by direct measurements.

It is reported in the literature that the accurate control of PNA (or DNA) probe density on gold electrodes could be achieved by the immobilisation of thiol-modified PNA (or DNA) with a thiol spacer (Keighley et al. 2008). Using this approach, a 385-fold change in R_{ct} was achieved upon hybridisation using electrochemical impedance spectroscopy (EIS). Hence this technique can be adopted in order to optimise the sensitivity of the assay. In this chapter we will be carrying out a detailed EIS-based study of various ratios of thiol-modified PNA to mercaptohexanol (MCH) on gold electrodes in order to identify the optimised ratio for the best hybridisation efficiency. Optimisation of the probe density is a crucial step prior to taking any further steps towards fabrication.

3. 2 Materials and methods

3.2. 1 Apparatus

The EIS experiments were carried out with PalmSense4 compact potentiostats (PalmSense, Netherlands) and a three-electrode cell system: an Ag/AgCl (KCl) reference electrode (BASi, USA) connected via a salt bridge filled with 10 mM of phosphate buffer (pH 7.3), a Pt counter electrode (ALS, Japan), and a gold working electrode (2.0 mm diameter from CH Instruments, USA).

The Faradaic EIS with PNA probe was conducted in 10 mM PB (pH 7.3) measurement buffer containing 10 mM of the ferro/ferrocyanide ($[Fe(CN)_6]$)$^{3-/4-}$ redox couple over a frequency range from 100 kHz to 100 mHz, with a 10 mV ac.voltage superimposed on a dc bias voltage of 0.2 V (formal potential of the redox couple) vs. Ag/AgCl. The Faradaic EIS with DNA probe was conducted in a buffer with a higher ionic strength, which is necessary for the screening of the negative charges of DNA (Keighley et al. 2008). As a result, the 10 mM PB buffer that was used for the EIS measurements with the PNA-probe was replaced with 50 mM PB containing 100 mM K_2SO_4 (pH 7.0) for the case of DNA-probe.

3.2. 2 Oligonucleotides

High performance liquid chromatography (HPLC) purified PNA probe sequences were purchased from Cambridge Research Biochemicals, UK, in lyophilised form, while synthetic oligonucleotide sequences were purchased from Sigma Aldrich, UK. The PNA and DNA probe sequences, listed in the first two rows in Table 3.1, were used for the probe optimisation studies presented in section 3.3.1 for the detection of long pathogenic DNA specific to the C.difficile bacteria (Joshi et al. 2014). The PNA probe sequence in the fourth row is complementary to the miRNA-21-5p sequence given in the fifth row. MiRNA-21-5p is specific to pancreatic cancer (Qu et al. 2017). The non-specific miRNA sequence in the final row of Table 3.1 was adopted for the control studies.

Table 3. 1 List of PNA probes, target DNA and miRNA sequences used in this work. AEEA is a glycol linker of nine atoms (8-amino-3, 6-dioxaoctanoic acid).

PNA probe 1 (fully complementary to DNA target 1)	SH-C6-AEEA TTT TTT TTA ATA CTA ACA CTG C
DNA probe 1 (fully complementary to DNA target 1)	5'-SH-C6-TTT TTT TTA ATA CTA ACA CTG C-3'
DNA target 1 (complementary to PNA probe 1 & DNA probe 1)	3'-AAA TTA TGA TTG TGA CGT AAT CCC AAT ACA ACG TCA ATG ACC TAC CGT T -5'
PNA probe 2 (fully complementary to miR-21-5p)	SH-C6-AEEA TTT TCA ACA TCA GTC TGA TAA GCT A
miR-21-5p sequence (fully complementary to PNA probe 2)	3'-AGU UGU AGU CAG ACU AUU CGA U-5'
Non-specific miRNA	3'-AGU UGU ACC AGA UAU CCG UAA A-5'

As compared to the C6 linker, when a C6-AEEA linker is adopted in PNA probes a significant reduction in the non-specific interactions is observed (Jolly et al. 2016). Such a property of the PEG-like linker (C6-AEEA) is due to the creation of a hydration layer because of the presence of the AEEA. Each PEG ether group is capable of H-binding to two water molecules creating a strong hydration shell (Wang & Kreuzer 1997). Hence, proteins and other charged molecules are prevented from penetrating the hydration layer and being adsorbed onto the surface (Jolly et al. 2016).

3.2. 3 Biosensor fabrication

The gold working electrodes were first mechanically polished for 2 minutes with 1 µM diamond solution (Buehler, USA) on a polishing pad (BASi, USA). This was followed by mechanical polishing using alumina slurry with decreasing particle sizes (starting with 1 µm, then 0.3 µm and finishing with 0.05 µm). Polishing was carried out for at least 2 minutes with each particle size. In between each polishing step, 5 minutes sonication in ethanol and rinsing in Milli-Q water were performed to remove any residues. After the final polishing, 10 minutes of sonication in ethanol followed by 10 minutes in Milli-Q water was carried out. Electrodes were then rinsed with Milli-Q water and electrochemically cleaned in 0.5 M H_2SO_4 (Sigma, Aldrich) by scanning the potential between the oxidation and reduction of gold, 0 V and +1.5 V vs. an Ag/AgCl reference electrode, for 50 cycles until the voltammogram graphs showed no further changes. Finally, the electrodes were rinsed with Milli-Q water and dry cleaned with a nitrogen gun.

The PNA probe fabrication was carried out by co-immobilisation of clean electrodes with the thiolated ssPNA probe sequence and 6-mercapto-1-hexanol (MCH, Sigma-Aldrich, UK) in 50% dimethyl sulfoxide (DMSO, Sigma-Aldrich, UK), 50% ultra-pure water (v/v) immobilisation solution for 16 h in a humidity chamber. The initial concentration of MCH (10 mM) was prepared in Ethanol (BioUltra for molecular biology, ≥99.8%, Sigma-Aldrich, UK) and diluted to the required concentration in the immobilisation buffer for the preparation of a range of molar ratios of ssPNA and MCH. All electrodes were prepared with 1 µM thiol modified PNA and with varying molar ratios of MCH (e.g. 1:4 molar ratio of PNA:MCH refers to 1 µM thiol modified

PNA + 4 µM MCH prepared in the same immobilisation solution). Each electrode was incubated in 100 µL of the immobilisation solution for 16 h at 4° C. A minimum of three electrode samples were prepared at each PNA:MCH mole fraction. After immobilisation, the electrodes were rinsed with excess Milli-Q water to remove any unattached thiols and were backfilled with 1 mM MCH at room temperature for one hour, in order to ensure complete thiol coverage. The electrodes were then rinsed with excess Milli-Q water and placed in the measurement buffer for 2 hours to stabilise the SAM.

The DNA probe fabrication was carried out by following the optimised protocol in literature (Keighley et al. 2008) which requires the co-immobilisation of clean electrodes with the thiolated ssDNA probe sequence and 6-mercapto-1-hexanol (MCH, Sigma-Aldrich, UK) in 0.8 M phosphate buffer (PB) + 1.0 M NaCl + 5 mM $MgCl_2$+ 1 mM ethylene diamine tetraacetic acid (EDTA), pH 7.0. The DNA charge is screened by the high ionic strength and Mg^{+2} ions which also allows high probe densities. All electrodes were prepared with 1 µM thiol modified DNA with varying molar ratios of MCH. A minimum of three electrode samples were prepared at each DNA:MCH mole fraction. Following the immobilisation, electrodes were sequentially rinsed with: immobilisation buffer, 200 mM PB, 10 mM PB and finally 10 mM PB + 10 mM EDTA to remove any remaining Mg^{2+}. The electrodes were then backfilled with 1 mM MCH for one hour in order to ensure complete thiol coverage. The electrodes were then rinsed with excess Milli-Q water and placed in the measurement buffer for 2 hours to stabilise the SAM.

3. 3 Results and discussion

3.3. 1 PNA-probe vs. DNA-probe studies using EIS technique

Initially, the better performance of the PNA-probes compared to DNA-probes was investigated for the detection of the target DNA. This is mainly because of the crucial need to develop an initial controlled fabrication strategy for the detection probe. As DNA is more stable compared to target miRNA, which has a higher vulnerability to RNase degradation (Qian et al. 2017), target DNA was adopted for the optimisation

studies. The DNA sequence that is specific to the human pathogen C.difficile that causes antibiotic associated diarrhoea in humans was selected (Joshi et al. 2014) for its potential application for clinical diagnosis. Electrochemical impedance spectroscopy measurements were carried out for the detection of the DNA sequence. The strategy was in turn adapted for the detection of the miRNA target in upcoming sections.

(a)
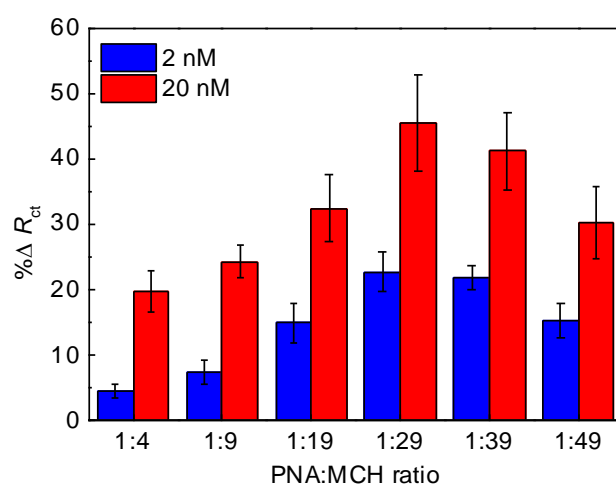
(b)
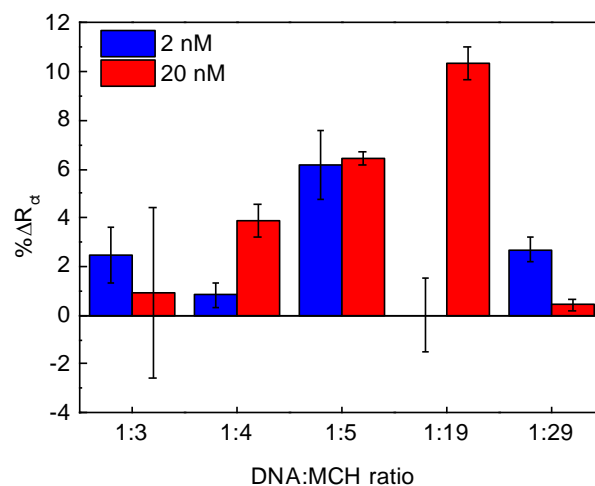
Figure 3. 1. Percentage variations of R_{ct} upon hybridisation with target DNA that is specific to the human pathogen C.difficile. Measurements were carried out with various ratios of (a) probe PNA to MCH and (b) probe DNA to MCH on the electrode surface, after incubation with 2 nM and 20 nM concentrations of complementary target

DNA. All EIS measurements with PNA-probes were carried out in 10 mM PB (pH 7.3) containing 10 mM of the ferro/ferrocyanide ($[Fe(CN)_6]$)$^{3-/4-}$. 10 mM PB buffer was replaced with 50 mM PB containing 100 mM K_2SO_4 (pH 7.0) for all DNA-probe measurements. The error bars represent the standard deviation between the three separate electrodes.

The % variation of R_{ct} shown in Figure 3.1 (a) increases significantly upon hybridisation as the ratio of PNA to MCH functionalised on the surface is reduced gradually from 1:4 to 1:29. However, further decreases in the PNA density at the surface results in a decreasing %R_{ct} upon hybridisation. The highest value of %ΔR_{ct}, hence the best hybridisation, was observed when a fraction of 0.03 (1:29 ratio) PNA to spacer molecule MCH was adopted on the surface. The further reduction of this ratio results in reduced hybridisation, this is due to the reduced amount of probe (ssPNA) on the surface, resulting in insufficient capture of the target. On the other hand, at ratios higher than 1:29 (e.g. 1:4), steric hindrance reduces the hybridisation efficiency with the target (Keighley et al. 2008). Another limiting factor at higher ratios could be the large initial R_{ct} that is significantly high compared to the overall %R_{ct} variation upon hybridisation.

The % variation of R_{ct} for the DNA-probe in Figure 3.1 (b), on the other hand, remained significantly lower upon incubation with the target DNA, and the results did not display consistency. The most consistent stabilisation and increase of surface charge transfer resistance after hybridisation was observed with electrodes immobilised with a DNA:MCH ratio of 1:5. Even then the %Rct variation upon incubation with 20 nM DNA, remained significantly low (6.4% ± 0.28). Hence our results suggested a better performance of the PNA probes for detection of DNA, with 7-times the hybridisation efficiency when compared to DNA probes. The strategy of using PNA-probes for DNA detection was re-investigated by using quartz crystal microbalance with dissipation (QCM-D) and field-effect transistor-based biosensor (Bio-FET) for proof of detection on different platforms (Appendix II & III).

3.3. 2 Investigation of miRNA detection using EIS technique

Following the justification of the success of PNA probes for DNA detection, the same strategy was adopted for the fabrication of the PNA-probe for the recognition of miR-21-5p. Faradaic mode EIS was adopted for the evaluation of the stability of the fabricated probe, its specificity, and target binding steps. The measurements were performed in 10 mM of $[Fe(CN)_6]^{-3/4-}$ the redox couple, to monitor the resistance to charge transfer upon target binding events. Initially the PNA biosensor was measured for its stability in a 10 mM PB (pH 7.3) buffer containing 10 mM of the ferro/ferrocyanide $([Fe(CN)_6])^{3-/4-}$ redox couple (Figure 3.2 a, red curve). Three rounds of incubations, each for 30 minutes, were carried out. An %R_{ct} variation that was less than 5% confirmed the stability of the PNA-probe. Finally, the PNA-probe was tested for its non-specific binding upon incubation in 10 mM PB (pH 7.3) which contained non-specific miRNA (Figure 3.2 a, blue curve). The results given in Figure 3.2 (a) indicate a negligible change in the R_{ct} of the platform upon incubation in blank buffer, as well as when the probe was exposed to 1 nM of non-specific miRNA sequences, which resulted in a 0.71% variation in R_{ct} (535.6 Ω → 539.2 Ω). After the successful evaluation of the system with non-specific interactions, the developed platform was tested for its binding efficiency to target miRNA (Figure 3.2 (b)). The probe surface was initially incubated with 10 nM of fully-complementary miRNA sequences. This has resulted in a change of R_{ct} from 566.5 Ω to 658.3 Ω, an increase of 16.2%, which was then doubled to 30.6% after incubation with a higher target concentration of 100 nM. Hence, this variation can be related to the PNA/miRNA duplex that forms as a result of hybridisation. The uncharged PNA platform alters to a negatively charged platform due to the presence of miRNA. The negatively charged miRNA on the electrode surface then in turn increases resistance (R_{ct}) to the redox ions inside the solution to reach the electrode surface.

a)   b)
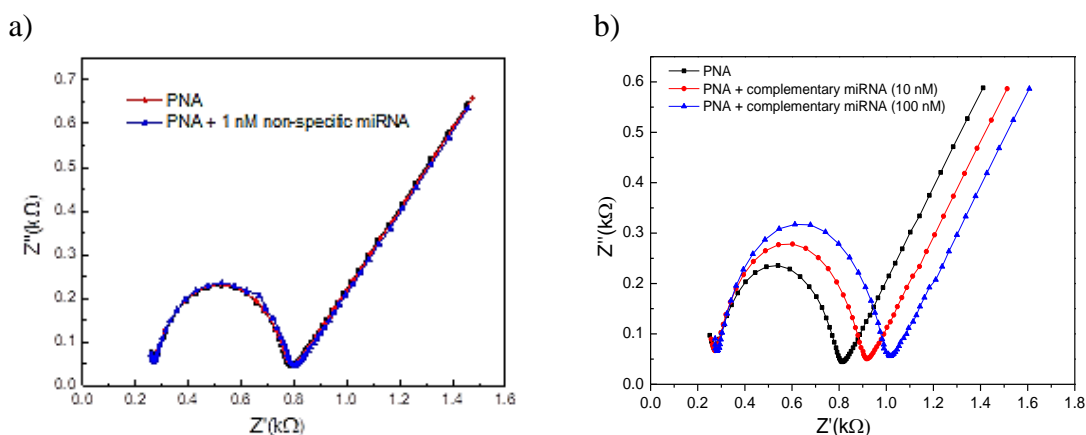
Figure 3.2   EIS characterisation of the PNA-probe. The Nyquist plot in (a) corresponds to the electrode surface stabilised with PNA probe followed by non-specific binding of 1 nM miRNA. The Nyquist plot in (b) corresponds to the electrode surface stabilised with PNA probe (black), followed by initial hybridisation with 10 nM complementary miRNA target (red) and second incubation of 100 nM complementary miRNA (blue). The plots in (a) and (b) correspond to two different electrodes, the reproducibility of the results are presented in the upcoming sections.

3.3. 3 Probe optimisation for the enhancement of PNA-miRNA hybridisation signals

EIS in Faradaic mode was adopted to investigate the result of various mole fractions of PNA to thiol (PNA to MCH) in the immobilisation solution for the enhancement of the hybridisation signal. Thiol-modified PNA probes and mercaptohexanol were co-immobilised onto gold electrodes and the charge transfer resistance for the electrode surface was determined by electrochemical impedance spectroscopy. Typical Nyquist plots for the PNA/MCH functionalised electrode surface before and after complementary miRNA incubation are shown in Figure 3.3.(a) & (b).

According to the results, a 1:5 ratio of PNA:MCH for the self-assembled layer performed an R_{ct} variation of 15.99% with a standard deviation of ±2.53% upon incubation with 10 nM of complementary miRNA. Such a result corresponds to a 7-

fold increase in the initial %ΔR_{ct} measured upon stabilisation of the probe (%ΔR_{ct} upon stabilisation = 2.33% ±2.37%).

Although the %ΔR_{ct} for the 1:2 ratio of PNA:MCH self-assembled layer performed a negligible variation upon stabilisation (ΔR_{ct} = 2.4% ±2.68%), this almost remained the same after incubation with 10 nM of complementary miRNA (ΔR_{ct} = 1.03% ±0.05%) which reflects a very poor hybridisation efficiency. The complete analysis of various PNA:MCH mole fractions and %ΔR_{ct} upon miRNA hybridisation is shown in Figure 3.3.c.

The %ΔR_{ct} increases significantly upon hybridisation as the ratio of PNA to MCH functionalised on the surface is reduced gradually from 1:2 to 1:15. A sharp drop is observed upon reducing the ratio further to 1:20. Although a high density of PNA, such as in the 1:5 ratio, is expected to result in a high density of hybridised DNA on the surface, further increases of the PNA fraction (ratio 1:2) results in a decrease of the fractional change in R_{ct} upon hybridisation. This is due to the combination of two effects (Keighley et al. 2008); first is the steric hindrance that reduces the hybridisation efficiency with the target, and the second is the larger initial R_{ct}.

The best hybridisation efficiencies were performed upon adopting 1:10 and 1:15 ratios of PNA to MCH on the surface. When the probe density was reduced further to a 1:20 ratio, the hybridisation efficiency drops due to an insufficient amount of probe on the electrode surface (Keighley et al. 2008). Although the 1:15 ratio displayed the highest hybridisation efficiency, it performed to be a less stable probe upon incubation with blank, compare to 1:10 ratio. Hence, we have decided to adopt a 1:10 ratio for further assays of miR-21-5-p detection. Although the literature reports a ratio of 1:4 (PNA:MCH) for the label-free detection of DNA/miRNA (Jolly et al. 2016) (Jolly et al. 2015) (Keighley et al. 2008) with EIS, our studies have shown that it is crucial to carry out a personalised optimisation study for any target sequence and adopt the most efficient ratio.

a)   b)

c)
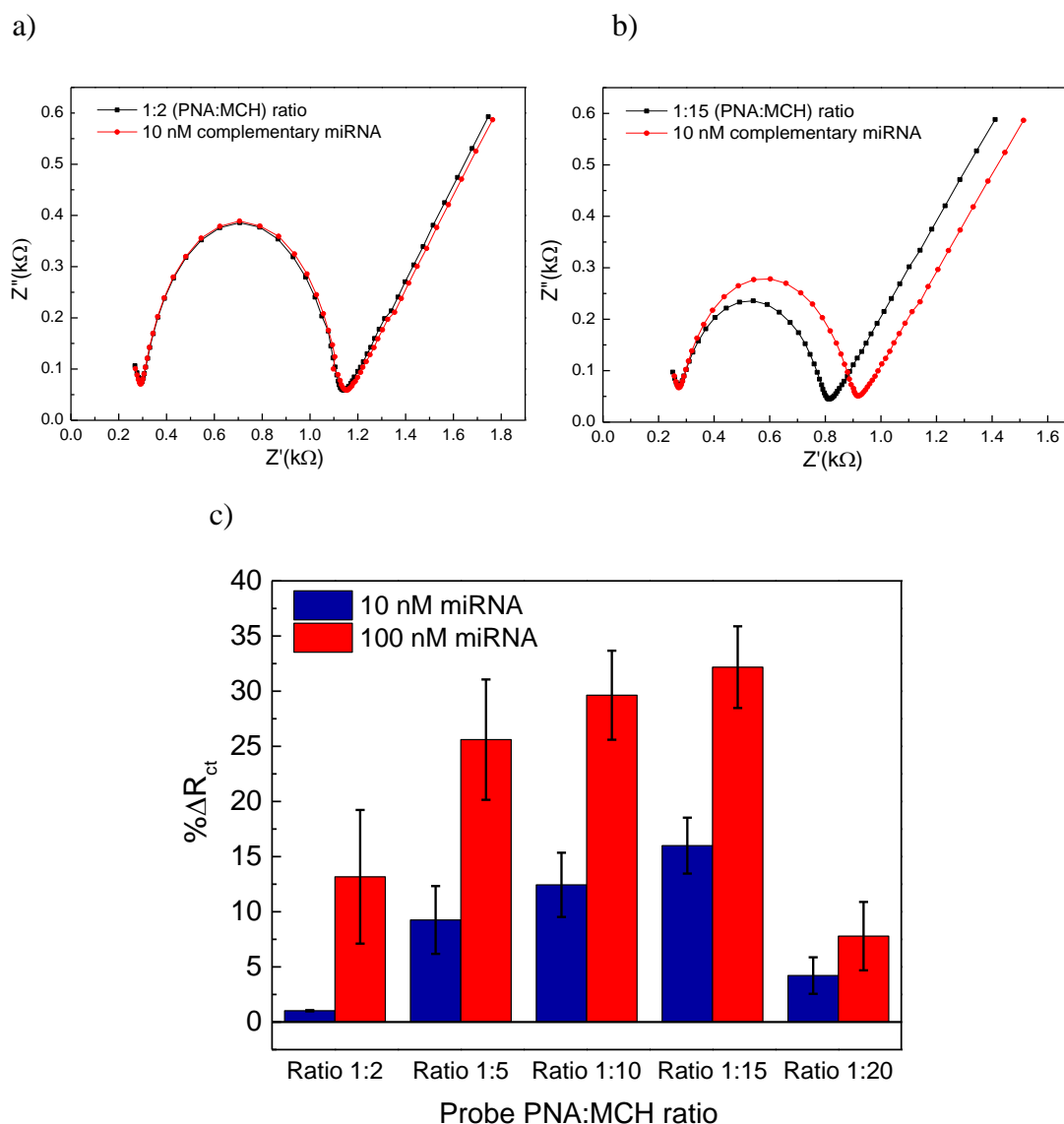
Figure 3. 3 (a) Nyquist response when 1:2 PNA to MCH ratio is adopted for detection. (b) Nyquist response when 1:15 PNA to MCH ratio is adopted for detection. (c) Percentage variations of R_{ct} upon hybridisation by adopting various ratios of PNA to MCH on electrode surface. All EIS measurements were carried out in 10 mM PB (pH 7.3) containing 10 mM of the ferro/ferrocyanide ($[Fe(CN)_6]$)$^{3-/4-}$. The error bars represent the standard deviation between three separate electrodes.

The results in Figure 3.3 once again confirm that it is crucial to carry out the optimisation study for any sequence, and the results will vary depending on the

sequence that is worked with. There is a possible explanation for this result. Such an observation for the case of a long DNA sequence (Figure 3.1 a) could be attributed to the fact that when dealing with longer target sequences, there is the need for better spacing of the probe-PNA. This is due to the fact that long sequences of DNA are even more negatively charged and when captured on the surface will perform an electrostatic repulsion force with the adjacent captured sequence, and this can result in poor binding if there isn't sufficient spacing of the probe. On the other hand, if the probes are spaced too loosely then they won't be sufficient to capture the target. Hence, it is crucial to perform the optimisation study to find the perfect trade-off between these factors.

3.3. 4 Detection limit of the optimised miRNA sensor

Limit of Blank (LOB), Limit of Detection (LOD) and Limit of Quantitation (LOQ) are terms used to describe the smallest concentration of the analyte that can be reliably measured by an analytical procedure (Armbruster & Pry 2008) and all of these parameters have distinct definitions that should not be confused. LOB and LOD are crucial terms in assays for the discrimination between the presence and absence of an analyte, whereas LOQ is used in clinical diagnosis for measuring reliable levels of analytes (Armbruster & Pry 2008).

LOB can be defined as the highest apparent analyte concentration expected to be found when replicates of a blank (containing no analyte) sample are tested, and the term is defined with the following formula (Armbruster & Pry 2008):

$$LOB = mean_{blank} + 1.645(SD_{blank}) \qquad \textbf{Equation 3. 1}$$

Where $mean_{blank}$ refers to the mean result of replicated measurements for blank and SD_{blank} refers to the standard deviation for blank.

On the other hand, LOD is defined as the lowest concentration of analyte that can be reliably distinguished from LOB at which the detection is feasible. LOD is evaluated

by using both the calculated LOB and the results from testing repetitions of samples known to contain a low concentration of the analyte. The LOD then becomes (Armbruster & Pry 2008);

$$\text{LOD} = \text{LOB} + 1.645(\text{SD}_{\text{low concentration sample}})\qquad \textbf{Equation 3. 2}$$

The optimised sensor with a 1:10 ratio of PNA to MCH on the gold electrode surface was initially challenged with a high concentration of non-specific miRNA (1 nM) for its selectivity, then with various concentrations of complementary miRNA for its sensitivity and evaluation of LOD.
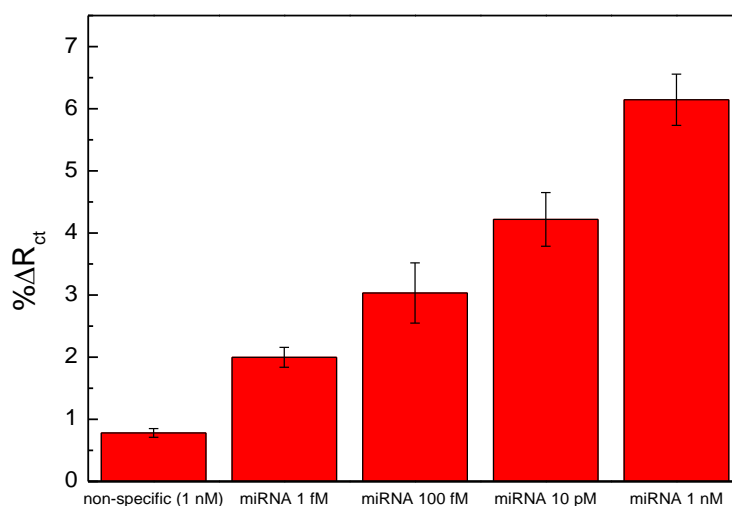
Figure 3. 4 Limit of detection study. The bars represent average percentage changes in R_{ct} upon incubation with non-specific solution followed by various concentrations of full-complementary target miRNA. The error bars represent the standard deviation between three separate electrodes.

The results in Figure 3.4, reveal a detection limit which is brought down to fM levels with no additional amplification steps, but only with the probe optimisation study. The variation of R_{ct} was observed to be at the negligible level of 0.78% ±0.07% upon non-specific interactions; and was observed to be gradually increased by increasing the concentration of complementary miRNA. By adopting Equation 3.2, the detection

limit for miR-21-5p was calculated to be 0.77 fM. LOQ on the other hand is the lowest concentration at which a reliable detection is possible, provided the predefined goals for bias and imprecision are met. LOQ could be the equivalent to LOD or higher. It cannot be lower than LOD as we expect that the LOD of a system lies somewhere below the experiment's functional sensitivity. Being initially introduced by a study for developing the clinical diagnosis tool to characterise thyroid stimulating hormone (TSH) assay efficiency for distinguishing euthyroid from hyperthyroid patients at low TSH concentrations, the functional sensitivity of the system is defined at a concentration that leads to a Coefficient Vector (CV) = 20% (Armbruster & Pry 2008). The coefficient vector is defined as the ratio of standard deviation to the mean. This is applicable to the clinical diagnosis and management where LOQ is adopted to measure low levels of hormones (e.g. TSH). In the case of our studies, we assumed a predefined limit of 15% for the standard deviation against corresponding analyte concentrations, that is a feasible assumption for analytical methods (Shrivastava & Gupta 2011). Upon evaluating the coefficient vector for each of our measured analyte concentrations, 100 fM revealed a CV of 15.8%. The value exceeds the pre-defined value of 15%, hence, 100 fM was decided as the LOQ (Shrivastava & Gupta 2011). For the analyte concentrations higher than 100 fM, the coefficient vector was evaluated to be much lower than the pre-defined value which corresponds to a good functional sensitivity.

3.3. 5 Detection in serum

After successful evaluation of the system with the target miRNA prepared in 10mM PB buffer, we proceeded to test the sensor for its efficiency with the target miRNA spike-in serum. Hence, an initial assay was carried out where the target miRNA concentrations were prepared in 10% serum for the incubations. Interestingly, the results show an improved variation on R_{ct} values when the miRNA samples were prepared in the 10% serum.
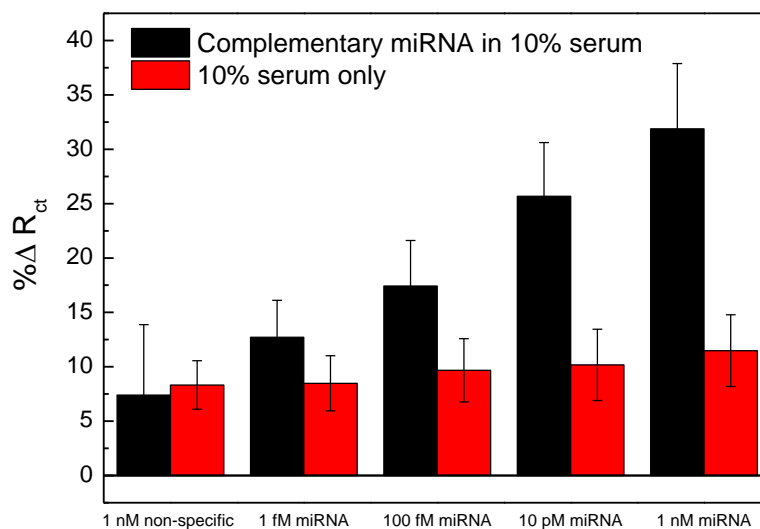
Figure 3. 5 Red bars represent the average R_{ct} variations upon incubations with 10% serum only. Black bars represent the incubations that initially started with 1 nM of non-specific miRNA spike-in 10% serum, followed by various concentrations of target miRNA prepared in 10% serum. The error bars represent three separate electrodes.

The results presented in Figure 3.5 indicate a significant increase (~4-fold) on R_{ct} values compared to the case of detection in 10 mM PB buffer (Figure 3.4). However, the background measurements with serum also had a high variation of R_{ct} at the same time which drops our LOQ in serum. For better investigation, both results of R_{ct} variations in Figures 3.4 & 3.5 were combined in a graph shown in Figure 3.6. The %R_{ct} variation due to non-specific interactions in both cases were eliminated from the results by adopting a normalisation line (dashed line) in Figure 3.6. Hence, it is confirmed that the 1.21% ±0.21% variation of R_{ct} upon 1 fM miRNA incubation was raised more than 4-fold to be 5.15% ±3.48% when incubation was carried out in 10% serum. LOQ in 10% serum was evaluated as 10 pM. Although the LOD is lower, the functional sensitivity of the system with serum samples is best represented by LOQ, as it reflects reliable measurements for clinical diagnosis (Armbruster & Pry 2008).
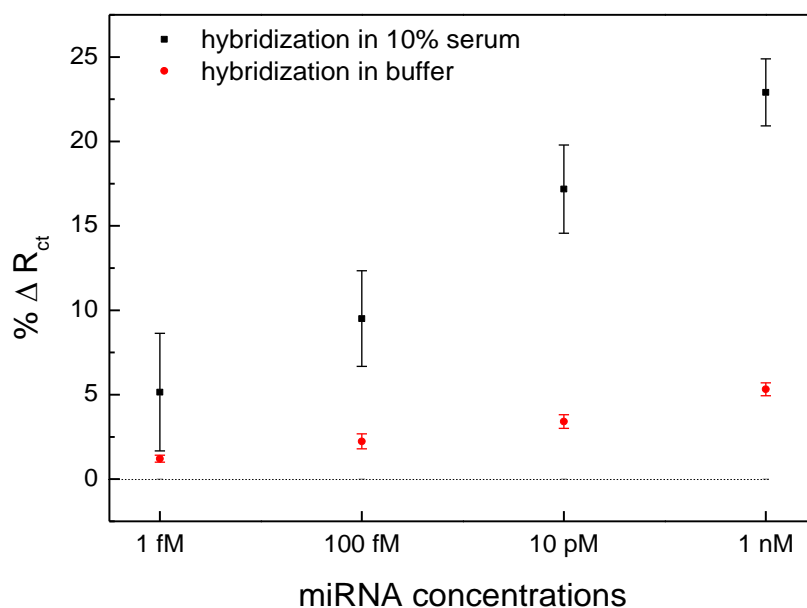
Figure 3. 6 Variation of R_{ct} in buffer and 10% serum. The error bars represent three separate electrodes.

There could be an explanation for such a result. It is a known fact that miRNA suffers from RNAse degradation when not shielded from a nuclease rich environment. Although the behaviour of miRNA, in circulating blood, remained enigmatic for a long period of time, recent evidence suggests that they are protected by encapsulation in microvesicles or proteins of the Argonaute (AGO) family in blood plasma/serum. Such encapsulation shields the extracellular miRNA from RNAse degradation (Taylor et al. 2013) (Etheridge et al. 2013) (Turchinovich et al. 2013) (Kinet et al. 2013).

Hence, the results shown in Figure 3.6, could be attributed to the fact that when miRNA is prepared in a buffer it is still exposed to environmental nucleases causing a drop in the actual yield, leading to less hybridisation. However, in a 10% serum, there are sufficient amount of proteins that attach to the major binding sites of miRNA (Malonga et al. 2006) and protect them from degradation. This could be the possible reason as to why the best yield of miRNA and hybridisation with the detection probe was obtained in a 10% serum. EIS measurements were repeated with a miRNA spiked in 100% serum (Appendix I). Although the variations of R_{ct} were higher compared to

control measurements there is still a need for improving the LOD of the platform in a 100% serum environment (Appendix I).

3. 4 Conclusions

The results presented in this chapter correspond to the experimental manifestation of high sensitivity in electrochemical detection platforms without the need for target labelling. With the aim of improving the miRNA sensing, the work in this chapter presents a simple and sensitive electrochemical PNA-based biosensor that functions with no additional amplification steps. By combining the electrochemical detection techniques found in the literature together with our approach of probe optimisation, we have achieved significant improvements in R_{ct} variations of the system upon target detection. With the current platform, a LOD of 0.77 fM of miR-21-5p was achieved in buffer that is almost as good as the previous results reported in literature by use of additional amplification steps (LOD of 0.38 fM) (Jolly et al. 2016). Despite the issues of non-specific binding in serum, we have achieved a LOQ of 10 pM in a serum environment which is a big step towards real case applications. The presented technique can be adopted for detection of any other oligonucleotides specific to various other diseases.

References

Akao, Y., Nakagawa, Y. & Naoe, T., 2007. MicroRNA-143 and -145 in colon cancer. *DNA and Cell Biology*, 26(5), pp.311–320.

Ambros, V., 2004. The functions of animal microRNAs. *Nature*, 431, pp.350–355.

Armbruster, D.A. & Pry, T., 2008. Limit of blank , limit of detection and limit of quantitation. *The Clinical Biochemist Reviews*, 29, pp.49–52.

Bartel, D.P., 2004. MicroRNAs : genomics , biogenesis , mechanism , and function genomics : the miRNA genes. *Cell Press*, 116, pp.281–297.

Dahiya, N. & Morin, P.J., 2010. MicroRNAs in ovarian carcinomas. *Endocrine-Related Cancer*, pp.77–89.

Esquela-kerscher, A. & Slack, F.J., 2006. Oncomirs – microRNAs with a role in cancer. *Nature Reviews Cancer*, 6(4), pp.259–269.

Etheridge, A. et al., 2013. The complexity , function , and applications of RNA in circulation. *Frontiers in Genetics*, 4(115), pp.1–8.

Ferracin, M., Calin, G.A. & Negrini, M., 2011. MicroRNAs in cancer (an overview). In W. C. S. Cho, ed. *MicroRNAs in Cancer Translational Research*. Springer, Dordrecht, pp. 1–73.

He, L. et al., 2005. A microRNA polycistron as a potential human oncogene. *Nature*, 435(7043), pp.828–833.

Ichimi, T. et al., 2009. Identification of novel microRNA targets based on microRNA signatures in bladder cancer. *International Journal of Cancer*, 125, pp.345–352.

Iorio, M. V & Croce, C.M., 2011. MicroRNA dysregulation in cancer : diagnostics , monitoring and therapeutics . A comprehensive review. *EMBO Molecular Medicine*, 4, pp.143–159.

Jolly, P. et al., 2015. A simple and highly sensitive electrochemical platform for detection of microRNAs. *Institute of Electrical and Electronics Engineers Sensors*, pp.803–806.

Jolly, P. et al., 2016. Highly sensitive dual mode electrochemical platform for microRNA detection. *Scientific Reports*, 6(36719), pp.1–9.

Joshi, L.T. et al., 2014. Extraction and sensitive detection of toxins A and B from the human pathogen clostridium difficile in 40 seconds using microwave-accelerated metal- enhanced fluorescence. *Public Library of Science*, 9(8).

Keighley, S.D. et al., 2008. Optimization of label-free DNA detection with electrochemical impedance spectroscopy using PNA probes. *Biosensors and Bioelectronics*, 24, pp.906–911.

Kinet, V. et al., 2013. Cardiovascular extracellular microRNAs : emerging diagnostic markers and mechanisms of cell-to-cell RNA communication. *Frontiers in Genetics*, 4, pp.1–7.

Lu, J. et al., 2005. MicroRNA expression profiles classify human cancers. *Nature*, 435, pp.834–838.

Malonga, H., Neault, J. & Tajmir-Riahi, H.-A., 2006. Transfer RNA binding to human serum albumin : a model for protein – RNA Interaction. *DNA and Cell Biology*, 25(7), pp.393–398.

Matsuzaki, J. & Ochiya, T., 2017. Circulating microRNAs and extracellular vesicles as potential cancer biomarkers : a systematic review. *International Journal of Clinical Oncology*, 22(3), pp.413–420.

Ng, E.K.O. et al., 2009. Differential expression of microRNAs in plasma of patients

with colorectal cancer : a potential marker for colorectal cancer screening. *Gut*, 58, pp.1375–1381.

Peng, Y. & Gao, Z., 2011. Amplified detection of microRNA based on ruthenium oxide nanoparticle-initiated deposition of an insulating film. *Analytical Chemistry*, 83, pp.820–827.

Qian, H. et al., 2017. Protecting microRNAs from RNase degradation with steric DNA nanostructures. *Chemical Science*, 8, pp.1062–1067.

Qu, K. et al., 2017. Circulating miRNA-21-5p as a diagnostic biomarker for pancreatic cancer : evidence from comprehensive miRNA expression profiling analysis and clinical validation. *Scientific Reports*, 7(1692), pp.1–12.

Ramaswamy, S. et al., 2001. Multiclass cancer diagnosis using tumor gene expression signatures. *Proceedings of the National Academy of Sciences*, 98(26), pp.15149–15154 MEDICAL.

Ren, Y. et al., 2013. A highly sensitive and selective electrochemical biosensor for direct detection of microRNAs in serum. *Analytical Chemistry*, 85, pp.4784–4789.

Shrivastava, A. & Gupta, V.B., 2011. Methods for the determination of limit of detection and limit of quantitation of the analytical methods. *Chronicles of Young Scientists*, 2(1), pp.21–25.

Spizzo, R. et al., 2013. miR-145 participates with TP53 in a death-promoting regulatory loop and targets estrogen receptor-α in human breast cancer cells. *Cell Death & Differentiation*, 17(2), pp.246–254.

Taylor, D.D. et al., 2013. The origin , function , and diagnostic potential of RNA within extracellular vesicles present in human biological fluids. *Frontiers in Genetics*, 4(142), pp.1–12.

Turchinovich, A. et al., 2013. Circulating miRNAs : cell – cell communication function ? *Frontiers in Genetics*, 4(119), pp.1–10.

Wang, J., 2006. Electrochemical biosensors: towards point-of-care cancer diagnostics. *Biosensors and Bioelectronics*, 21(10), pp.1887–1892.

Wang, P. et al., 2013. The serum miR-21 level serves as a predictor for the chemosensitivity of advanced pancreatic cancer , and miR-21 expression confers chemoresistance by targeting FasL. *Molecular Oncology*, 7, pp.334–345.

Wang, R.L.C. & Kreuzer, H.J., 1997. Molecular Conformation and Solvation of Oligo (ethylene glycol) -Terminated Self-Assembled Monolayers and Their Resistance to Protein Adsorption. *The Journal of Physical Chemistry B*, 101(47), pp.9767–9773.

Chapter 4 Simple fishing and pre-concentration of microRNA with LNA-modified magnetic beads for electrochemical detection

Electrochemical detection seems promising for future miniaturised point-of-care applications (Silva et al. 2017) and studies so far revealed promising results for the electrochemical detection of circulating miRNAs, which are ideal candidates to serve as cancer biomarkers (Jolly et al. 2016). The levels of circulating miRNAs provide valuable information about cancer in its early stages, before the symptoms arise (Lawrie et al. 2008; Chen et al. 2008; Mitchell et al. 2008). Herein, we present the development of a new methodology for the simple fishing of target miRNAs from solution via magnetic beads which results in the separation and pre-concentration of the target prior to analysis, that is crucial for signal amplification for detection. The methodology is developed in order to offer detection in complex solutions (e.g. blood) which is a major complication for current platforms. Magnetic beads are known to be robust and versatile tools for the separation of nucleic acids and are a well known solid support for electrochemical detection (Palecek & Fojta 2007). Our methodology utilises magnetic beads for capture of the target miRNAs from solution and brings the concentrated target to the sensor surface. Herein, we modify the magnetic beads with locked nucleic acids (LNA), which have a high affinity for their complementary RNA/miRNA sequence, therefore they further encourage the capture of the target (Natsume et al. 2007). The separated, hence concentrated miRNAs, are in turn brought to a sensor surface that is immobilised with peptide nucleic acids (PNA). Electrochemical Impedance Spectroscopy (EIS) is one of the electrochemical measuring techniques that tracks the variation of charge transfer resistance (R_{ct}) upon hybridisation. The studies of EIS so far on adopting PNA probes has reported the detection of 100 times larger R_{ct} values compared to previous DNA probe studies

(Keighley et al. 2008b). As a result, PNA probes are incredibly promising tools for impedance sensing. Upon adopting the methodology, we have achieved an average R_{ct} variation of 32.4% ± 5.4% upon hybridisation of the PNA-probe with its target miRNA using LNA-modified magnetic beads. This is significantly higher than the 0.71% variation of R_{ct} that was observed for hybridisation with non-specific miRNA. Hence, the EIS results confirm the success of our methodology for the fishing of miRNA from solution and its direct electrochemical detection on PNA-immobilised gold electrode surfaces. To the best of our knowledge, our study is the first experimental work for the magnetic beads-based capture of miRNA from solution using high affinity LNA-probes, that doesn't require prior sample preparation for target labelling or the adoption of enzymatic labelling on the probe surface for detection.

4. 1 Background

Magnetic beads hold many applications and are a well-known solid support for electrochemical detection (Wang et al. 2002; Katz et al. 2004; Palecek & Fojta 2007). Recently there has been an interest in the design of new electrochemical biosensors for nucleic acid detection using magnetic beads that offer efficient magnetic separation (Gogotsi & Uvarova 2003). The adoption of the beads for the electrochemical detection of miRNA was initially suggested by *Bettazzi et al. (Bettazzi et al. 2013)* and the study revealed a detection limit of 7 pM for miR-222, where the sequence was chosen as a model due to its involvement in brain, lung and liver cancers. The methodology required the functionalisation of the streptavidin coated magnetic beads with a biotinylated DNA probe that was specific to the target miRNA. This was followed by the extraction of the target miRNAs from the cell samples and their labelling with biotin. The biotinylated target was then hybridised with the DNA capture probe on the magnetic bead. The resulting biotinylated hybrid was labelled with a streptavidin-alkaline phosphatase conjugate. The magnetic beads that hold the biotinylated DNA-miRNA hybrid with streptavidin-alkaline phosphatase conjugate were then magnetically entrapped on to a screen-printed electrode. The substrate was added for measuring the enzymatic product, and the measurements were carried out using differential pulse voltammetry. The assay was integrated into a microfluidic device that facilitated multiplexed analysis.

The following year, in 2013, a similar study reported detection limits as low as femtomolar (fM, 10^{-15}) levels for voltammetric detection of miRNA by designing a magnetic beads based assay on a multi-channel screen-printed array of electrodes (Erdem et al. 2013). In the same year, another study achieved the creation of a highly sensitive platform that revealed attomolar (aM, 10^{-18}) level detection of oral-cancer related miRNAs (Wang et al. 2013). Similar to previous studies streptavidin coated magnetic beads were initially modified with a biotinylated capture probe (P_c). The methodology showed a slight variation from previous methods, as a second probe was adopted as signal probe (P_s) that was modified with a biotin tag at two ends. In the absence of target microRNA, the P_c and P_s would not hybridise due to low melting points. Whereas when incubated with target miRNA (T), the capture probe (P_c) would be able to hybridise with T (target miRNA) and P_s (signal probe) forming "Y" junction structures on the magnetic beads. This step was followed by the capture of horseradish peroxidase (HRP) conjugated streptavidin by the biotinylated signal probes and the resulting HRP-tagged surface of magnetic beads were adsorbed onto the working electrode surface that was electrically magnetic-controllable, enabled by a voltage on the electric coil. The resulting HRP-tagged magnetic beads catalyse the H_2O_2-mediated oxidation of TMB (3,3',5,5'-tetramethylbenzidine sulfate). The electrically magnetic-controllable electrochemical biosensor allowed the detection of miRNA concentrations at attomolar levels, with a linear range of 1 aM~10 fM. (Wang et al. 2013).

In 2013, *Bartosik et al (Bartosik et al. 2013)* reported another study for the detection of miRNA using magnetic beads. This work utilised target miRNA pre-labelled with the electroactive Os(VI)bipy (six-valent osmium and 2,2′-bipyridine) complex on the ribose sugar molecule at the 3′-end of miRNA. The magnetic beads that were immobilised on the complementary probe were then used to capture Os(VI)bipy-labelled miRNAs followed by the thermal release of the target and electrochemical detection at a hanging mercury drop electrode at femtomole levels (Bartosik et al. 2014). It was not long after in 2014 that an electrochemical magnetosensor platform for the direct detection of miRNAs in raw RNA samples on commercial screen-printed electrodes was suggested (Campuzano et al. 2014). The method eliminated the pre-labelling of the target as suggested by previous studies. Carnarian Italian ringsport

virus (CIRV) p19 protein was immobilised through its terminal chitin-binding domain (CBD) to chitin-functionalised magnetic beads and utilised to capture previously hybridised duplexes of miRNA/anti-miRNA. The captured hybrid was labelled with Strep-HRP polymer and the resulting magnetic beads were then magnetically anchored onto screen-printed carbon electrodes. The method performed a detection limit of 0.04 nM by measuring the catalytic amperometric current upon the addition of H_2O_2 and hydroquinone.

An even lower detection limit of 10 aM was achieved in 2017 (Vargas et al. 2017) by adopting a similar methodology to Campuzano et al, which eliminates the pre-labelling of target miRNAs. The methodology utilised the direct hybridisation of the target miRNA (miRNA-21) with a biotinylated DNA capture probe that was previously immobilised on streptavidin-modified magnetic beads. The resulting helix was initially labelled with a specific DNA–RNA antibody and the bacterial protein A (ProtA) conjugated with horseradish peroxidase (HRP) homopolymer (Poly-HRP40) as an enzymatic label for signal amplification. Then the modified magnetic beads were anchored onto a working electrode surface of commercial screen-printed electrodes utilising the H_2O_2/hydroquinone (HQ) system. Finally, amperometric detection was performed.

With the aim of advancing the current technologies of magnetic bead-based electrochemical detection, the first and most crucial step forward is the analysis of how well the current methodologies satisfy the requirements of a final product that is commercially viable. Through a gap analysis, one can identify the space between where the current technology is and where it has to be in order to desing a demanded sensor. This analysis is extremely beneficial in order to develop a new methodology that fulfils the weaknesses of current models. Hence, Table 4.1 provides an insight into the design methodologies of the studies discussed earlier, and enables one to make comparisons.

Table 4. 1 List of current magnetic beads-based electrochemical detection methodologies for miRNA detection

Assay Description	LOD	Pre-labelling of target	Number of assay steps	Type of capture probe	Reference
Electrochemical detection of miRNA-222 by use of a magnetic bead-based bioassay	7 pM	Yes	7	DNA	(Bettazzi et al. 2013)
Electrically magnetic-controllable electrochemical biosensor for the specific detection of oral cancer-related microRNA	0.22 aM	No	7	RNA	(Wang et al. 2013)
Magnetic bead-based hybridisation assay for electrochemical detection of microRNA	~fM level	Yes	6	DNA	(Bartosik et al. 2013)
Magnetobiosensors based on viral protein p19 for microRNA determination in cancer cells and tissues	0.04 nM	No	6	RNA	(Campuzano et al. 2014)
Magnetic beads-based sensor with tailored sensitivity for rapid and single-step amperometric determination of miRNAs	10 aM	No	6	DNA	(Vargas et al. 2017)

4.1. 1 New Assay Design

In order to improve the current methodologies in literature, we designed a new assay that combines the high affinity and separation properties of LNA modified magnetic beads with the high stability of PNA probes on gold electrode surfaces in order to develop a magnetic-beads based direct electrochemical detection of miRNAs from solution. Our methodology initially replaces the DNA/RNA capture probe that is adopted in the literature with a probe that has a higher affinity to miRNAs. One nucleic acid that is known for displaying extraordinary hybridisation affinity towards RNA is Locked Nucleic Acid (LNA). The enhanced affinity is a result of the modified chemical structure of LNA (Laschi et al. 2009) that leads to the high melting points of LNA-RNA (Natsume et al. 2007) and makes LNA well suited for miRNA detection and analysis for cancer diagnosis. Hence, a biotinylated LNA probe was adopted and LNA-modified streptavidin coated magnetic beads were utilised for capturing miRNA from solution. After separation of the target miRNA from solution, a number of thermal and chemical denaturation methods were investigated for the most efficient release of the captured miRNA target from magnetic beads. A PNA-immobilised gold electrode was adopted for the identification of the miRNA that was captured by magnetic beads. PNA oligonucleotides when immobilised on gold electrode surfaces provide exceptional stability and great detection limits for the identification of low concentrations of miRNA in a solution (Jolly et al. 2015; Jolly et al. 2016). Hence, such a methodology does not only eliminate the pre-labelling step of target but also benefits from the high affinity properties of LNA-probes for capturing low concentrations of miRNA from solution, and their quantification by highly stable PNA-probes.
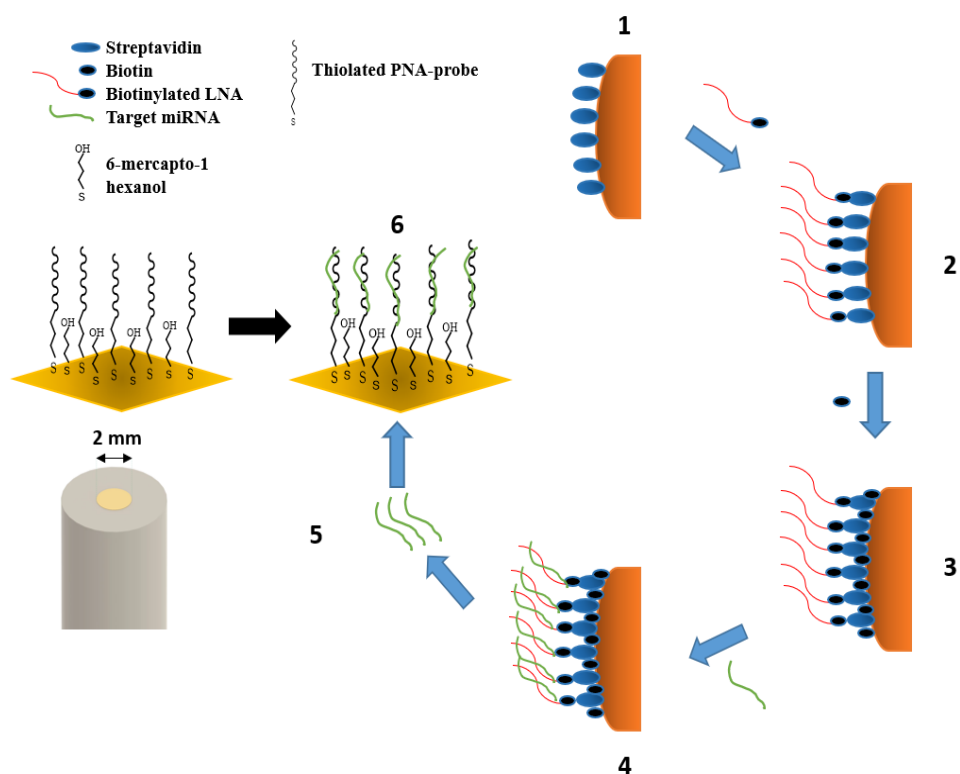
Figure 4. 1 Schematic diagram of the assay. (1) Streptavidin coated magnetic beads ready for probe modification. (2) Biotinylated LNA capture probes are immobilised on magnetic beads via streptavidin-biotin bonding. (3) Surface blocking carried out with biotin in order to prevent non-specific binding. (4) Probe-modified and biotin blocked beads incubated with miRNA target (diluted for desired concentration in 10 mM PB) (5) chemical or thermal release of the miRNA from magnetic beads surface. (6) Re-hybridisation of captured miRNA with PNA-probe for electrochemical detection.

4. 2 Materials and Methods

4.2 1 Preparation of magnetic beads

Prior to any assay, the Pierce^{TM} Streptavidin Magnetic Beads (Thermo Scientific) were washed with 25 mM Tris-buffered saline containing 0.1% Tween^{TM}-20 Detergent (Thermo Scientific). This was carried out by adding 30µL (0.3 mg) of magnetic beads into 1.5mL micro centrifuge tube that was placed on a magnetic stand to collect the

beads to the side of the tube. The supernatant was removed with the help of pipette and discarded. Then 1 mL of wash buffer (Tris-buffered saline) was added to the tube. The tube was inverted several times and gentle vortex was applied for an even mix. The beads were then collected with magnetic stand to the side of the tube and the supernatant was removed. It is crucial not to allow beads to dry and if necessary, the beads were stored in wash buffer until the incubation with the LNA probe was carried out.

4.2 2 Oligonucleotides

The synthetic biotinylated LNA capture probe was purchased from Eurogentec, UK, in lyophilised form while the HPLC purified synthetic miRNA sequences were purchased from Sigma-Aldrich, UK, in lyophilised from. The PNA probe was purchased from Cambridge Research Biochemical, UK. The sequences are shown in Table 4.2.

Table 4. 2 LNA, PNA and miRNA sequences used by this study. The full complementary sequence on the first row corresponds to the miR-21-5p sequence specific to pancreatic cancer. TEG stands for tetra-ethyleneglyco linker (15 atoms) which is used to add Biotin to an oligonucleotide. AEEA is a glycol linker of nine atoms (8-amino-3,6-dioxaoctanoic acid). LNA modification sites in each sequence are represented by (ln).

miR-21-5p sequence (full complementary)	3'-AGU UGU AGU CAG ACU AUU CGA U-5'
LNA Probe: 5'-Biotin-TEG	T(lnC)A-A(lnC)A-TCA-G(lnT)C-TGA-T(lnA)A-G(lnC)T-(lnA)-'3
PNA probe: SH-C6-AEEA-TTT	TCA ACA TCA GTC TGA TAA GCT A
Non-specific miRNA sequence	3'-AGU UGU ACC AGA UAU CCG UAA A-5'

4.2 3 Bio-functionalisation of magnetic beads

Prior to bio-functionalisation, the Pierce^{TM} Streptavidin Magnetic Beads (Thermo Scientific) were washed by following the procedure given in section 4.2 1. This was then followed by washing the beads within the immobilisation buffer (10 mM PB buffer, pH 7.3) that was carried out by adding 1 mL of 10 mM PB buffer (pH 7.3) to the tube that contained the pre-washed dry beads. The tube was inverted several times, and a gentle vortex was applied for an even mix and the beads were collected with the magnetic stand. The supernatant was removed, and the dry beads were incubated with 300 µL of 1 µM biotinylated LNA-probe solution immediately. 1 µM of biotinylated LNA-probe solution was prepared in 10 mM PB buffer (pH 7.3) prior to immobilisation with magnetic beads. The incubation with LNA-probe solution was carried out at room temperature for 1 hour with continuous mixing. In the end, modified beads were collected by placing the tube on the magnetic stand again and removing the supernatant for further analysis. Then the modified beads were washed with 10 mM PB buffer twice and were incubated with 100 µM biotin (prepared in 10 mM PB buffer, pH 7.3) in order to block the remaining streptavidin active sites on the probe-functionalised surface, hence eliminating the undesired binding of other biotinylated oligonucleotides. After biotin blocking, the beads were collected with the magnetic stand, and supernatant was removed for further analysis. This was followed by a final wash of the beads in 10 mM PB buffer.

4.2 4 Hybridisation of LNA-functionalised magnetic beads with target miRNA

1 µM of 300 µL target miRNA was prepared in 10 mM PB (pH 7.3) and heated at 95˚C in a water bath for 5 minutes prior to incubation. The heating was carried out in order to prevent the formation of hairpins or secondary structures, as the evidence suggests that miRNAs have a tendency to form both hairpin and homoduplex structures in solution (Belter et al. 2014). This was followed by incubating the dry LNA-functionalised (bio-functionalised) magnetic beads with 300 µL of the target miRNA solution for 30 minutes at room temperature, with continuous mixing for the hybridisation to take place. In the end, the beads were collected with the magnetic

stand, and the remaining solution was removed for further analysis. The beads that contained the LNA-miRNA hybrids were washed twice in 10 mM PB buffer and then a number of thermal/chemical denaturation methods were studied for the most efficient release of the target miRNA from the magnetic beads surface. These methods are explained further in Section 4.2 5. Following the denaturation step, the beads were separated from the solution by use of the magnetic stand and the solution that contained the captured miRNA target was removed for electrochemical detection on PNA-probes.

4.2 5 Physical and Chemical Methods for LNA-miRNA Denaturation

A variety of physical and chemical denaturation methods were investigated for the optimum release of miRNA target from the surface of magnetic beads after being captured by the LNA-probe. This study is crucial for the optimum yield of the target sequence for the detection studies.

4.2.5. 1 Heating

The final solution of LNA-modified magnetic beads (300 µL) that were previously hybridised with target miRNA, was heated in a water bath at 95˚C for 10 minutes.

4.2.5. 2 Removal of Salts

A low salt concentration can lead to the denaturing of DNA double-strands due to the removal of ions that stabilise the negative charges on each of the two single strands. Electrochemical detection studies have shown that successful hybridisation of DNA-DNA (Keighley et al. 2008a), DNA-RNA (Wang et al. 2001) or LNA-RNA (Laschi et al. 2009) requires the presence of ions that will provide the screening for the negative backbone phosphate groups that are present both in DNA and RNA single strands. Hence, for the denaturation experiments 300 µL of Milli-Q water that was free from salts was added to the tube containing LNA-functionalised magnetic beads previously hybridised with target miRNA. The mixture was incubated at ambient temperature for 10 minutes prior to measurements with UV spectrophotometry.

4.2.5. 3 Alkaline solution

In previous studies, various concentrations of NaOH (0.01, 0.1 and 1 M) were investigated for their efficiency for the denaturation studies of DNA duplexes. Amongst the three concentrations, 1 M NaOH achieved 90% denaturation of DNA fragments in one minute followed by complete denaturation in 10 minutes (Wang et al. 2014). Hence, we adopted the same concentration for the chemical denaturation studies of the LNA-miRNA duplex. The stock solution of NaOH (10 M) was prepared upon dissolving 4 g of NaOH (Sigma-Aldrich) in 10 mL of Milli-Q water. The NaOH was diluted from 10 to 1 M in Milli-Q for the assays. 300 µL of 1 M NaOH were added to the tube containing LNA-functionalised magnetic beads previously hybridised with target miRNA. The mixture was incubated at ambient temperature for 10 minutes prior to measurements with UV spectrophotometry.

4.2.5. 4 Dimethyl Sulfoxide (DMSO)

DMSO is another agent that has proven to provide efficient denaturation by lowering the melting temperature of the DNA. Upon trying various concentrations of DMSO (25%, 50% and 60%), *Wang & Son et al.* achieved complete denaturation of DNA in 60% DMSO in one minute followed by further denaturing to 90% over time (Wang & Son 2013). On the other hand, another study (Wang et al. 2014) revealed the denaturation capability of DMSO with higher concentrations and proved that 60% DMSO is sufficient for the complete denaturation of DNA in contrast to low concentrations. Hence, DMSO was purchased from Sigma-Aldrich at a grade for molecular biology use (99.9%). 300 µL of 60% DMSO was prepared in Milli-Q water. The solution was added to the tube containing LNA-functionalised magnetic beads that were previously hybridised with target miRNA. The mixture was incubated at ambient temperature for 10 minutes prior to measurements with UV spectrophotometry.

4.2.5. 5 Urea

The denaturation ability of urea has been widely attributed to its capability to disturb interpeptide and interchain hydrogen bonds (Herskovits 1963). Several early studies looking into the effects of urea on suitable model compounds (Levy & Magoulas 1961) and detergent micelles (Bruning & Holtzer 1961) have suggested this property of urea is grossly oversimplified and at least partly attributed to the destabilisation of hydrophobic interactions. Hence, the urea was considered capable of destroying not only hydrogen bonds but also other sources of stabilisations, like hydrophobic interactions. *Shen et al.* adopted a 50% (w/w) urea solution for target DNA dehybridisation on the surface of magnet submicrobeads following their capture with DNA-probes (Shen et al. 2012). The technique achieved a limit of detection of 8.5 fM. In addition, *Zhang et al* also used a 50% (w/w) urea solution to release target DNA from the surface of magnetic nanobeads immobilised with probe DNA (Zhang et al. 2009). Hence, we employed the same methodology and 300 µL of 50% (w/w) urea were prepared for incubation in a tube containing LNA-functionalised magnetic beads previously hybridised with target miRNA. The mixture was incubated at ambient temperature for 10 minutes prior to measurements with UV spectrophotometry.

4.2 6 UV-Spectrophotometer measurements for validation of design steps

A Shimadzu UV-1800 with Thermal Melt Analysis System was adopted in order to validate the assay steps. The solutions of LNA-probe and target miRNA prior to their bio-functionalisation and hybridisation on magnetic beads surface were analysed by UV-spectrophotometry. This was followed by the analysis of the final solution of target miRNA after its capture on the magnetic beads surface and release. 8-series micro cells with silicone plugs that fit inside the spectrophotometer were adopted in order to measure the samples; this has the benefit of allowing the user to analyse 8 different samples during one measurement. The amount of light that is absorbed by the solution is dependent on the concentration, the path length of the light through the cuvette and how well the analyte absorbs the light at a certain wavelength. It is a known fact that single or double stranded DNA, RNA or LNA oligonucleotides, absorb

ultraviolet (UV) light due to the existence of heterocyclic rings of the nucleotides. The absorbance levels are usually observed to be around 260 nm (Tinoco et al. 1980; Okonogi et al. 2002) and these absorbance properties can be adopted for their quantification (Engman et al. 2004). Hence, UV spectrophotometry was run within the region of 190 nm-800 nm, which allows enough room to identify the LNA-probe, initial target miRNA, and the captured target miRNA. Initially, a baseline measurement was carried out by adding 80 µL of buffer solution (10 mM PB) to each of the micro-cells which sets a reference baseline prior to the actual measurements of nucleic acids within the same buffer. Following the baseline measurement, each micro-cell was emptied and re-filled with 80 µL of solutions which contained the nucleic acids prepared in the same buffer (10 mM PB) for the analysis.
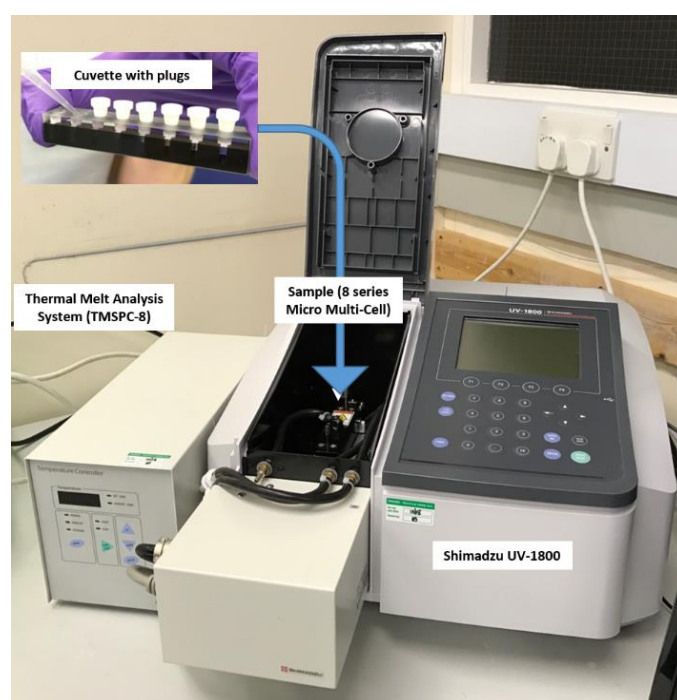

Figure 4. 2 Shimadzu UV-1800 spectrophotometer with Thermal Melt Analysis System (TMSPC-8) consisting of 8 series micro multi-cell cuvette

4.2 7 Electrochemical detection of captured miRNA

Gold working electrodes were mechanically polished for 2 minutes with 1 µM diamond solution (Buehler, USA) on a polishing pad (BASi, USA). This was followed by mechanical polishing using alumina slurry with decreasing particle sizes (starting with 1 µm, then 0.3 µm, and finishing with 0.05 µm). Polishing was carried out for at least 2 minutes in each particle size. In between each polishing step, 5 minutes of sonication in ethanol and rinsing in Milli-Q water were performed to remove the residues. After the final polishing, 10 minutes of sonication in ethanol followed by 10 minutes in Milli-Q water was carried out. Electrodes were then rinsed with Milli-Q water and electrochemically cleaned in 0.5 M H_2SO_4 (Thermo Fisher Scientific, UK) by scanning the potential between the oxidation and reduction of gold, 0 V and +1.5 V vs. an Ag/AgCl reference electrode, for 50 cycles until the voltammogram graphs suggest no further changes. Finally, the electrodes were rinsed with Milli-Q water and dry cleaned under a nitrogen gun.

Clean electrodes were then co-immobilised with the thiolated ssPNA probe sequence and 6-mercapto-1-hexanol (MCH, Sigma-Aldrich, UK) in 50% dimethyl sulfoxide (DMSO, Sigma-Aldrich, UK) 50% ultra-pure water (v/v) immobilisation solution for 16 h in a humidity chamber. After immobilisation, electrodes were rinsed with excess Milli-Q water to remove any unattached thiols and were backfilled with 1 mM MCH for one hour in order to ensure complete thiol coverage. Electrodes were then rinsed with excess Milli-Q water and placed in the measurement buffer for 2 hours to stabilise the SAM.

The experiments were carried out with a PalmSense4 compact potentiostat (PalmSense, Netherlands) and a three-electrode cell system: An Ag/AgCl (KCl) reference electrode (BASi, USA) connected via a salt bridge filled with 10 mM phosphate buffer (pH 7.3), to a Pt counter electrode (ALS, Japan), and gold working electrode (2.0 mm diameter from CH instruments, USA). The Faradaic EIS was conducted in 10 mM PB (pH 7.3) measurement buffer containing 10 mM of the ferro/ferrocyanide ($[Fe(CN)_6])^{3-/4-}$ redox couple over a frequency range from 100 kHz to 100 mHz, with a 10 mV ac voltage superimposed on a dc bias voltage of 0.2 V vs. Ag/AgCl (corresponding to the formal potential of the redox couple).

4. 3 Results and discussion

4.3. 1 The use of UV-Spectrophotometry for validation of design steps

Shimadzu UV-1800 spectroscopy was initially adopted for the identification of the solutions in order to validate the feasibility of each design step. UV measurements provided the absorbance levels for the solutions containing the probe and the target (LNA and miRNA) adopted in the experiments, and the residue solutions of magnetic beads before/after their functionalisation with the LNA-probe, hybridisation with the target sequence and subjection to heat (or chemical denaturation methods).

An absorbance peak at around 260 nm is reported in the literature for the representation of nucleic acids (Tinoco et al. 1980). Hence, a similar absorbance peak for the final solution of target miRNA captured by the magnetic beads would prove the success of the methodology for fishing for miRNA from solution.

Prior to analysis, we have tested the thermal stability of Pierce™ Streptavidin Magnetic Beads that were modified with biotinylated LNA, under extreme heat conditions (95˚C for 10 minutes). Such a study is crucial in order to make sure that the stability of streptavidin-biotin binding (between the beads and the LNA-probe) is conserved under high temperatures. The application of high temperatures was required for the denaturation of the probe LNA-target miRNA helix for the final release of target. An inability of the magnetic beads-LNA binding to resist high temperatures could result in the release of the LNA probe together with the target miRNA from the magnetic beads' surface, hence lead to false signal in the final solution for captured target miRNA. Although the biotin, after binding streptavidin, increases the thermal stability of streptavidin significantly (Gonzalez et al. 1999), there are studies that reported the reversible breakage of the bond under elevated temperatures (Holmberg et al. 2005). Hence, we functionalised the Pierce™ Streptavidin Magnetic Beads with LNA-probes and observed the behaviour of the solution when heated at 95˚C for 10 minutes.
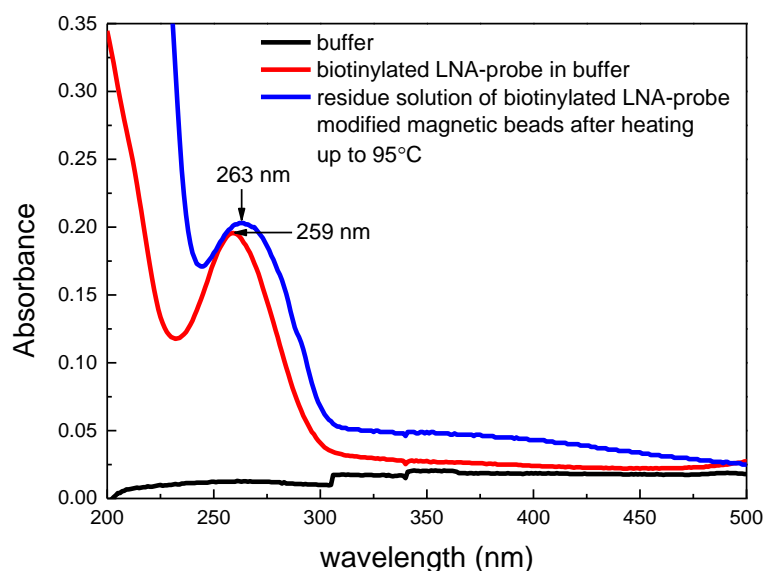
Figure 4. 3 A UV absorbance graph for blank buffer (black line), biotinylated LNA probe in buffer (red line), and the residue buffer solution after the heating up of LNA modified magnetic beads at 95˚C for 10 minutes (blue line). The absorbance levels below 230 nm were considered to be noise due to the increased absorbance of the quarts cuvette itself, upon being subjected to light at wavelengths lower than 250 nm.

Following the heating of LNA-modified magnetic beads at 95˚C for 10 minutes, UV spectrophotometry results in Figure 4.3 for the residue solution (blue line) indicated an absorbance peak at 263 nm. This value is very close to the initial absorbance peak, at 259 nm, that was obtained for the LNA probe prior to its immobilisation on magnetic beads. Such results could be attributed to the fact that under high temperature conditions, a disruption is made in streptavidin-biotin binding between the magnetic beads and the probe. This results in the discharge of the LNA-probe into solution. Additionally, the slight shift of the absorbance peak (Figure 4.3, red peak → blue peak), after the heating up of the LNA-modified beads, towards the right end of the spectrum could be attributed to the additional discharge of the streptavidin coating of the magnetic beads into solution (Stoscheck 1990). This condition was confirmed by

a second assay that analysed the residue solution of magnetic beads (without the LNA probe) before and after heat was applied.
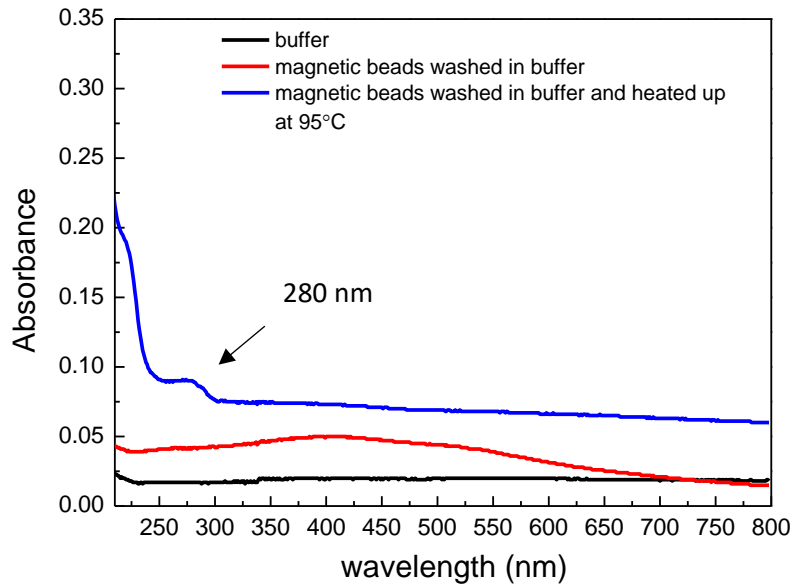
Figure 4. 4 UV absorbance graph for blank buffer (black line), residue solution of magnetic beads after being washed in buffer (red line), residue solution of magnetic beads after being washed and heated up at 95˚C for 10 minutes in buffer (blue line). The absorbance levels below 230 nm were considered as noise due to the increased absorbance of the quarts cuvette itself upon being subjected to light at wavelengths lower than 250nm.

The results in Figure 4.4 suggest no significant absorbance peak in the residue solution of magnetic beads upon being washed in buffer. This indicates no dissociation of the streptavidin coating from the magnetic beads surface upon washing. However, an absorbance peak at 280 nm was observed within the residue solution after heating up the beads to 95˚C. This could be attributed to the discharge of the streptavidin coating of the magnetic beads upon heating, and resulting in the absorbance at 280 nm that indicates the presence of proteins (Stoscheck 1990). This also explains the slight shift of the absorbance towards 280 nm (blue peak) in Figure 4.3 for the residue solution of

LNA-modified magnetic beads upon heating, as the peak corresponds to the dissociation of the LNA-probe together with the streptavidin into solution.

The results indicated the degradation of the streptavidin coating of magnetic beads upon heating and the crucial need for an alternative method for the denaturing step of the LNA probe-target miRNA duplex that eliminates heat. For this purpose, another set of assays were performed which compared the efficiency of denaturation and target release using a number of chemical methods. Four different methods were adopted: incubation with Milli-Q water (ion-free), 50% (w/w) urea solution, 60% DMSO solution and 1 M NaOH (alkaline) solution for 10 minutes at ambient temperature. Prior to the assays, the LNA-functionalised magnetic beads were incubated with each solution in order to confirm that the biotin-streptavidin bonding between the probe and the magnetic beads was not disrupted upon incubation with these solutions. Hence, the absorbance peaks observed in the residue solution after denaturation of the LNA probe functionalised magnetic beads-target miRNA can be attributed only to target release and no interference due to probe dissociation from the magnetic beads surface into solution.

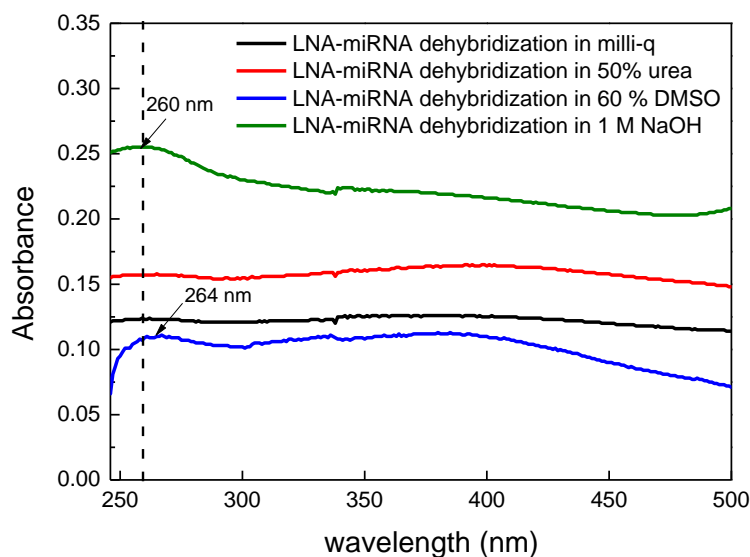**Figure 4. 5** UV-absorbance graph of the final solution of target miRNA after performing dehybridisation in Milli-Q solution (black line), in 50% (w/w) urea solution (red line), in 60% DMSO solution (blue line), and in 1 M NaOH solution

(green line) for 10 minutes. For each measurement, a baseline measurement was carried out within the solution of investigation prior to the UV-analysis. The absorbance levels below 230 nm were considered to be noise due to the increased absorbance of the quarts cuvette itself upon being subjected to light at wavelengths lower than 250nm.

As suggested by the results in Figure 4.5, a distinguishable nucleic acid absorbance peak was observed only in two cases: one with the adoption of 1 M NaOH, and one with the adoption of 60% DMSO for the denaturation of the LNA capture probe-miRNA hybrid duplex. The peak is most significant and clear at 260 nm for the case of 1 M NaOH where this peak is slightly shifted to 264 nm upon the adoption of 60% DMSO which also presented very noisy data upon being measured. Therefore, we have decided to pursue the rest of the assays by adopting 1 M NaOH as a chemical denaturation method, which presented promising results for the release of target miRNA.

Another assay was carried out for the comparison study of the expected absorbance peak of miRNA in solution, with the absorbance peak obtained after its capture and then its release into solution. Such a method would prove the presence of captured miRNA in the final solution. The results presented in Figure 4.6 revealed an absorption peak at 259 nm for the biotinylated LNA probe (Figure 4.6(a), step i), 258 nm for the target miRNA in solution before its capture (Figure 4.6(a), step ii), and 259 nm for the solution that contains the captured target miRNA that was released by chemical denaturation in 1 M NaOH solution (Figure 4.6(a), step 5). The results match closely with literature that identifies an absorbance peak at around 260 nm for the representation of nucleic acids (Tinoco et al. 1980). The presence of an absorbance peak at 259 nm in the final target solution that is very close to the initial absorbance peak of the target solution indicates a successful capture by the magnetic beads and the subsequent release into final solution. Hence, the final solution of target miRNA was utilised for its electrochemical detection with PNA-probes (Section 4.3.2) for the approval of our methodology of fishing of miRNA from solution by use of magnetic beads.

(a)
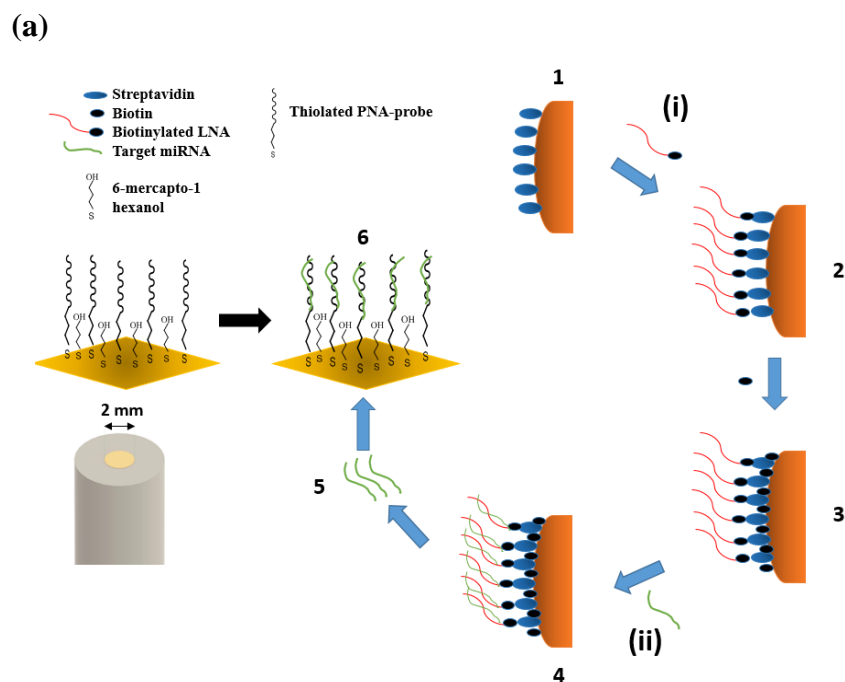
(b)
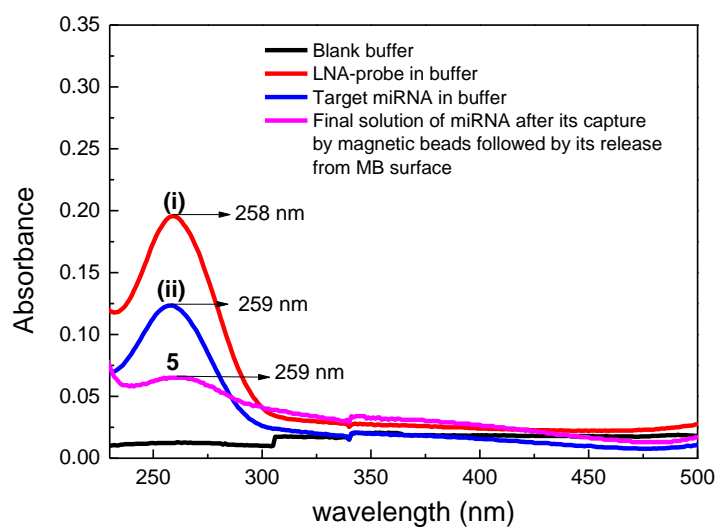
Figure 4.6 (a) Representation of the design steps (i, ii and 5) that were tested by UV spectrophotometry measurements. (b) UV absorbance of the biotinylated LNA probe (red), target miRNA (blue), and the magnetic beads captured miRNA (pink). Buffer was set as the baseline measurement (black line) of the spectrophotometer prior to UV analysis. The absorbance levels below 230 nm were considered to be noise due to the increased absorbance of the quarts cuvette itself upon being subjected to light at wavelengths lower than 250 nm.

4.3. 2 Electrochemical Impedance Spectroscopy (EIS) results

Faradaic EIS was selected for the evaluation of the stability of the fabricated PNA-probe prior to analysis with target miRNA (Figure 4.7a). PNA-probes are known for their high specificity to complementary targets and are expected to perform no hybridisation with a non-specific target. This was confirmed by an assay that was performed by incubation of PNA-immobilised electrodes with a high concentration of non-specific miRNA (1 nM) target sequences, that resulted in an R_{ct} variation of only 0.78±0.07%.

(a)

(b)
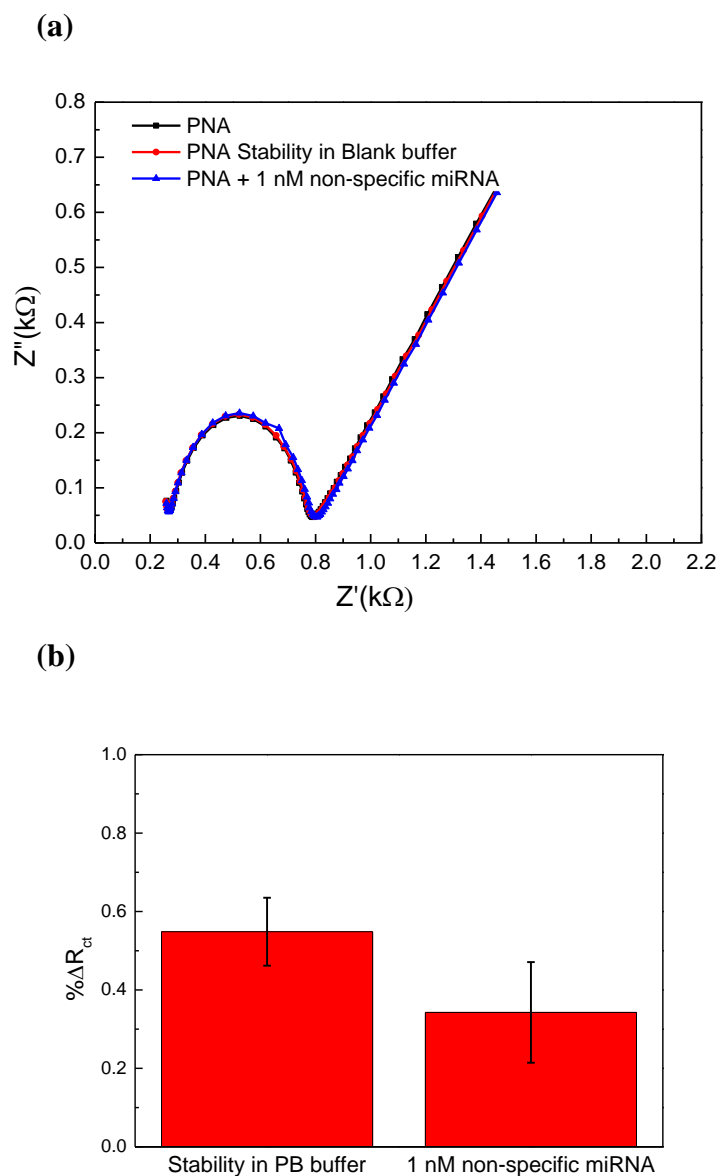
Figure 4. 7 (a) EIS characterisation of the PNA immobilised probe stability in 10 mM PB (pH 7.3) buffer followed by hybridisation in 10 mM PB (pH 7.3) that contains 1 nM non-specific miRNA. (b) Percentage variations of R_{ct} upon hybridisation of PNA immobilised probe with a non-specific miRNA target. All measurements were performed in 10 mM PB that contains 10 mM of [Fe (CN)6]$^{-3/4-}$ redox couple. Error bars represent three separate electrodes.

The next two assays were carried out in order to observe the hybridisation of the PNA-probe with the target miRNA captured by LNA-modified magnetic beads. The measurements were performed in 10 mM of [Fe (CN)6]$^{-3/4-}$ redox couple to monitor the resistance to charge flow transfer upon target binding events. The first assay adopted the solution of thermally released miRNA from the magnetics beads' surface for its hybridisation on complementary PNA probes. In previous sections we have observed that high temperatures lead to the dissociation of the streptavidin coating from the magnetic beads surface and the release of probe-LNA. Hence, upon EIS measurements no variation of R_{ct} was expected due to the lack of a target in the solution. On the other hand, the second assay eliminated the use of high temperatures and adopted a chemical denaturation method (incubation of magnetic beads containing LNA-miRNA helix in 1 M NaOH) for the release of target from the magnetic beads' surface. Hence, EIS measurements were expected to display an increased value of R_{ct} due to the presence of captured miRNA, inside the solution, that is complementary to the probe-PNA. Binding of the target to the PNA-probe is expected to increase the resistance to charge flow (R_{ct}).

(a)

(b)

Figure 4. 8 (a) EIS characterisation of the PNA immobilised probe and its stability in blank buffer followed by hybridisation with solution that contains thermally released miRNA from magnetic beads surface. (b) 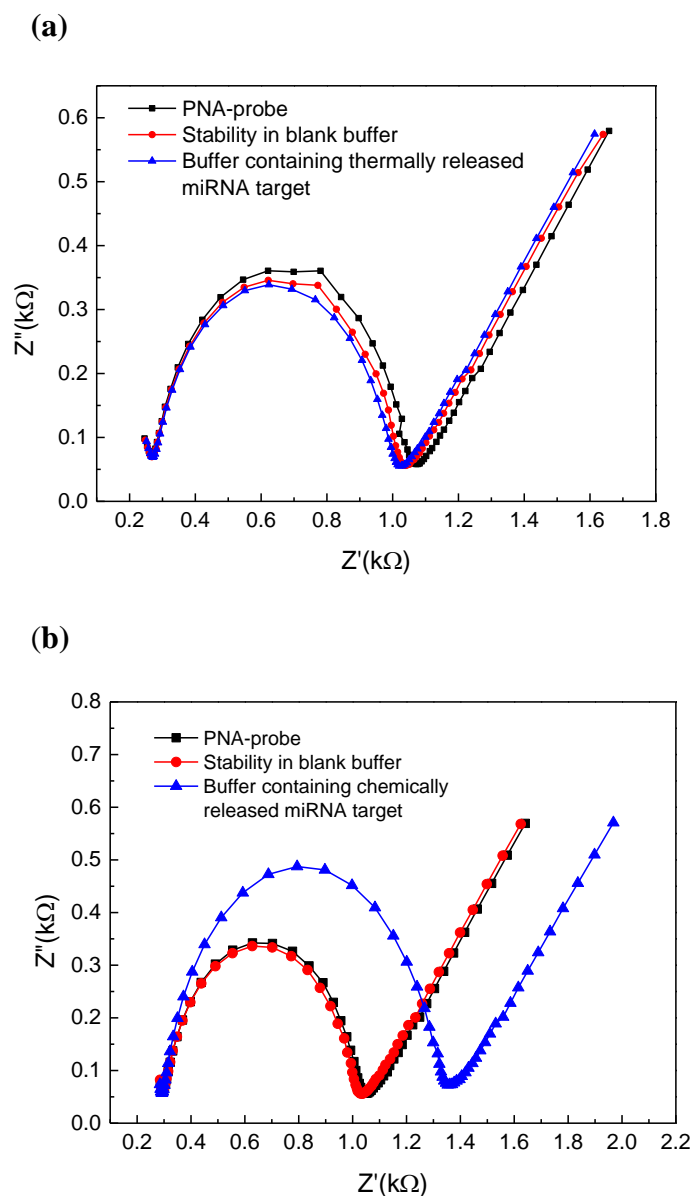EIS characterisation of the PNA immobilised probe and its stability in blank buffer followed by hybridisation with chemically released miRNA from magnetic beads surface. All measurements were performed in 10 mM PB that contains 10 mM of [Fe (CN)6]$^{-3/4-}$ redox couple. For the stability measurements, the electrodes were incubated in 10 mM PB for 30 minutes prior to measurement in redox couple.

The results given in Figure 4.8 (a) represent the measurements of the assay design that used the method of thermal denaturation for the release of target miRNA from the magnetic beads' surface. A PNA/MCH self-assembled layer with a ratio of 1:10 had an R_{ct} variation of 2.24% upon stabilisation, which reflects the formation of a stable PNA-MCH SAM. Initial incubation with the blank buffer showed no significant change of Rct (ΔRct = 3.8%), which demonstrates a strong stability of the probe before its incubation with the target. This was followed by incubation with the solution that was expected to contain the magnetic beads-captured miRNA, free in solution, upon thermal release. However, the EIS results showed almost no variation in R_{ct}, (785.6 Ω $\rightarrow$765.9 Ω, ΔRct=6.2%) upon target incubation, as shown in Figure 4.8 (a). This has once again proven the poor efficiency of thermal release, with possible disruption of the magnetic beads surface, and encourages the application of chemical denaturation methods. As a result, the assay was repeated by replacing thermal denaturation with the incubation in an alkaline solution (1 M NaOH diluted in Milli-Q). The target miRNA that was released into the alkaline solution was in turn re-hybridised with the PNA probe for EIS detection. The conditions for the re-hybridisation with the PNA probe was achieved by mixing 10 µl of the target solution (in 1 M NaOH solution) with 100 µl of 10 mM PB solution (at pH 7.3). This is necessary to represent the hybridisation buffer, and reduce the pH of the alkaline solution for the required hybridisation efficiency with the complementary PNA probe. The results shown in Figure 4.8 (b) once again suggest the strong stability of PNA-MCH SAM prior to incubation with target. In this case, a significant R_{ct} variation of 40.1% was observed after incubation with the target, which corresponds to successful hybridisation. The assay was repeated on three different electrodes in order to approve the reproducibility of detection.
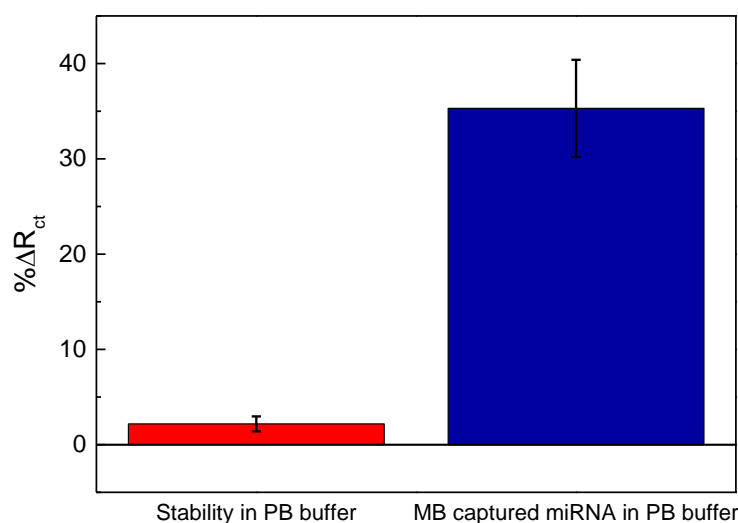
Figure 4. 9 Percentage variations of R_{ct} upon hybridisation of PNA immobilised probe with chemically released target miRNA. Error bars corresponds for the standard deviation for three separate electrodes.

The results in Figure 4.9 revealed the reproducibility of the method upon detection on three different PNA-immobilised electrodes that suggested an average R_{ct} variation of 32.4 ± 5.4 % upon hybridisation with the target miRNA. This is significantly higher than the blank buffer incubation that had an R_{ct} variation of 2.18 ± 0.78 %. Hence, our methodology of fishing for miRNA from solution by use of LNA-modified magnetic beads was proven to successfully separate the target from solution and its direct electrochemical detection on a PNA-immobilised probe.

4. 4 Conclusions

In this work, we have developed a new method for magnetic beads based electrochemical detection of miRNA that involves separation and pre-concentration of the target miRNA sample from solution, and its direct electrochemical detection on a PNA-immobilised gold electrode. By optimising the various assay steps found in the literature, we have developed an improved methodology which offers direct detection of target miRNAs with no need for pre-labelling of target sequences or enzymatic labelling on the detection probe. In an ideal world, it is crucial to develop technologies that provide accurate results without the requirement for many amplification steps. Although the literature offers various magnetic beads-based detection methodologies with great limits of detection, there is still the need for the elimination of a number of the assay steps that are not suitable for real world applications. In the healthcare industry there is a need for point-of-care testing that is simple, and offers results in a short time after patient contact. For this purpose, we have investigated the feasibility of a methodology that eliminates the need for sample preparation, hence the requirement for trained labour, or for additional signal enhancement steps. Additionally, an important and neglected aspect of miRNA detection is distinguishing between the pool of miRNA sequences which can lead to false positives in the results of patients. For this purpose, the LNA-probes that were utilised have a special affinity for complementary miRNAs, and offer improved hybridisation efficiencies. Such a property of LNA-probes was combined with the separation properties of magnetic beads so that LNA favoured capturing of target miRNA from solution was achieved. Following the capture of the target, we have carried out chemical denaturation of the hybridised LNA-miRNA helix for the release of the miRNA from the magnetic beads' surface. Then we utilised PNA-immobilised gold electrodes for the EIS based detection of miRNA, which demonstrates a significant variation in R_{ct} (32.4 ± 5.4 %) upon target incubation. We believe such a model for detection is a crucial step towards the easy fishing of miRNAs from complex solutions, such as blood, and pre-concentration of the target prior to its direct electrochemical detection for quantification. The idea can be easily translated to manufacturing by utilising the "Lab-on-chip" technology for diagnostics (Herold & Rasooly 2009; Erickson et al. 2014), which is further explained and demonstrated in Chapter 6. EIS measurements,

by using PNA-probes, revealed a strong specificity by having almost no variation in R_{ct} (0.78±0.07%) with a non-specific miRNA solution. Hence, we have demonstrated the feasibility of a methodology for the detection of miRNA, that combines the highly specific separation properties of LNA-modified magnetic beads with the sensitive and specific electrochemical detection properties of PNA-probes. To the best of our knowledge, our experimental work is the first PNA-probe based electrochemical detection study that utilises LNA-modified magnetic beads for capture and pre-concentration of miRNA prior to analysis. Up to date, direct electrochemical detection of miRNAs from complex solution, such as blood continues to be a challenge. We hope our methodology, upon further investigations, will be applicable for the detection of miRNAs expressed in circulating blood or body fluids.

References

Bartosik, M. et al., 2014. Magnetic bead-based hybridization assay for electrochemical detection of microRNA. *Analytica Chimica Acta*, 813, pp.35–40.

Bartosik, M. et al., 2013. Os (VI) bipy-based electrochemical assay for detection of specific microRNAs as potential cancer biomarkers. *Electrochemistry Communications*, 33, pp.55–58.

Belter, A. et al., 2014. Mature miRNAs form secondary structure,which suggests their function beyond RISC. *Public Library of Science One*, 9(11), pp.1–23.

Bettazzi, F. et al., 2013. Electrochemical detection of miRNA-222 by use of a magnetic bead-based bioassay. *Analytical and Bioanalytical Chemistry*, 405(2-3), pp.1025–1034.

Bruning, W. & Holtzer, A., 1961. The effect of urea on hydrophobic bonds: the critical micelle concentration of n-dodecyltrimethylammonium bromide in aqueous aolutions of Urea. *Journal of American Chemical Society*, 83(23), pp.4865–4866.

Campuzano, S. et al., 2014. Magnetobiosensors based on viral protein p19 for microRNA determination in cancer cells and tissues. *Angewandte Chemie International Edition*, 53, pp.6168–6171.

Chen, X. et al., 2008. Characterization of microRNAs in serum : a novel class of biomarkers for diagnosis of cancer and other diseases. *Cell Research*, 18, pp.997–1006.

Engman, K.C. et al., 2004. DNA adopts normal B-form upon incorporation of highly fluorescent DNA base analogue tC : NMR structure and UV-Vis spectroscopy characterization. *Nucleic Acids Research*, 32(17), pp.5087–5095.

Erdem, A., Congur, G. & Eksin, E., 2013. Multi channel screen printed array of electrodes for enzyme-linked voltammetric detection of MicroRNAs. *Sensors & Actuators: B. Chemical*, 188, pp.1089–1095.

Erickson, D. et al., 2014. Smartphone technology can be transformative to the deployment of lab-on-chip diagnostics. *Lab on a Chip*, 14, pp.3159–3164.

Gogotsi, Y.G. & Uvarova, I. V. eds., 2003. *Nanostructured Materials and Coatings for Biomedical and Sensor Applications*, Kluwer academic publishers.

Gonzalez, M., Argaran, C.E. & Fidelio, G.D., 1999. Extremely high thermal stability of streptavidin and avidin upon biotin binding. *Biomolecular Engineering*, 16, pp.67–72.

Herold, K.E. & Rasooly, A., 2009. *Lab on a chip Technology: Volume 1 Fabrication and Microfluidics*, Caister Academic Press.

Herskovits, T.T., 1963. Nonaqueous solutions of DNA ; denaturation by urea and its methyl derivatives. *Biochemistry*, 2(2), pp.335–340.

Holmberg, A. et al., 2005. The biotin-streptavidin interaction can be reversibly broken using water at elevated temperatures. *Electrophoresis*, 26, pp.501–510.

Jolly, P. et al., 2015. A simple and highly sensitive electrochemical platform for detection of microRNAs. *Institute of Electrical and Electronics Engineers Sensors*, pp.803–806.

Jolly, P. et al., 2016. Highly sensitive dual mode electrochemical platform for microRNA detection. *Scientific Reports*, 6(36719).

Katz, E., Willner, I. & Wang, J., 2004. Electroanalytical and bioelectroanalytical systems based on metal and semiconductor nanoparticles. *Electroanalysis*, 16(2), pp.19–44.

Keighley, S.D. et al., 2008a. Optimization of DNA immobilization on gold electrodes for label-free detection by electrochemical impedance spectroscopy. *Biosensors and Bioelectronics*, 23, pp.1291–1297.

Keighley, S.D. et al., 2008b. Optimization of label-free DNA detection with electrochemical impedance spectroscopy using PNA probes. *Biosensors and Bioelectronics*, 24, pp.906–911.

Laschi, S. et al., 2009. Enzyme-amplified electrochemical hybridization assay based on PNA , LNA and DNA probe-modified micro-magnetic beads. *Bioelectrochemistry*, 76(1-2), pp.214–220.

Lawrie, C.H. et al., 2008. Detection of elevated levels of tumour-associated microRNAs in serum of patients with diffuse large B-cell lymphoma. *British Journal of Haematology*, 141, pp.672–675.

Levy, M. & Magoulas, J.P., 1961. Effect of urea on hydrogen bonding in some dicarboxylic acids. *Journal of the American Chemical Society*, 84(8), pp.1345–1349.

Mitchell, P.S. et al., 2008. Circulating microRNAs as stable blood-based markers for cancer detection. *Proceedings of the National Academy of Sciences USA*, 105(30), pp.10513–10518.

Natsume, T. et al., 2007. Hybridization energies of double strands composed of DNA , RNA , PNA and LNA. *Chemical Physics Letters*, 434, pp.133–138.

Okonogi, T.M. et al., 2002. Phosphate backbone neutralization increases duplex DNA flexibility : A model for protein binding. *Proceedings of the National Academy of Sciences*, 99(7), pp.4156–4160.

Palecek, E. & Fojta, M., 2007. Magnetic beads as versatile tools for electrochemical DNA and protein biosensing. *Science Direct*, 74, pp.276–290.

Shen, L., Zhang, X. & Jin, W., 2012. Signal amplification based on DNA hybridization – dehybridization reaction on the surface of magnet submicrobeads for ultrasensitive DNA detection. *Analyst*, 137, pp.4849–4854.

Silva, E.T.S.G. da et al., 2017. Electrochemical Biosensors in Point-of-Care Devices : Recent Advances and Future Trends. *ChemElectroChem*, 4, pp.778–794.

Stoscheck, C.M., 1990. [6] Quantification of protein. *Methods in Enzymology*, 182, pp.50–68.

Tinoco, I., Bustamante, J. and C. & Maestre, M.F., 1980. The optical activity of nucleic acids And their aggregates. *Annual Review of Biophysics and Bioengineering*, 9, pp.107–41.

Vargas, E. et al., 2017. Magnetic beads-based sensor with tailored sensitivity for rapid and single-step amperometric determination of miRNAs. *International Journal of Molecular Sciences*, 18(2151).

Wang, J. et al., 2002. Genomagnetic electrochemical assays of DNA hybridization. *Talanta*, 56, pp.931–938.

Wang, J. et al., 2001. Magnetic bead-based label-free electrochemical detection of DNA hybridization. *Analyst*, 126, pp.2020–2024.

Wang, X., Lim, H.J. & Son, A., 2014. Characterization of denaturation and renaturation of DNA for DNA hybridization. *Environmental Health and Toxicology*, 29, pp.1–8.

Wang, X. & Son, A., 2013. Effects of pretreatment on the denaturation and fragmentation of genomic DNA for DNA hybridization. *Environmental Science Processes & Impacts*, 15, pp.2204–2212.

Wang, Z. et al., 2013. A novel electrically magnetic-controllable electrochemical biosensor for the ultra sensitive and specific detection of attomolar level oral cancer-related microRNA. *Biosensors and Bioelectronics*, 45, pp.108–113.

Zhang, X. et al., 2009. Ultrasensitive electrochemical DNA assay based on counting of single magnetic nanobeads by a combination of DNA amplification and enzyme amplification. *Analytical Chemistry*, 81(5), pp.8083–8089.

Chapter 5 Redox-tagged peptide supported SAM for direct capacitive assaying

In this chapter, we report on the adoption of a redox-active self-assembled monolayer for direct and capacitive based recognition of the target binding. The methodology can significantly benefit electrochemical biosensing platforms due to the redox active nature of the SAM. Incorporation of a peptide possessing ferrocene moieties that has self-assembling capability to metal surfaces, for the recognition of target biomolecules, has proven to be a success in previous studies. Hence, our methodology modifies the existing method for its use with PNA probes for the detection of DNA which can eventually be adapted for miRNA detection. This is mainly due to DNA being less vulnerable to RNAse degradation than miRNA, which provides an advantage when performing optimisation studies. If successfully implemented, such a methodology comes with the major advantage of eliminating the need for the doping of the measurement solution with redox active ions, and it offers a direct and sensitive capacitive based recognition of the target that is more applicable for real sensor devices. The work presented in this chapter has fostered collaboration with the Nanobionics Research Group in São Paulo State University, who have synthesised the ferrocene-tagged peptide utilised in our studies. The entirety of the experimental work presented in this chapter, including the fabrication of the sensor surface, electrochemical measurements and the SPR measurements was carried out by the author. A specific level of roughness of the electrode surface had been a crucial factor for obtaining optimum immobilisation of the peptide. Additional investigations were carried out for maintaining it below a certain value in all measurements. Additional work is not presented for the sake of clarity, and to ensure we maintain confidentiality with our collaborators.

5. 1 Background

Advancing beyond blood glucose analysis, electrochemical biosensors are becoming a prominent alternative for point-of-care applications due to being easy to miniaturise (Moschou & Tserepi 2017), integrate with mobile devices (Roda et al. 2016; Zhang et al. 2016), their low power requirements and ease of use. There is currently an increasing interest in the possibility of nucleic acids and protein markers reporting on diseases at early stages, before any symptoms arise (Santos et al. 2014). Although a wide range of strategies exist for their detection (optical methods such as Colorimetric, Surface Plasmon Resonance, Optical Microarray, ELISA, Interferometry and mass sensitive platforms such as Quartz Crystal Microbalance) (Haab 2003; Homola 2008; Ray et al. 2010; Speight & Cooper 2012; Santos et al. 2014), these methods either require target labelling, te utilisation of an appropriate sandwich form, rely on specific induced variation in excitable surface plasmons or modification with nanoparticles for increased sensitivity. However, electrochemical methods are known for possessing a high sensitivity and are readily scalable at a low cost. In addition, there is a significantly growing body of work in label free approaches in electrochemical platforms that can achieve high levels of selectivity via controlled interfacial chemistry (Santos et al. 2014; Santos et al. 2015; Fernandes et al. 2015; Piccoli et al. 2016; Piccoli et al. 2018).

In the past, a vast range of strategies have been suggested for the improvement of electrochemical sensor performance for oligonucleotide detection. A few examples include label-based methods which involve the adoption of electroactive markers such as redox indicators and intercalators, nanoparticles, quantum dots and enzymes (Pumera et al. 2005; Pan 2007; Wei et al. 2011; Jolly et al. 2016; Gaiji et al. 2017). Along with improving the sensor performance by such methods, self-assembly approaches were adopted to modify the surface for advanced detection. As an alternative surface, studies were conducted that designed a mixed SAM as a potential electroanalytical assay platform for point-of-care applications. The mixed SAM is composed of a redox layer with an antibody receptive component that comes on top for the purpose of redox capacitive detection for the recognition of target molecules (Santos et al. 2015; Fernandes et al. 2015; Piccoli et al. 2018). Our experimental work

in this chapter adopts a similar methodology and benefits from the redox properties of ferrocene that is integrated within the SAM. Such a strategy aims to eliminate the need for labelling the target or for additional steps, such as the use of intercalators for signal amplification. A faradaic probe is developed with a molecular layer of ferrocene-tagged peptides that offers the sensitive label-free recognition of a target in solution. It is stated in recent literature that the redox activity of a confined group leads to the formation of an interfacial charging signal that is detected by an EIS derived complex capacitance (C_r) signal (Santos et al. 2014). Such a signal depends heavily upon its electrostatic environment. In this case the C_r of a surface confined electroactive film does not depend on its dimensions, but rather on the redox centre energy levels and occupancy (Bueno et al. 2012; Bueno et al. 2013). Hence, such a methodology eliminates the need for pre-labelling of the target and the need for doping of the measurement solution with redox active ions. If the methodology is coupled successfully with PNA-probes, it will allow for the label-free and sensitive detection of DNA/miRNA targets that is more applicable in the development of point-of-care technology.

5.1. 1 Redox active peptide for capacitive diagnostic assays

This section will introduce the methodology behind the development of a platform that contains redox active elements built inside the SAM layer that offers capacitive based direct analysis of target binding. In order to obtain such an electrochemically active capacitive interface, studies in literature introduced the synthesis of a peptide bearing a ferrocene (fc) molecular (redox) group, which comes with the sequence Fc-Glu-Ala-Ala-Cys, via solid phase peptide synthesis (Piccoli et al. 2018). In order to achieve the self-assembling capability together with the electrochemically active capacitive response of the peptide, the side chain of cysteine (Cys) was covalently bound to the gold electrode (via sulphur groups) and the side chain of glutamic acid (Glu) was used to attach the ferrocene in the peptide chain (Piccoli et al. 2018). The redox-tagged peptide was immobilised on the gold electrode and a recognition probe was attached onto the peptide via the activation of the terminal carboxyl group of the glutamic acid side chain of the peptide (Piccoli et al. 2016; Piccoli et al. 2018). Such a methodology establishes a Faradaic probe that offers sensitive and label-free recognition of a target

in solution (Bueno et al. 2012; Santos et al. 2015; Piccoli et al. 2018). The strategy is based upon mapping the perturbations in the interfacial charging of the redox elements incorporated in the SAM after the binding of the target.

The methodology adopts impedance based electrochemical capacitance spectroscopy (ECS), that has shown to be a convenient and highly sensitive mode of detection among the broad range of label free electronic biomarker assay methodologies currently available (Santos et al. 2014; Fernandes et al. 2015; Piccoli et al. 2016).

The main difference between Faradaic and non-Faradaic impedance approaches is the requirement for redox doping of the measurement solution. In non-Faradaic mode, the assessment is made not through the changes in the resistance to charge transfer in solution, but through the variation of double layer capacitance, C_{dl}, that is a measurable quantity and observed to be very sensitive to interfacial variations. Such a variation is observed, for instance, when a target protein attaches to a receptor that is already immobilised on an electrode surface and displaces water and ions from the surface (Tkac & Davis 2009), or as a result of the conformational change of a protein after the binding of an analyte (Berggren et al. 2001). The capacitive behaviour of the biorecognition surface in non-Faradaic mode can be described as a combination of two capacitances: C_m that refers to an insulating layer comprised of a SAM and double layer, and C_{rec} that corresponds to the biorecognition layer. A third layer of C_a is generated upon the binding event of a target.
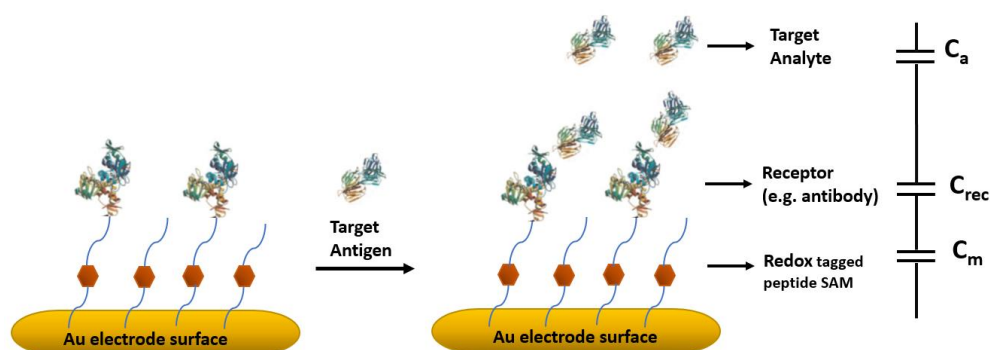

Figure 5. 1 Schematic representation of a traditional capacitive biosensor. The capacitive behaviour can be explained in three capacitors: the one due to the

insulating layer (C_m), the one due to receptive layer (C_{rec}) and the final one due to the biorecognition layer (C_a).

Hence, the total capacitance is given as followed:

$$\frac{1}{C} = \frac{1}{C_m} + \frac{1}{C_{rec}} + \frac{1}{C_a}$$

Equation 5. 1

According to Equation 5.1, the lowest element dominates the total capacitance. This is crucial for the sensor design based on capacitive measurements as the capacitance of the insulating layer must be as high as possible to allow one to detect changes in the system as a result of target binding (Berggren et al. 2001). In addition, the construction of an impermeable insulating layer to ions in solution will lead to the prevention of signal loss (Berggren et al. 2001).

The studies adopted capacitive approaches commonly used in aptamers and antibodies as recognition elements (Berggren & Johansson 1997; Limbut et al. 2006a; Limbut et al. 2006b). For instance, one of the methodologies immobilised a specific antibody (MD-2) above SAM on a gold electrode surface for the detection of a biomarker for autoinflammatory (and autoimmune) diseases that is called interferon-γ. The study revealed a direct detection of the protein interferon-γ at attomolar levels (Dijksma et al. 2001).

Placing a voltage polarised metallic interface, containing a molecular film with a redox active entity, into an electrolyte results in two contributions to capacitance. The initial contribution is due to the double layer capacitance that results from the contact of the metal interface with solution. The second contribution to capacitance is due to the presence of an element within the molecular film that can be Faradaically charged (redox active) and termed as pseudocapacitance, C_r (Santos et al. 2014). Although the magnitudes of these two capacitive elements are sensitive to surface and solution composition, pseudocapacitance is known to be considerably higher. Very recent studies performed measurement of this capacitance, that can be also referred as redox capacitance (C_r) through impedance-derived electrochemical spectroscopy, ECS (Santos et al. 2015; Piccoli et al. 2018).

This impedance derived capacitance (C_r) is in fact composed of two distinct contributions (Santos et al. 2014):

$$\frac{1}{C_r} = \frac{1}{C_e} + \frac{1}{C_q}$$

Equation 5. 2

Where C_e is attributed to the electrostatic or geometrical capacitance that is a result of charge separation in the normal sense and can be simply defined as $C_e = dq/dV$ (where q is the net charge and V represents the potential). C_q on the other hand is the quantum capacitance that arises specifically from the variations of chemical potential changes associated with charging a nanoscale mesoscopic entity. The pseudocapacitance (C_r) is associated with surface confined redox events and is a representation of a specific manifestation of the general mesoscopic capacitance principles reported by Marcus Büttiker (Büttiker et al. 1993).

The quantum capacitance (C_q) is explicitly defined with the following formula (Bueno & Davis 2014):

$$\frac{1}{C_q} = \frac{1}{e^2} \left(\frac{1}{g_m(E)} + \frac{1}{g_r(E)} \right)$$

Equation 5. 3

Where g_m represents the energy density of states in metal and g_r represent that of the molecular density of states chemically attached over the electron reservoir. The quantum capacitance, C_q, arises explicitly from the chemical potential variations associated with charging a nanoscale mesoscopic entity (Büttiker et al. 1993). In such an approach, since $q_m(E) \gg q_r(E)$, as the electronic density states in the metal are much higher compared to those associated with the molecular redox states chemically attached over the electron reservoir, the formula simplifies to $C_q = e^2 g_r$ (Bueno & Davis 2014). We can further define g_r by a Gaussian redox density of states:

$$g_r(\mu_e) = \frac{1}{\sigma\sqrt{2\pi}} \exp\left[-\frac{(E_r - \mu_e)}{2\sigma^2} \right]$$

Equation 5. 4

where σ refers to standard deviation (and σ^2 the variance) of the multiple possible energetic states.

The reported studies in literature have shown that the element of C_r is sensitive to the local environment (Fernandes et al. 2014) and any variations in redox site occupancy should be experimentally reported through C_r. In other words, the hypothesis states that any local change in the dielectric constant or electrostatics will result in perturbation of the charging fingerprint in a detectable manner (Lehr et al. 2014). Hence, if one manages to couple this ability within a selective target-recruiting molecular film, then one can generate a feasible sensor that eliminates the need for target labelling or solution doping with redox markers. A number of studies were recently performed which show the resolved C_r charging element can be effectively adopted as a transduction of biological recognition events (Bedatty et al. 2013; Fernandes et al. 2014; Lehr et al. 2014).

The C_r signal is resolved from electrochemical impedance spectroscopy, $Z^*(\omega)$, which is converted to capacitance by using the mathematical relationship $C^*(\omega)=1/j\omega Z^*(\omega)$ where ω is the angular frequency and $j =\sqrt{-1}$ (Goes et al. 2012) (Bueno et al. 2012). Any change in the environment of redox tethered sites leads to a change in the storage capability of the peptide-SAM layer with a resulting change in C_r. The behaviour was demonstrated experimentally in recent studies for the label-free detection of C-reactive protein (CRP) (Bedatty et al. 2013), by utilising a mixed SAM that contains a tethered redox probe (11-ferrocenyl-undecanethiol) pentadecanethiol on which the receptive antibodies were physisorbed. This same methodology was further approved in additional studies (Johnson et al. 2012; Bryan et al. 2013).

Prior to any impedance derived capacitive analysis with such a redox active molecular layer, it is required to adopt cyclic voltammetry in order to approve the Faradaic activity and identify the potential windows of maximum redox activity (the half wave potential $E_{1/2}$) and redox inactivity (E_{out}) (Santos et al. 2015; Fernandes et al. 2015; Piccoli et al. 2018). This provides one with the analysis of maximal and minimal capacitive analysis. Following that, comes the electrochemical impedance spectroscopy (EIS) measurement over a range of frequencies (10 mHz – 1 MHz)

within the potential windows of redox activity and inactivity. In EIS measurements, a modulating potential $[V(t) = V_o \sin(\omega t)]$ (where V_o is the maximum voltage, t is the time, and ω is the angular frequency) is applied and the resulting sinusoidal current response of the system is monitored $[I(t) = I_o \sin(\omega t + \phi)]$ (where I_o is the maximum current and ϕ is the phase shift) which allows one to derive various functions such as impedance (Z^*). Hence, the impedance can be converted to capacitive data ($C^* = 1/j\omega Z^*$) (Santos et al. 2014).

In this chapter we will introduce an experimental study that couples the capacitive sensing ability of a ferrocene tagged peptide SAM with highly specific PNA probes for the detection of a target DNA sequence that is specific to Human Pathogen Clostridium difficile {Formatting Citation} (Joshi et al. 2014). If the successful demonstration of the methodology is achieved for DNA detection, then the methodology can be further adapted for miRNA detection that will offer a label-free alternative for the detection of circulating miRNAs.
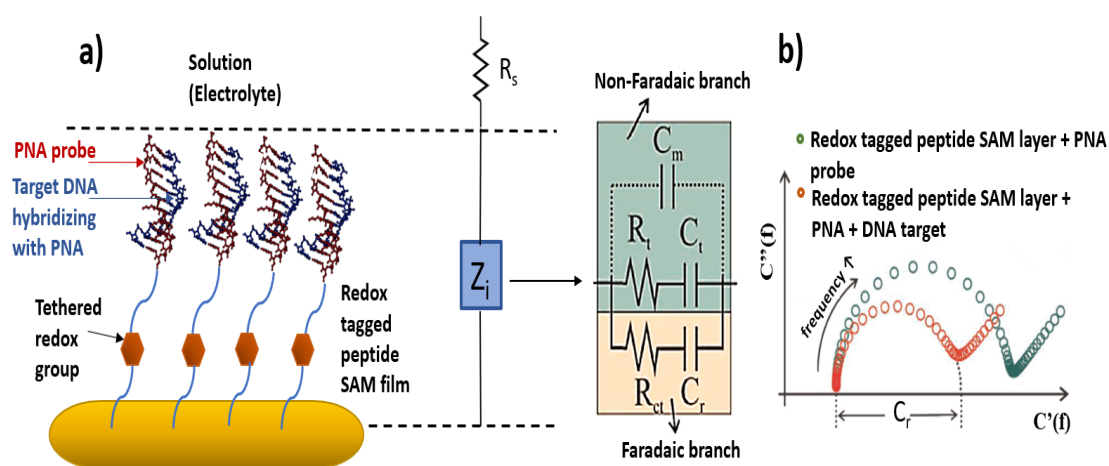
Figure 5. 2 (a) Schematic representation of the redox-tagged peptide SAM layer with PNA probe immobilised on top that captures the target DNA through hybridisation. The schematic of the methodology is recreated for DNA detection by using PNA-probes (Santos et al. 2015; Piccoli et al. 2016). Z_i and R_s represent the interfacial impedance and the solution resistance respectively of a generic receptive interface used in capacitive biosensing. Supportive SAM contains a tethered redox group that

represent the Faradaic branch and able to store charge in the electrode-solution interface. Sensing/receptive probe (PNA) is attached on top that is complementary to target DNA (specific to C.difficile bacteria). Appropriate equivalent circuit capable of modelling electrochemical capacitive biosensors is comprised of two series capacitances: that of the monolayer (C_m) and of the double layer (C_{dl}) where $C_{dl} \gg C_m$ which means the domination of C_m in the analysis and is represented in the circuit (Bueno et al. 2012; Bueno et al. 2013). The resistive (R_t) and capacitive (C_t) terms represent the ideal response of the dipolar layer (since $C_m \ll C_t$, consequently R_t and C_t control the monolayer dielectric (ionic) response (Santos et al. 2015). In contrast the faradaic response is controlled by R_{ct} (charge transfer resistance) and C_r (redox capacitance). (b) C_r can be directly determined from the diameter of the semi-circle of the capacitance Nyquist plot.

5. 2 Materials and methods

5.2. 1 Chemical reagents

The redox-tagged peptide with the sequence Fc-Glu-Ala-Ala-Cys was synthesised via solid phase peptide synthesis by using standard methods provided in literature (Piccoli et al. 2018). All solvents and chemicals unless, otherwise stated, were of analytical grade and purchased from Sigma Aldrich (UK).
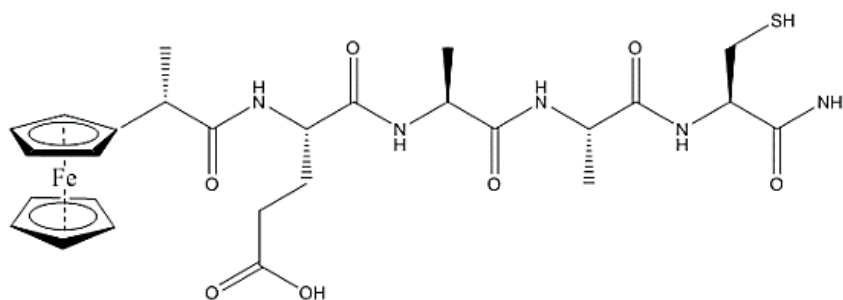

Figure 5. 3 Chemical structure of the redox (ferrocene) tagged peptide (Piccoli et al. 2018). The thickness of the peptide SAM was resolved by ellipsometry as 1.80 ± 0.03 nm.

5.2. 2 Oligonucleotides

The HPLC purified PNA probe sequence was purchased from Cambridge Research Biochemicals, UK in lyophilised form. The synthetic DNA sequence that is specific to Human Pathogen Clostridium difficile (Joshi et al. 2014) was purchased from Sigma Aldrich, UK. The sequences are shown in Table 5.1 below.

Table 5. 1 List of PNA probe and complementary DNA sequence used in this work.

PNA probe:	(N term) - NH_2 - TTT TTT TTA ATA CTA ACA CTG C - (C term)
DNA sequence (49 bases), *specific to C. difficile bacteria*	3'-AAA TTA TGA TTG TGA CGT AAT CCC AAT ACA ACG TCA ATG ACC TAC CGT T - 5'

5.2. 3 Electrode surface preparation for CV and EIS measurements

A gold working electrode was first mechanically polished on a polishing pad for at least 5 minutes with aluminium oxide with decreasing particle size (starting with 1μm, then 0.3 μm and finishing with 0.05 μm). Between each step, the electrode was rinsed with Milli-Q water and sonicated in Milli-Q for 2 minutes in order to remove adhered particles. Cyclic voltammetry was then carried out on the electrode surface for the reduction of surface oxides, by using 0.5 M KOH solution (-0.3 V to -1.6 V at a scan rate of 100 mV s^{-1}) for 75 scans, which was followed by electrochemical cleaning in 0.5 M H_2SO_4 (-0.2v to 1.5 V at 100 mV·s^{-1}) until stabilisation of the gold reduction peak in CV was obtained (25 scans). Additional CV was carried out in 0.5 M H_2SO_4 by setting the potential from 0.2 to 0.6 V at 100 mV·s^{-1} for 10 scans. This final CV was performed in order to assure a capacitive current that is not higher than 0.6 μA at 0.3 V vs. Ag|AgCl. Following the electrochemical cleaning, the electroactive areas were evaluated by mathematical integration of the cathodic peak with the potential from voltammograms for electrode cleaning, by using a conversion factor of 410

μC.cm^{-2} (Santos et al. 2015). The roughness factor was controlled by maintaining it below 1.7 in all measurements.

The biosensor was prepared by the immersion of a clean gold electrode in a solution containing 2 mM of redox-tagged peptide in H$_2$O/ACN (1:1) for 16 h (at 4˚C). After being thoroughly rinsed with Milli-Q water, the carboxyl groups of the glutamic acid side chain were activated with an aqueous solution of 0.4 M N-(3-(dimethylamino)-propyl)-N'-ethylcarbodiimide (EDC)/ 0.1 M N-hydroxysuccinimide (NHS) for 30 minutes. The activated electrodes were then rinsed with Milli-Q water followed by a second rinse in 50% DMSO and then immediate incubation with 1 μM of PNA probes (prepared in 50% DMSO) for 2 hours at room temperature. At the end of the PNA-probe immobilisation (via covalent bonding between the amino group terminated PNA and the activated carboxyl group of the peptide glutamic acid side chain), the electrode was rinsed with Milli-Q followed by measurement buffer. Then CV and EIS were performed to confirm the successful immobilisation. This was followed by 0.1% BSA (bovine serum albumin) solution incubation for 1 hour at room temperature to eliminate any active carboxyl groups.

5.2. 4 Electrochemical measurements

Electrochemical measurements were conducted in a cell that contains 20 mM tetrabutylammonium perchlorate (TBAClO$_4$) as a supporting electrolyte dissolved in acetonitrile and water (1:4 (v/v)). The supporting analyte was replaced with 10 mM of PB (pH 7.3) for only the final set of EIS experiments as required. CV was performed at a scan rate of 100 mV·s^{-1} between -0.2 V and 0.7 V relative to Ag|AgCl. Electrochemical impedance spectroscopy measurements were carried out in the ac frequency range of 100 kHz to 0.1 Hz with a 10 mV amplitude (peak to peak). The dc bias was set to the formal potential of the ferrocene redox-tagged peptide determined by CV prior to running EIS measurements (i.e. 0.363 V relative to Ag|AgCl). Impedance derived capacitance analysis adopted the mathematical relationship $C(\omega)^* = 1/j\omega Z(\omega)^*$, where ω is the angular frequency (Bueno et al. 2012).

5.2. 5 Preparation of gold sensor chip for SPR measurements

The gold sensor chip was sonicated in acetone, ethanol and Milli-Q water respectively for 3 minutes. Following the sonication, the chip was dried under a nitrogen pump followed by UV/Ozone cleaning for 30 minutes. Then the clean gold surface was covered completely with 2 mM of redox-tagged peptide in H_2O/ACN (1:1) and placed inside a chamber in order to prevent evaporation of the sample. The incubation was carried out for 16 h. In the end, the chip was rinsed thoroughly with H_2O/ACN (1:1) followed by a rinse with Milli-Q water. The carboxyl groups of the glutamic acid side chain were activated by incubating the chip with an aqueous solution of 0.4 M N-(3-(dimethylamino)-propyl)-N'-ethylcarbodiimide (EDC)/0.1 M N-hydroxysuccinimide (NHS) for 30 minutes. Then the chip was rinsed thoroughly with Milli-Q water and dried under nitrogen for SPR measurements.

5.2. 6 SPR measurements

SPR measurements were carried out using a Reichert SPR 7000DC dual channel flow spectrometer at 25°C. The measurement buffer, 10 mM PB (pH 7.3), was filtered through 0.2 μm filters, and degassed for 2 h by sonication before the measurements. 500 µl of 1 µM PNA probe, 0.1% BSA and 100 nM DNA target were prepared separately in 10 mM PB (pH 7.3). These incubation samples were degassed prior to injecting into the SPR in order to avoid the formation of any bubbles within the system. The peptide-SAM modified chip was placed under the SPR module for the measurements and was injected with 1 µM PNA probe for 30 minutes under a flow rate of 8 µL/min. Then the chip was washed with buffer, 10 mM PB (pH 7.3), under a flow rate of 25 µL/min for 10 minutes for the dissociation of any unbound molecules and until a stable baseline was achieved. This was followed by the injection of 0.1% BSA for 7 minutes and then a wash under buffer until reaching stabilisation again. After stability was achieved, the chip was injected with three rounds of blank samples followed by a target concentration, where each incubation was carried out for 7 minutes under a flow rate of 25 µL/min. A wash under buffer was carried out for 10 minutes after each incubation for the dissociation of any unbound molecules.

5. 3 Results and discussion

5.3. 1 Cyclic voltammetry (CV) analysis of electrochemical activity of peptide SAM

The electrochemical characterisation of the redox-tagged peptide was performed by the self-assembly of the peptide to the gold electrode and measuring cyclic voltammetry responses in the presence and absence of the peptide. The ability of the synthesised peptide to attach on gold is expected to occur due to the presence of a thiol group in the Cys residue. Figure 5.4 displays the comparison of cyclic voltammetry results for the bare gold electrode surface and the electrode surface when immobilised with redox-tagged peptide overnight. There is a clear appearance of oxidation and reduction peaks associated with the ferrocene/ferrocenium (Fc/Fc^1) redox coupling activity. The CV response resulted in an associated half-wave potential (E_{in} or $E_{1/2}$) of 0.363 V relative to the Ag|AgCl reference electrode, that agrees closely with the value reported in literature (Piccoli et al. 2018). The difference between the oxidation and reduction potential peaks is 22 mV and the ratio between anodic (j_{pa}) and cathodic (j_{pc}) current is almost a unit ratio. Such results can be attributed to the successful attachment of redox-tagged peptide onto the gold electrode surface and performing typical redox reversible processes (Piccoli et al. 2018).
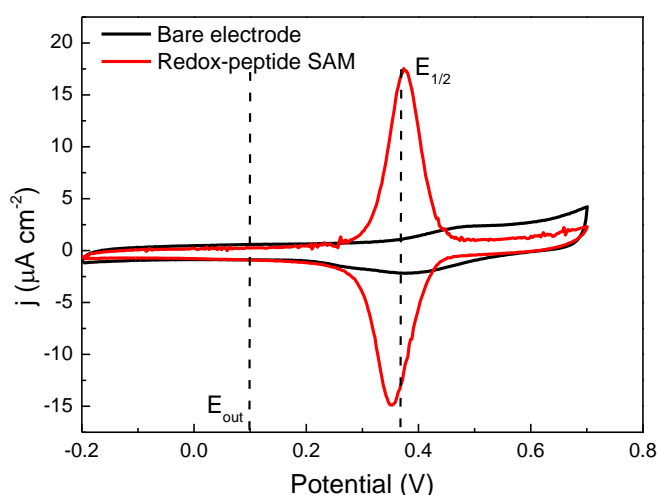

Figure 5. 4 Cyclic Voltammetry response of redox-charging peptide-aptamer SAM and its comparison to bare gold electrode. Dashed lines placed on the graph represent

the potentials for non-faradaic (0.1V) and faradaic (0.363 V) outputs. CV measurements were carried out in 20 mM TBACl04 in ACN/H$_2$O 1:4 at a scan rate of 100 mV·s^{-1}.

(a)   **(b)**
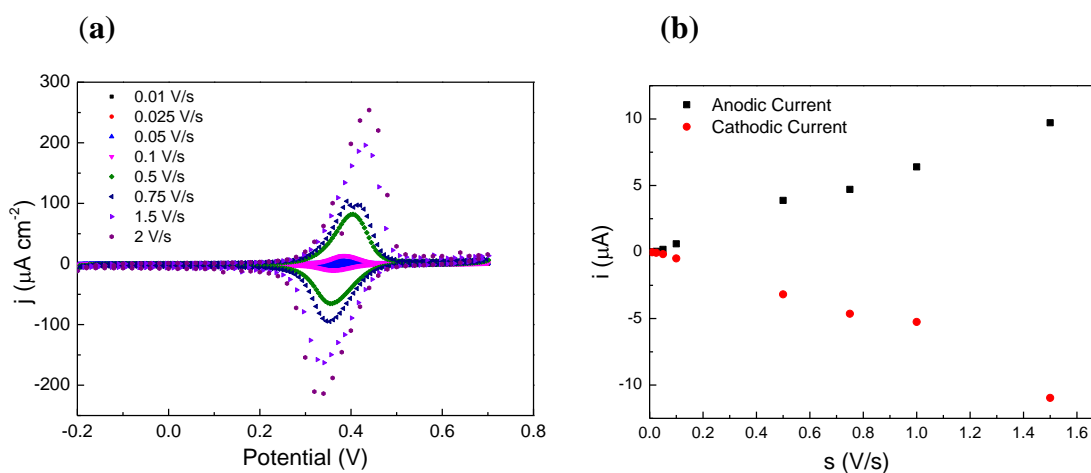

Figure 5. 5 Additional CV measurements at different scan rates where anodic and cathodic peak currents were observed for further approval of reversibility of the peptide SAM system (a) Cyclic voltammetry graph of the peptide SAM at various scan rates (b) Anodic and cathodic peak currents for peptide SAM at various scan rates.

The reversibility of the redox activity of the peptide SAM was further approved by repetitions of the cyclic voltammetry measurements upon using various scan rates (Figure 5.4). The resulting anodic and cathodic peak currents for each scan rate were compared in a graph displayed in Figure 5.5 (b) which put the ratio between anodic (j_{pa}) and cathodic (j_{pc}) current close to a unit ratio for each scan rate.

The molecular surface density can be quantified from cyclic voltammetry by measuring the oxidative charge associated with ferrocene oxidation (Piccoli et al. 2018). The positive peak area in Figure 5.3 divided by the scan rate of 100 mV s^{-1} corresponds to the oxidative charge (Trasatti & Petrii 1991):

$$\text{Oxidative Charge, } Q = \frac{1}{s} \int i.\, V'\, dV' \qquad\qquad \textbf{Equation 5. 5}$$

Electrochemical surface area (ESA), A_e in cm^2, is then (Trasatti & Petrii 1991) (Santos et al. 2015) :

$$\text{ESA, } A_e = \frac{Q}{410 \text{ X } 10^{-6}}$$ **Equation 5. 6**

The molecular surface coverage is then evaluated (Γ, mol cm^{-2}) as:

$$\Gamma = \frac{Q}{F \text{ x } A_e}$$ **Equation 5. 7**

Where, F is Faraday's constant (9.649 x 10^4 $Cmol^{-1}$) and A_e is the electrochemical surface area.

Hence, the molecular surface density was evaluated to have a value of 1.33 x 10^{-10} mol.cm^{-2} which is in agreement with the prior reports for peptide SAM on a gold surface (Gatto et al. 2012; Piccoli et al. 2018). The slightly lower value in comparison with the expected theoretical values reported in literature for cysteine-anchored peptide SAMs could be attributed to the fact that the theoretical values for the surface molecular coverage are usually higher due to the assumption of vertical orientation and a close hexagonal packing of helical peptides (Gatto et al. 2008). However, in reality peptide SAMs are never perpendicularly oriented and their axis has a tilt angle of 30−60° with respect to the surface (Kai et al. 2008; Okamoto et al. 2009; Piccoli et al. 2018).

5.3. 2 Electrochemical impedance spectroscopy analysis of immobilisation of peptide SAM and its stability

Following the studies of the peptide SAM on gold using cyclic voltammetry, further investigation of the SAM immobilisation was made using electrochemical impedance spectroscopy. The hypothesis of this study is that the redox properties of the peptide SAM, when resolved by impedance derived capacitance techniques, is capable of the sensitive reporting of the binding of biological targets (Santos et al. 2014; Santos et al. 2015; Fernandes et al. 2015; Piccoli et al. 2016; Piccoli et al. 2018). This analytical

methodology is distinctive from what is offered by traditional impedance methodologies in that it reports the charge transfer resistance upon data fitting. A redox capacitance signal originates from the charging capability of the ferrocenyl redox-tagged peptide. As a result, the "charging identity" can be provided by converting the impedance data to capacitance. The signal measured in this case is not based on charge transfer resistance but on non-Faradaic capacitive charging. As a result, the interfacial recognition is detected by converting the same raw data into a complex capacitance Nyquist diagram as shown in Figure 5.6.
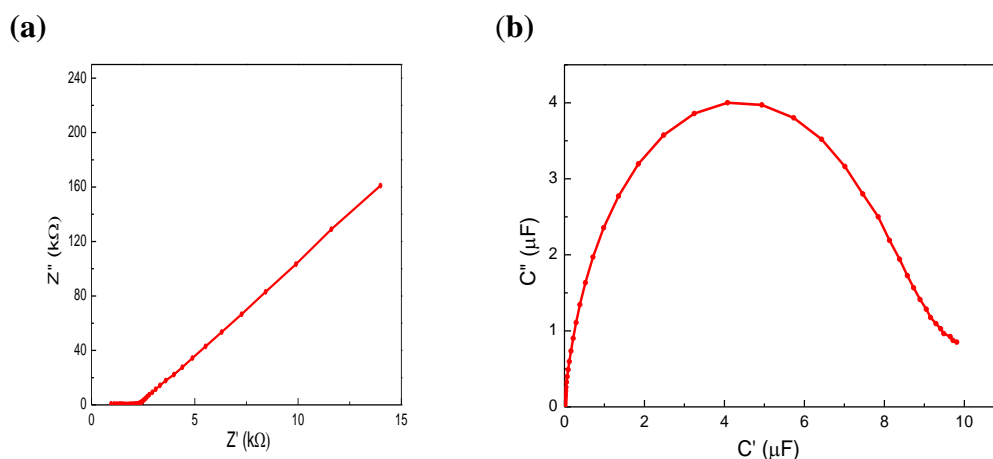
(a)   **(b)**

Figure 5. 6 (a) Nyquist impedimetric plot of Z" versus Z' for electroactive peptide-SAM immobilised on gold electrode surface at electrode potential corresponding to half-wave potential (b) The analogous capacitive response of C" versus C', C_r itself is obtained from the semicircle diameter.

Figure 5.6 (a) displays a resolved C_r value of 176.3 $\mu F\ cm^{-2}$ at half-wave potential ($E_{1/2}$) that is markedly greater than either the capacitance of bare gold (11.52 $\mu F\ cm^{-2}$) or the SAM at redox out potentials (E_{out}), which is the potential where no Faradaic redox activity is observed (6.8 $\mu F\ cm^{-2}$). Although the measured C_r value is smaller than the reported value in literature, 267.0 $\pm$ 7.1 $\mu F\ cm^{-2}$ (Piccoli et al. 2018), it is worth mentioning the variable factors such as electrode quality, different electrochemical apparatus, and measurement solution quality that could lead to slightly

different values to what is reported by other groups. However, the significant variation of the Nyquist derived capacitance at $E_{1/2}$ in comparison to redox out potential and the bare electrode case, indicates the successful immobilisation of the peptide-SAM and the adoption of its redox properties.
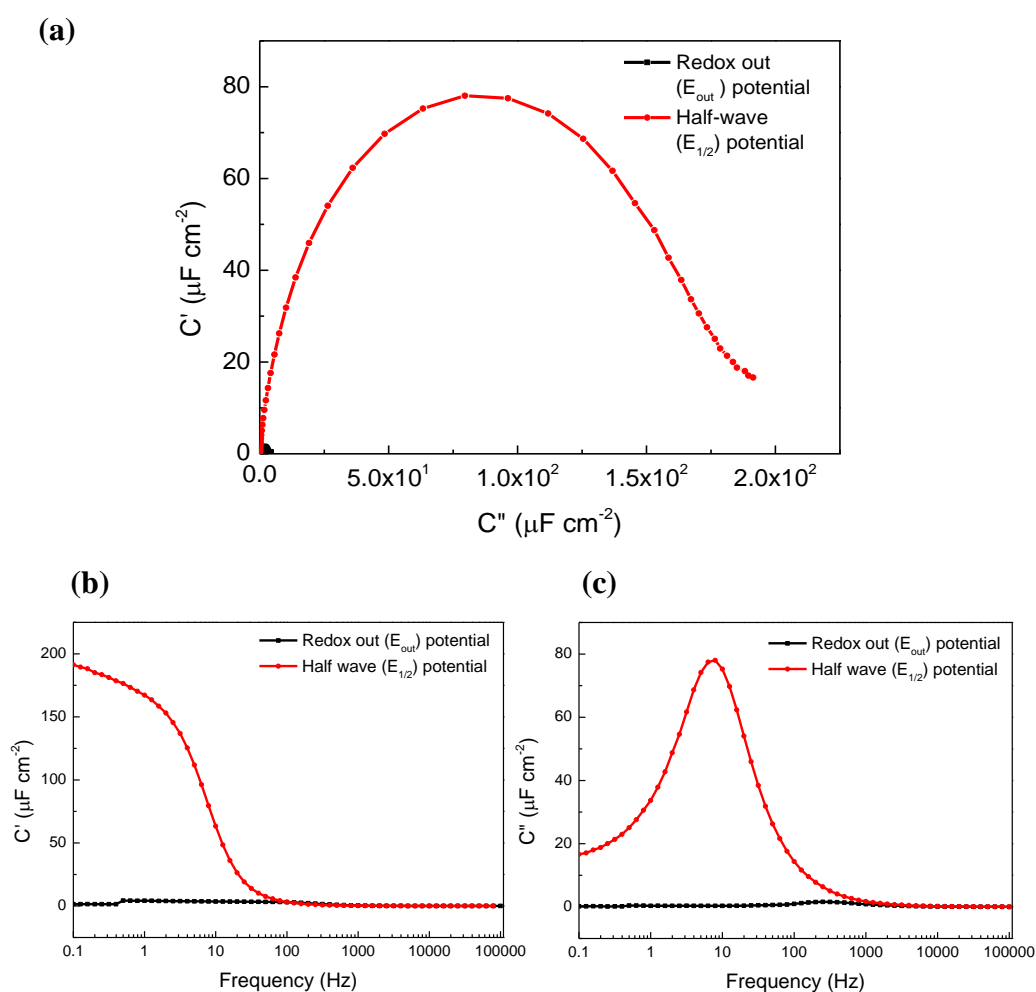
Figure 5. 7 (a) Capacitive Cole-Cole plot after immobilisation of the electroactive peptide-SAM, measurements carried out at electrode potentials corresponding to half-wave potential ($E_{1/2}$, evaluated as 0.363 V from Figure 5.4) and redox-out (E_{out}, evaluated as 0.1 V from Figure 5.4) vs. Ag|AgCl potentials. (b) The real part of the capacitance of the ferrocene-tagged peptide SAM at both electrode potentials (half-wave and redox out). (c) The imaginary part of the capacitance of the ferrocene-tagged peptide SAM at both electrode potentials (half wave and redox out).

Prior to any covalent immobilisation of PNA-probe, it is imperative to assess the stability of the SAM. Nyquist resolved capacitive response in Figure 5.8 displays the signal output change during five rounds of incubations in the absence of target. A significant drop, 24.49%, was observed on the initial C_r value of the peptide SAM by the end of three incubations. A well stable SAM was reported only after four incubations where 3.49% fluctuation was observed between the last two incubations (Figure 5.7, Stability 4 & 5) that indicates for good stability of the platform. This once again demonstrates the critical requirement for sufficient number of blank incubations for complete stability before any further investigation.
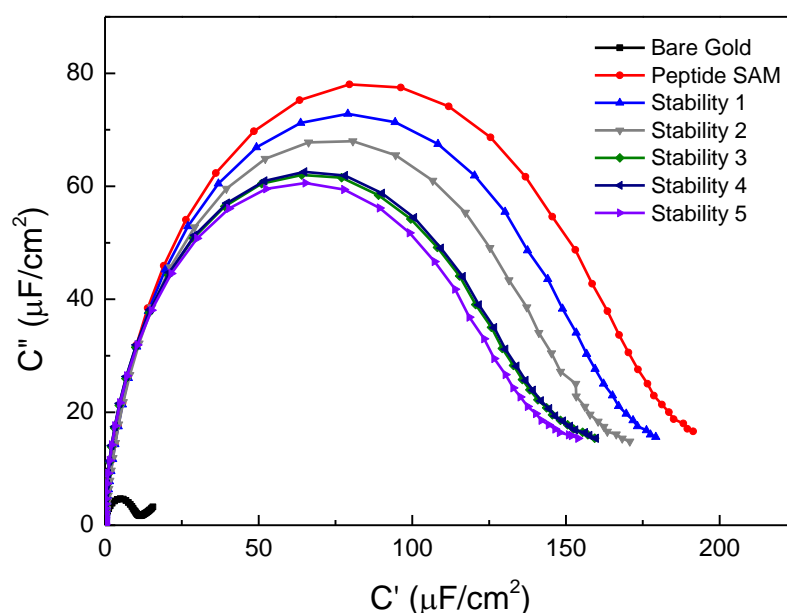
Figure 5. 8 EIS measurements taken in 20 mM TBAClO$_4$ ACN/H$_2$O 1:4, for blank electrode surface followed by measurement after its immobilisation with the peptide SAM. Then 5 rounds of stability measurements were carried out for the electrode surface immobilised with the peptide SAM. For or each stability measurement the electrode surface was incubated in 10 mM PB, pH 7.0 for 30 minutes and rinsed with Milli-Q water before measuring.

5.3. 3 Surface Plasmon Resonance (SPR) Analysis for the Validation of Attachment of PNA-Probe on peptide-SAM

Following the CV and EIS characterisation of the peptide-SAM, and prior to the further investigation of the attachment of the PNA-probe on the redox-tagged SAM by EIS, a constructive step provides validation of the methodology on a different measurement platform. The real time monitoring of the immobilisation of the PNA-probe on the redox-tagged peptide was carried out by using surface plasmon resonance. A gold planar SPR chip was functionalised with redox-tagged peptide for this purpose. SPR is an optical technique that detects the molecular binding on a thin metal (e.g. gold) film in terms of variations of refractive index. The measured signals reflect the molecular weight of the adsorbed biomolecules and can be used for the quantification of the number density of different types of adsorption. The plot given in Figure 5.8 (black line) corresponds to the real-time monitoring of the injection of the PNA probe under the flow of measurement buffer (10mM PB, pH 7.3) for its capture by the SPR chip that was previously immobilised by the ferrocene-tagged peptide. A control measurement was carried out at the same time where the other half of the same chip was incubated with a blank buffer instead of PNA-probe (red line). The shift in the reflectivity curve indicates the molecular binding taking place on half of the gold film, where no shift (hence no binding) was observed for the control (Bhalla et al. 2015). PNA upon binding on the surface of the gold is functionalised with redox peptide-SAM and revealed a change of 467.7 µRIU, whereas the incubation with the control revealed no change. The SPR chip was washed under flow of measurement buffer, until reaching stability once again, after the probe injection.
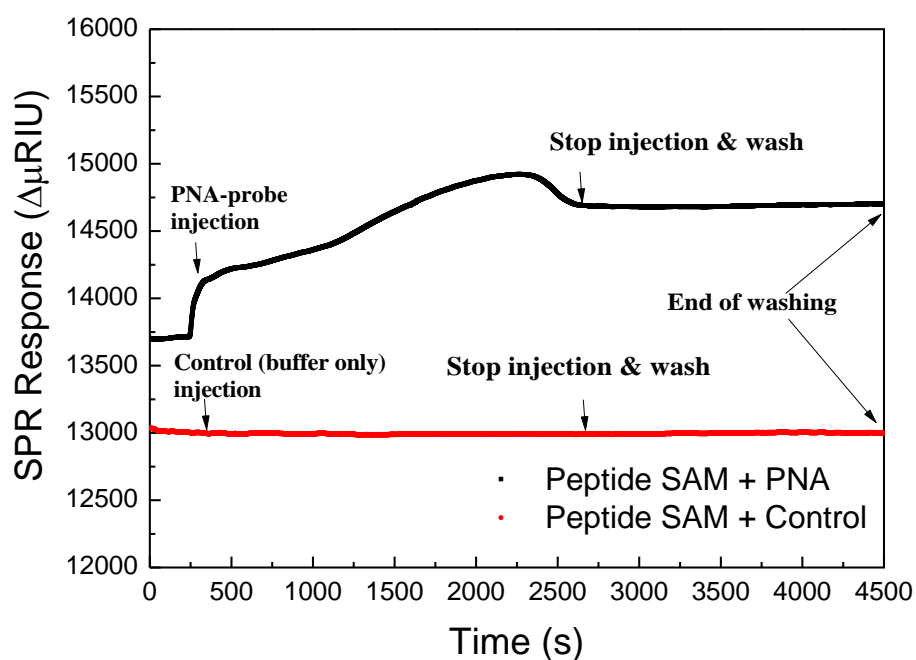
Figure 5. 9 Real time SPR response for PNA-probe attachment on ferrocene-tagged peptide immobilised SPR chip (black line). Red line corresponds to control (blank buffer) incubation. All measurements were carried out under flow, in 10 mM PB (pH 7.3).
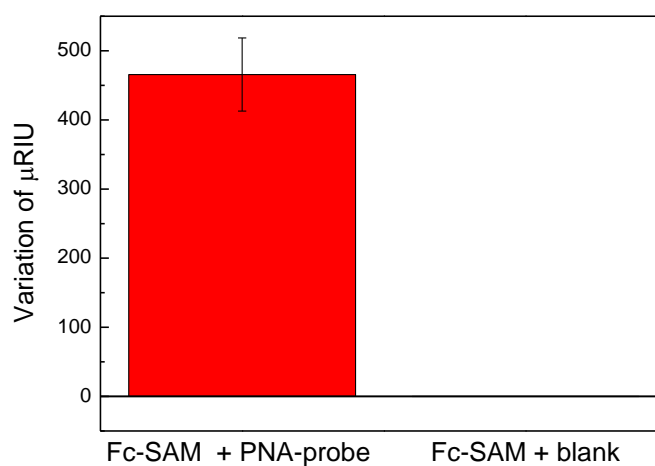
Figure 5. 10 Evaluation of change in μRIU after the PNA probe immobilisation upon using SPR real time response and its control (Figure 5.9). The error bar represents the standard deviation for three different chips.

Following the confirmation of immobilisation of the PNA-probe by SPR measurements, further analysis was carried out in order to test the stability of the designed redox tagged PNA-probe. Following the probe injection, the chip was injected with 0.1% BSA (prepared in 10 mM PB, pH 7.3) for the complete coverage of the gold surface for the elimination of non-specific binding. This was then followed by three consecutive blank buffer incubations (each for half hour). The evaluated %Δ μRIU results are displayed in Figure 5.10 and are found to be in good agreement with a stable system.
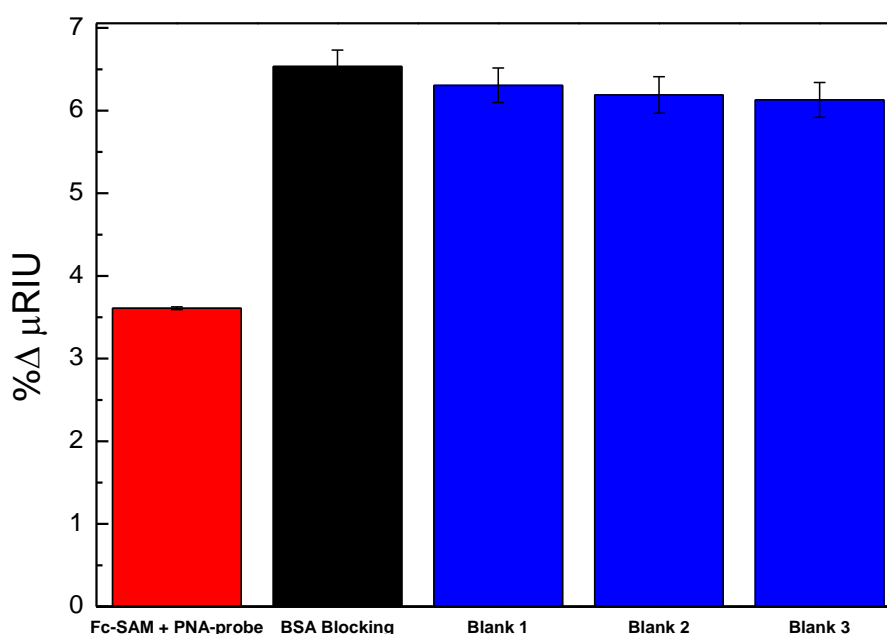
Figure 5. 11 Evaluation of % variation of μRIU upon using SPR real time response. All measurements were carried out under flow, in 10 mM PB, pH 7.3. Error bars represent the standard deviation for repetitions (n=2).

Following the approval of a stable system, the redox probe was investigated for its ability to capture the target DNA sequence. The SPR chip that was functionalised with redox probe was injected with 100 nM target DNA (*specific to C.difficile*) under flow. Control measurement was carried out with blank buffer incubation.

Upon incubation with the DNA target, a shift of 70 µRIU was observed on the reflectivity curve (Figure 5.12) where no shift was observed for the case of the blank buffer. Hence, the SPR responses, upon RIU variations, successfully demonstrated the phases of PNA-probe immobilisation, stability of probe, and molecular binding upon incubation with target DNA.

Figure 5. 12 Real time SPR response for attachment of PNA-probe followed by its surface blocking, stability measurements and incubation with 100 nM target DNA (black line). Red line corresponds to control where the fabricated probe was incubated with blank buffer instead of target after stability measurements.
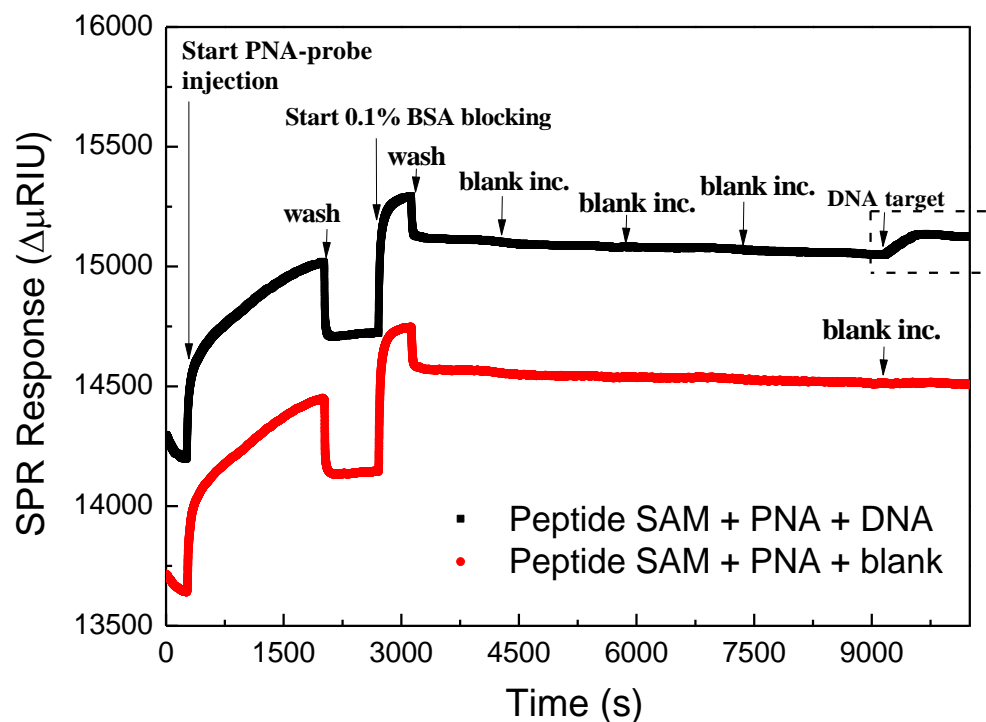
5.3. 4 Electrochemical Impedance Spectroscopy Analysis for the Attachment of PNA-Probe on Peptide-SAM

Following the SPR validation of the successful attachment of PNA-probe to the redox tagged SAM, the same process was repeated for DNA detection on the EIS platform. Upon covalent immobilisation of the Peptide Nucleic Acid (PNA) probe, the redox capacitance, C_r, (at E_{in}) is expected to change (decrease), indicating the successful covalent bonding of the probe with peptide (Santos et al. 2015; Piccoli et al. 2018).

The results in Figure 5.13 show a 13% decrease in the C_r (109 µF cm^{-2} →94.08 µF cm^{-2}) upon the immobilisation of the PNA probe on the peptide SAM. The previous studies reported a significant reduction of C_r (54%) for the case of immobilisation of CRP aptamer on the developed SAM (Piccoli et al. 2018). However, there are no published studies for PNA immobilisation on the electroactive peptide SAM and how it affects the electrostatic environment of the SAM. This leaves one with the question if the lower C_r drop indicates insufficient probe immobilisation on the SAM or if this is due to the neutrally charged nature of PNA. Previous attempts to detect CRP aptamer benefits the negative charges of the CRP bound for electrochemical impedance-based detection platform and its negative influence on the impedance derived capacitance measurements with peptide-SAM. However, due to its neutrally charged nature it could be reasonable not to expect such a large response for the case of a PNA-probe.
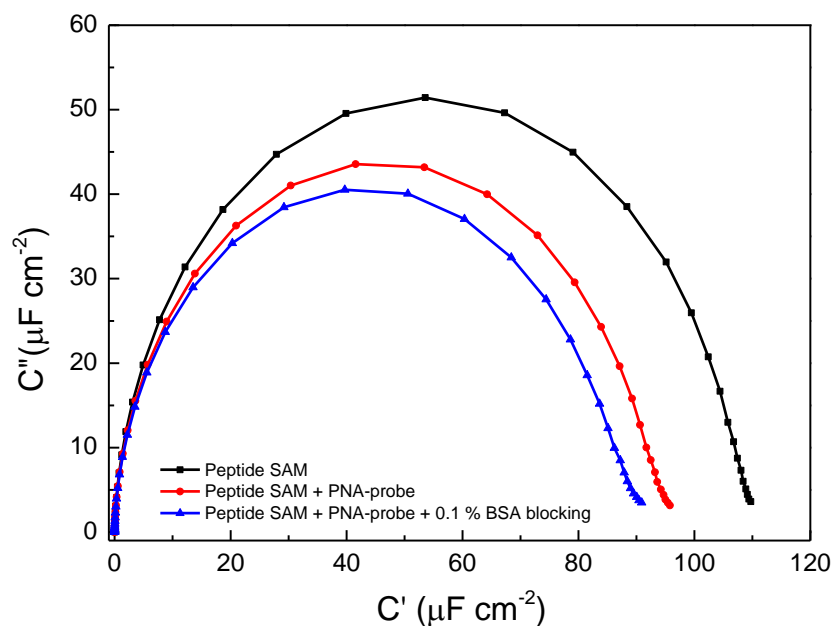
Figure 5. 13 EIS measurements taken in 20 Mm TBAClO$_4$ ACN/H$_2$O 1:4, for peptide-SAM (black curve) followed by covalent immobilisation of PNA-probe (red curve) and 0.1% BSA blocking for complete coverage of the surface (blue curve).

In order to benefit fully from the electrochemical activities of the redox peptide, 20 mM TBAClO$_4$ ACN/H$_2$O (1:4) has been adopted as this is the measurement buffer that is reported in literature (Piccoli et al. 2018). However, certain buffer conditions are essential when it comes to the hybridisation of PNA-probes with DNA. Due to the neutral backbone of PNA, the hybridisation of PNA oligomers to complementary DNA are known to be essentially independent of the ionic strength of the solution. Detection limits as low as fM levels have been obtained previously in our group, using different methods, by adopting 10 mM PB (pH 7.3) (Jolly et al. 2016) as both the measurement and hybridisation buffer. Additionally, SPR results performed successful binding of the target DNA, under a flow of 10 mM PB, pH 7.3.

Hence, the behaviour of the hybridised PNA-DNA duplex is not known in 20 mM TBAClO$_4$ ACN/H$_2$O 1:4 when used as the measurement buffer. Although the method has given stable measurements for the peptide-SAM and covalent attachment of PNA-

probe, the investigation of binding has not shown any significant variations on the C_r value (Figure 5.14). The results required further investigation of the measurements by replacing the measurement buffer with 10 mM PB (pH 7.3).
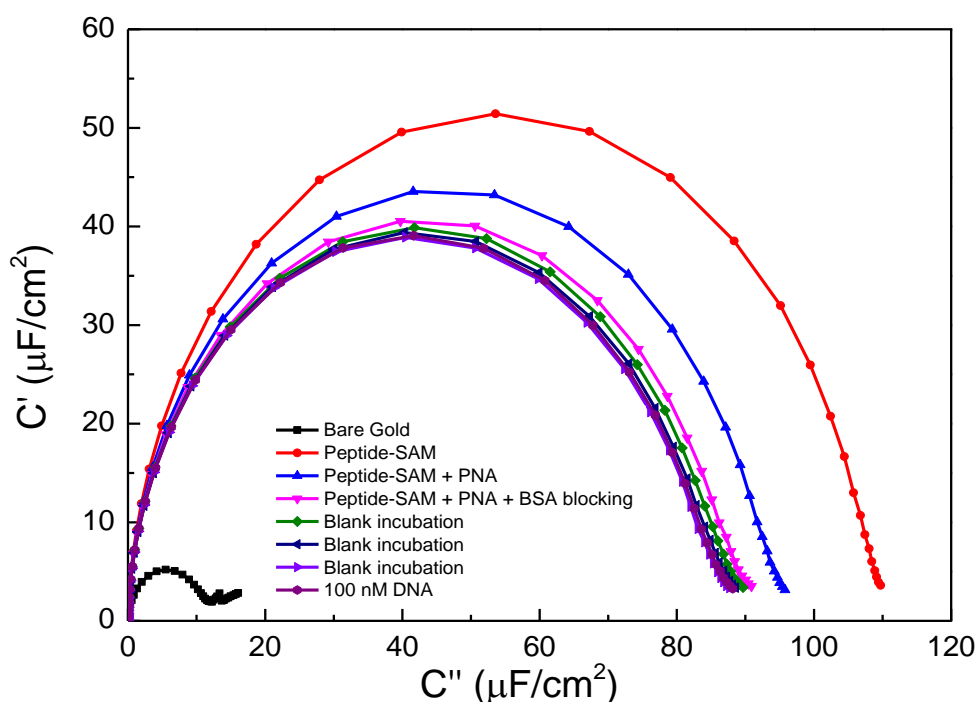
Figure 5. 14 EIS measurements taken in 20 mM TBAClO4 ACN/H2O 1:4, for peptide-SAM (red curve) followed by covalent immobilisation of PNA-probe (blue curve) and 0.1% BSA blocking for complete coverage of the surface (pink curve), three consecutive blank incubations for stability and finally incubation with 100 nM target DNA.

In order to encourage better hybridisation of probe PNA with target DNA, the measurement buffer was replaced with 10 mM PB (pH 7.3). The assay was repeated by keeping all the other factors the same as previously. The C_r response upon incubation with various concentrations of *C.difficile* specific DNA performed increased variation upon increasing target concentrations (Figure 5.15) when the measurement buffer was replaced with 10 mM PB (pH 7.3). Good reproducibility was

observed upon repetition of the assay on three different electrodes. A second assay was designed as control measurement by replacing the target incubations with blanks. This was done in order to observe if the capacitive shift (C_r) that is displayed in Figure 5.15 is due to binding of the target and does not correspond to any fluctuation/instability of the capacitance of the system over time.

Figure 5. 15 Evaluation of change in %Cr upon incubation of the peptide SAM-PNA probe functionalised electrode with various concentrations of target DNA. Target incubations were carried out after stabilisation of the platform with blank incubations. The measurements and incubations were carried out in 10 mM PB (pH 7.3). The error bars represent the standard deviation between three different electrodes.

Unfortunately, the results for the control measurements in Figure 5.16, showed a variation of the resolved capacitance (C_r) upon consecutive blank incubations. However, the C_r values were observed to be even more variable for the case of blank measurements compared to target incubations which leaves one in doubt if the result were due to a fault in the assay. Therefore, this has revealed the further need for the repetition of control measurements for the approval of target binding. The assays could not be taken any further due to limited supply of the peptide.
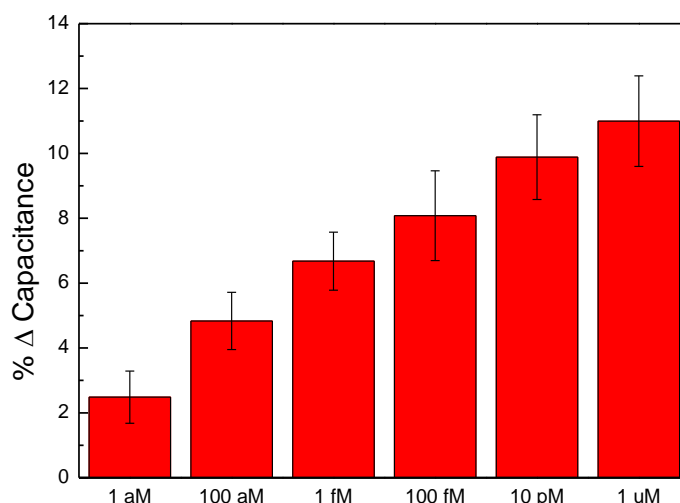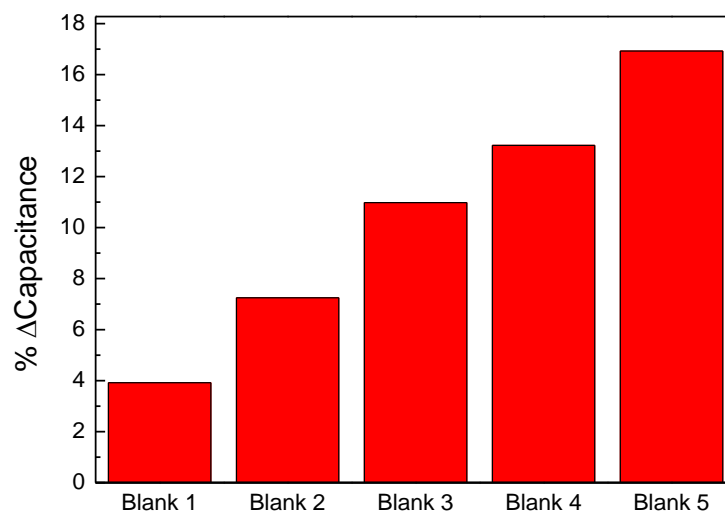
Figure 5. 16 Evaluation of change in %C_r upon incubation of the peptide SAM-PNA probe functionalised electrode with control (blank). The measurements and incubations were carried out in 10 mM PB (pH 7.3).

5. 4 Conclusions

A diverse range of interfacial strategies that adopt redox active elements exist for the detection of nucleic acids. Of the methods which are quantifiable and sensitive, those which do not require pre-labelling of the target analyte and the measurement solution are the most flexible in format and capability. In addition, elimination of redox labelling will drop the cost and help with scalability.

We have introduced a new analytical methodology based on the adoption of redox active SAM as surface tethered redox reporters in establishing a sensitive and label-free capacitive based detection of target DNA specific to *C.difficile*. The design steps for the immobilisation of the peptide-SAM on the gold electrode, stability of the SAM, attachment of PNA-probes onto the SAM, and detection of DNA were initially approved by using surface plasmon resonance. Then the steps were repeated for detection by electrochemical impedance derived capacitance spectroscopy. A few obstacles were encountered during the electrochemical measurements. The control

assays indicated a shift in the impedance derived capacitance (C_r) of the system over time. There could be possible explanations for such results. Such results and the poor stability of the peptide-SAM was observed only after utilising a new batch of the synthesised redox tagged peptide. Although we expect the quality of the synthesised peptide to be the same all the time, the observed results could be due to a fault in the batch under use. Due to limited synthesis of the peptide by suppliers and limited time, the control experiments could not be taken any further. As a result, future improvement would be the repeat of control measurements for the further approval of the results obtained for target detection. On the other hand, if the results are not due to the instability of the peptide, then another factor to look into would be the decision of using a different buffer for the measurements. A buffer is required that makes best use of the capacitive properties of the peptide as stated in the literature (Piccoli et al. 2018). However, it should at the same time encourage the hybridisation efficiency between PNA-DNA for the case of our study. The SPR results revealed successful immobilisation of the peptide-SAM on the gold electrode, and attachment of the PNA-probe on the SAM followed by DNA target detection. This is attributed to the fact that the buffer (10 mM PB, pH 7.3) adopted for the SPR analysis provided the required conditions for the hybridisation to take place (Jolly et al. 2016), and was sufficient enough for SPR analysis that it did not require the enhancement of the capacitive properties of the peptide-SAM. On the other hand, for the case of the electrochemical measurements there is the requirement for a buffer that will both enhance the capacitance value of the peptide-SAM and provide a sufficient environment for the hybridisation of the probe PNA with the target DNA. As a result, further research is required into finding the best buffer that will offer a good trade off between these two factors.

Overall, our experimental study introduced the design of a sensitive capacitive biosensor using a redox-tagged peptide supported SAM. The methodology proved its application in literature for the detection of C-reactive protein with a sensitivity that significantly exceeds that attainable with an analogous antibody interface (Piccoli et al. 2018). Therefore, redox active self-assembled monolayers are predicted to be useful in the development of biosensor devices to precisely detect biomarkers of clinical relevance, in a label-free form. In the case of our study, there is still the

requirement for a better modification of the method for enhancing the hybridisation efficiency of PNA with DNA. However, the design methodology proved its capability to detect target DNA after monitoring the fabrication steps of SPR. Hence, a constructive future plan would be the optimisation of the buffer and a repeat of the assays for an improvement in the electrochemical impedance derived capacitance studies.

References

Bedatty, F.C. et al., 2013. Label free redox capacitive biosensing. *Biosensors and Bioelectronics*, 50, pp.437–440.

Berggren, C., Bjarnason, B. & Johansson, G., 2001. Capacitive biosensors. *Electroanalysis*, 13(3), pp.173–180.

Berggren, C. & Johansson, G., 1997. Capacitance measurements of antibody-antigen interactions in a flow system. *Analytical Chemistry*, 69, pp.3651–3657.

Bhalla, N. et al., 2015. Plasmonic ruler on field-effect devices for kinase drug discovery applications. *Biosensors and Bioelectronics*, 71, pp.121–128.

Bryan, T. et al., 2013. An optimised electrochemical biosensor for the label-free detection of C-reactive protein in blood. *Biosensors and Bioelectronics*, 39, pp.94–98.

Bueno, P.R. et al., 2012. Capacitance spectroscopy : a versatile approach to resolving the redox density of states and kinetics in redox-active self-assembled monolayers. *The Journal of Physical Chemistry*, 116, p.8822−8829.

Bueno, P.R. & Davis, J.J., 2014. Measuring quantum capacitance in energetically addressable molecular layers. *Analytical Chemistry*, 86, pp.1337–1341.

Bueno, P.R., Fabregat-santiago, F. & Davis, J.J., 2013. Elucidating capacitance and resistance terms in confined electroactive molecular layers. *Analytical Chemistry*, 85, pp.411–417.

Büttiker, M., Thomas, H. & Prêtre, A., 1993. Mesoscopic capacitors. *Physics Letters A*, 180, pp.364–369.

Dijksma, M. et al., 2001. Development of an electrochemical immunosensor for direct detection of interferon- γ at the attomolar level. *Analytical Chemistry*, 73(5), pp.901–907.

Fernandes, F.C.B. et al., 2014. Comparing label free electrochemical impedimetric and capacitive biosensing architectures. *Biosensors and Bioelectronics*, 57, pp.96–102.

Fernandes, F.C.B. et al., 2015. Optimized diagnostic assays based on redox tagged bioreceptive interfaces. *Analytical Chemistry*, 87, p.12137−12144.

Gaiji, H. et al., 2017. A peptide nucleic acid (PNA) -DNA ferrocenyl intercalator for electrochemical sensing. *Electroanalysis*, 29, pp.917–922.

Gatto, E. et al., 2008. Electroconductive and photocurrent generation properties of self-assembled monolayers formed by functionalized , conformationally-constrained peptides on gold electrodes. *Journal of Peptide Science*, 14, pp.184–191.

Gatto, E. et al., 2012. Playing with peptides: how to build a supramolecular peptide nanostructure by exploiting helix ⋯ helix macrodipole interactions. *Langmuir*, 28, p.2817−2826.

Goes, M.S. et al., 2012. A dielectric model of self-assembled monolayer interfaces by capacitive spectroscopy. *Longmuir*, 28, p.9689−9699.

Haab, B.B., 2003. Methods and applications of antibody microarrays in cancer research. *Proteomics*, 3, pp.2116–2122.

Homola, J., 2008. Surface plasmon resonance sensors for detection of chemical and biological species. *Chemical Reviews*, 108, pp.462–493.

Johnson, A. et al., 2012. Sensitive affimer and antibody based impedimetric label-free assays for C-reactive protein. *Analytical Chemistry*, 84, p.6553−6560.

Jolly, P. et al., 2016. Highly sensitive dual mode electrochemical platform for microRNA detection. *Scientific Reports*, 6(36719).

Joshi, L.T. et al., 2014. Extraction and sensitive detection of toxins A and B from the human pathogen clostridium difficile in 40 seconds using microwave-accelerated metal- enhanced fluorescence. *Public Library of Science*, 9(8).

Kai, M. et al., 2008. Distance dependence of long-range electron transfer through helical peptides. *Journal of Peptide Science*, 14, pp.192–202.

Lehr, J. et al., 2014. Label-free capacitive diagnostics: exploiting local redox probe state occupancy. *Analytical Chemistry*, 86, pp.2559–2564.

Limbut, W. et al., 2006a. A comparative study of capacitive immunosensors based on self-assembled monolayers formed from thiourea , thioctic acid , and 3-mercaptopropionic acid. *Biosensors and Bioelectronics*, 22, pp.233–240.

Limbut, W. et al., 2006b. A reusable capacitive immunosensor for carcinoembryonic antigen (CEA) detection using thiourea modified gold electrode. *Analytica Chimica Acta*, 561, pp.55–61.

Moschou, D. & Tserepi, A., 2017. The lab-on-PCB approach : tackling the μTAS commercial upscaling bottleneck. *Lab on a Chip*, 17, pp.1388–1405.

Okamoto, S., Morita, T. & Kimura, S., 2009. Electron transfer through a self-assembled monolayer of a double-helix peptide with linking the terminals by ferrocene. *Langmuir*, 25(5), pp.3297–3304.

Pan, J., 2007. Voltammetric detection of DNA hybridization using a non-competitive enzyme linked assay. *Biochemical Engineering Journal*, 35, pp.183–190.

Piccoli, J. et al., 2018. Redox capacitive assaying of C - reactive protein at a peptide supported aptamer interface. *Analytical Chemistry*, 90, pp.3005–3008.

Piccoli, J.P. et al., 2016. The self-assembly of redox active peptides: synthesis and electrochemical capacitive behavior. *Peptide Science*, 106(3), pp.357–367.

Pumera, M. et al., 2005. Magnetically trigged direct electrochemical detection of DNA hybridization using Au 67 quantum dot as electrical tracer. *Langmuir*, 21, pp.9625–9629.

Ray, S., Mehta, G. & Srivastava, S., 2010. Label-free detection techniques for protein microarrays : Prospects,merits and challenges. *Proteomics*, 10, pp.731–748.

Roda, A. et al., 2016. Smartphone-based biosensors : a critical review and perspectives. *Trends in Analytical Chemistry*, 79, pp.317–325.

Santos, A. et al., 2015. Redox-tagged peptide for capacitive diagnostic assays. *Biosensors and Bioelectronics*, 68, pp.281–287.

Santos, A., Davis, J.J. & Bueno, P.R., 2014. Fundamentals and applications of impedimetric and redox capacitive biosensors. *Journal of Analytical & Bioanalytical Techniques*, S7.

Speight, R.E. & Cooper, M.A., 2012. A survey of the 2010 quartz crystal microbalance literature. *Journal of Molecular Recognition*, 25, pp.451–473.

Tkac, J.A.N. & Davis, J.J., 2009. Label-free field effect protein sensing. In J. J. Davis, ed. *Engineering the Bioelectronic Interface: Applications to Analyte Biosensing and Protein Detection*. Royal Society of Chemistry, pp. 193–224.

Trasatti, S. & Petrii, O.A., 1991. Real surface area measurements in electrochemistry. *Pure and Applied Chemistry*, 63(5), pp.711–734.

Wei, M., Guo, L. & Famouri, P., 2011. DNA biosensors based on metallo-intercalator probes and electrocatalytic amplification. *Microchimica Acta*, 172, pp.247–260.

Zhang, J. et al., 2016. An immobilization-free electrochemical impedance biosensor

based on duplex-specific nuclease assisted target recycling for amplified detection of microRNA. *Biosensors and Bioelectronic*, 75, pp.452–457.

Chapter 6 Summary and Outlook

With the main objective of improving the early diagnosis of cancer, the work in this thesis is a step forward towards the development of point-of-care technologies for the electrochemical based detection of circulating miRNAs. The breakthrough of a broad range of studies proving the relationship of circulating miRNAs to early states of cancer, and the lack of blood-based biomarkers currently in clinical diagnosis, has been the major motivation of this thesis. The main focus has been given to the adoption of oligonucleotide-based probes for the capture of target miRNAs from solution. A highly-sensitive PNA-based capture probe was demonstrated in the first experimental study for direct detection of miRNA. A new method was developed within the second experimental study, which was for the direct detection of miRNA in a serum environment, in order to overcome the difficulties that were encountered during second study. Hence, the second study examined the efficient separation and pre-concentration of miRNA from solution prior to detection. In the last experimental study, a redox active self- assembled monolayer was investigated for label-free and capacitive based detection. If successfully implemented, such a biosensor eliminates the need for doping of the measurement solution used within the first and second experimental work, further simplifying the detection. The strategies that have been experimented with in these studies are; label-free and amplification-free detection of low concentrations of miRNAs using PNA probes, the separation of target miRNA from complex solutions with LNA modified magnetic beads, pre-concentration of the target prior to detection, and the coupling of redox active SAMs with PNA probes for the detection of nucleic acids.

6. 1 Summary

The main focus has been given to the adoption of oligonucleotide-based probes for the capture of target miRNAs from solution. The key reasons for such an adoption in the development of biosensor devices are; their binding affinity for the target, their ease of chemical modification, the ability to create controlled surface chemistry for reproducible results, and their excellent stability as probes. Due to natural DNA not being free from limitations, which prevents their use in electrochemical biosensors, we have investigated the adoption of novel classes of synthetic DNA analogues (PNA and LNA). In these analogues, the backbone phosphate groups of DNA are subjected to a variety of chemical modifications for improved specificity and affinity of hybridisation with natural DNA and RNA/miRNA targets. The fine-tuning of these synthetic probes with various detection methodologies have been investigated.

In Chapter 3, our work in the development of a PNA-probe based biosensor for the detection of miR-21-5p revealed the crucial role of the optimisation of PNA-probe coverage density on the electrode surface for the enhancement of hybridisation efficiency. This was achieved with the incorporation of a spacer molecule, MCH, which was adopted as a surface blocker that is crucial for the prevention of non-specific binding. Upon the investigation of various ratios of PNA-probe to MCH on the electrode surface, the ratio of 1:15 (PNA:MCH) resulted in the maximum R_{ct} change of 32.2 % $\pm$ 3.7% upon hybridisation with the target miRNA, measured by means of Faradaic EIS. Although one might expect a better hybridisation with higher densities of probe on the surface, the R_{ct} change was observed to drop significantly upon adopting a larger probe density on the electrode surface (1:2 ratio of PNA:MCH). Hence, such results reveal the fact that high probe density does not necessarily lead to better hybridisation with a target, and the surface chemistry optimisation is a crucial step prior to the fabrication of a successful biosensor. These results are due to the combination of two effects: steric hindrance that leads to reduced hybridisation, and the large initial R_{ct} that leads to less apparent variation in R_{ct} after hybridisation. Such a methodology was reinforced with an additional study presented in the same chapter where similar surface chemistry optimisations were carried out for the detection of a C.difficile specific DNA (49 bases long) using PNA-probes. For the detection of such

a long sequence, there is a need for better spacing of the PNA-probe, and the optimised ratio is not expected to be the same as cases that use a shorter sequence, such as for miRNA. Hence, the results supported our methodology and the optimised detection was achieved with a lower probe density of 1:29 (PNA:MCH) on the electrode surface. This strategy can be easily translated to any other oligonucleotide probes (DNA/LNA) for the detection of nucleic acids. We have achieved a detection level as low as 0.77 fM for miRNA detection with no additional steps, which was previously achieved in literature only with the adoption of amplifications steps. However, the complex sample composition of blood makes it difficult to detect blood biomarkers such as miRNA. Our experimental efforts revealed a quantification limit of 10 pM when target miRNA was prepared in the serum environment. Upon replacing the solution with 100% serum, the increased interference of non-specific interactions lead to a negative variation of R_{ct}, and the electrochemical readings for target concentrations were disrupted.

In order to address the major issue of non-specific binding, we have developed a new assay in Chapter 4, for the magnetic beads based separation of target miRNA from complex solutions. The methodology is well established in literature for the pre-concentration of miRNA from biological samples. In general, magnetic beads offer an easy, effective option for sample preparation and separation of target miRNA. If developing a biosensor device for PoC purposes, the coupling of such effective separation methodologies with oligonucleotide-based electrochemical detection probes, would create very powerful biosensors. In this study, we have modified the magnetic beads with locked nucleic acid (LNA) probes which are known for their high affinity to complementary miRNA. As a result, the capture of the target was encouraged further. The captured miRNA was then brought to the sensor surface that was immobilised with PNA probes and recognised through hybridisation with complementary PNA. PNA probes are adopted due to their excellent stability for electrochemical detection studies, and their ability to produce low limits of detection for miRNA sensing, which was proved earlier in Chapter 3.

Our final experimental study in Chapter 5, demonstrates a new detection methodology, in collaboration with the Nanobionics group in São Paulo State University, for the development of label-free diagnostic assays. The successful implementation of the

methodology will offer the elimination of the need for redox markers in measurement solutions, and provide one with the capability to carry out direct electrochemical measurements, which is crucial for real case PoC devices for clinical applications. In this study we have introduced a new analytical methodology based on the adoption of redox active SAMs as surface tethered redox reporters in establishing a sensitive and label free capacitive based detection of the target. The study aimed to adopt the capacitive sensing ability of a ferrocene-tagged peptide SAM that is fairly sensitive to any electrostatic and chemical potential variations in its environment. Hence, if the SAM is coupled with a selective probe that captures the target, one can generate a feasible sensor that monitors the capture process by depending on the capacitive variations on the SAM due to binding processes.

6. 2 Future Work

Part of the work presented in this dissertation has fostered collaboration with another research group for label-free detection of circulating miRNAs (or any other disease specific nucleic acids). The future work of this collaborative study that is presented in Chapter 5, will be taken further with the continued collaboration between our group and the Nanobionics group in São Paulo State University.

On the other hand, some research that has been performed, but not presented in this dissertation, on transferring the methodologies from Chapters 3 & 4 to manufacturing are as follows:

6.2. 1 Lab-on-a-chip

The rapid expansion of mobile technology is also leading to a transformation in healthcare applications. The methodology of lab-on-a-chip (LOC) diagnostics (Moschou & Tserepi 2017) is now offering informative molecular diagnostics tests directly to the user with a smartphone, allowing them to take better control of their own health (Li Shen et al. 2012; Stemple et al. 2014; Chen et al. 2014). A lab-on-a-chip device integrates one or several laboratory functions down to a single chip. Hence, the laboratory functions are reduced to the size of a chip that it at most centimetres in size, in order to achieve automation and high-throughput (Hwang et al. 2006; Alyassin

et al. 2009; Moschou & Tserepi 2017). An ideal POC test requires the following: high sensitivity and specificity, affordability, rapid evaluation of results, ease of use (no need for trained labour), and functioning without the need for additional apparatus (Yetisen et al. 2013; Jolly, Rainbow, et al. 2019). As a result, LOC takes up the challenge by offering integrated sensors for specificity and sensitivity, rapid analysis by a miniaturised design, ease of use due to sample-in-answer-out microsystems, minimised reagent volumes for affordability and fabrication of cost-effective devices, and the elimination of additional equipment by implementing autonomous systems (e.g. integration of sample handling, sample pre-treatment and sensor read-outs). Upon using microfluidics the technology reveals the fact that, under flow, a biosensor saturates with much lower concentrations of nucleic acids (Jolly, Rainbow, et al. 2019). This discipline has its origins in the early 1990's and has grown exponentially. The technology is gaining the attention of both industry and academic researchers as an essential tool for life science research.

The methodologies developed in Chapters 3 & 4 can be incorporated for the fabrication of a strong biosensor for miRNA separation and detection. The idea can be easily translated to manufacturing by utilising the "lab-on-a-chip" technology for diagnostics (Herold & Rasooly 2009; Erickson et al. 2014). In a miniaturised microfluidic system, we can integrate the various functional units that are required for our design methodology that initially involves the separation of miRNAs from solution followed by their detection on an electrode surface. An increase in speed and automation can be achieved by performing these processes with microfluidics. To provide one with the preliminary idea of the implementation of our methodology on a miniaturised platform, we have created the flow diagram in Figure 6.1. The diagram presents how the methodology can be transformed to a LOC design that integrates all the functional units required for the functioning of our detection methods on a POC device. The complex sample composition of blood usually makes it harder to detect biomarkers directly from blood. For this purpose, the research into miniaturised systems for blood plasma separation has been thriving over the last 14 years (2005-2019) (Crowley & Pizziconi 2005; Browne et al. 2011). With further investigation of available miniaturised technologies for efficient separation of blood plasma, an appropriate filter can be coupled with our design. The first inlet of the mixer in Figure 6.1 (or

micromixer) receives blood plasma/serum that is separated from blood upon collection, by use of an appropriate filter system. Then the blood plasma/serum will be mixed with a solution that contains magnetic beads modified with LNA probes that are complementary to the target miRNA. The beads will separate the target miRNA from the blood plasma/serum under flow. Then the beads that hold the target miRNA will be separated from the solution by use of magnetism. The remaining blood plasma/serum will be discarded and the solution that holds the magnetic beads will be diverted to the inlet of a mixer that allows in an alkaline solution from its second inlet. The alkaline solution will be mixed, under flow, with the magnetic beads that hold the target miRNAs and lead to the release of target miRNA from the surface of the magnetic beads due to the denaturation of the LNA-target miRNA duplexes. Following this will be the separation of the magnetic beads waste, by use of a second magnetic separation module. In the end we will be left with a solution that holds only the target miRNA. Appropriate pH adjustment will be made in the target solution in order to bring the high alkaline nature of the solution down to pH 7. This is an essential step for the hybridisation with the PNA capture probe. After providing the required pH environment, the solution that contains the target miRNA will be sent for its electrochemical analysis on a PNA-probe immobilised on a gold-plated sensing electrode layer on a commercial printed circuit board (PCB).

A maximum volume of 400 µL serum or plasma has proven to be enough for the detection of cancer-derived circulating miRNA biomarkers whereas even smaller volumes (i.e. 25 µL) would be sufficient if highly abundant circulating miRNAs are being measured (Kroh et al. 2010; Murray et al. 2018). Hence, the development of miniaturised LOC technology that is capable of working with such volumes requires the active handling of small volumes of fluid (active microfluidics) by components such as microfluidic pumps or microfluidic valves (Haeberle & Zengerle 2007; Suzuki & Yoneyama 2003). For the development of micro-fluidic based POC diagnostic devices, the handling of such small volumes of fluid by external pumps is not ideal as they will require trained persons to handle them. In order to facilitate the easy handling of the device for untrained people, many strategies have been developed for on-chip fluid manipulation (Lei 2012). Microfluidic pumps are adopted for supplying the fluids in a continuous way whereas microfluidic valves are used for injecting precise volumes

of samples and buffers. This not only reduces the handling faults but also standardises the analytical conditions for each measurement. In future, for an ideal automated diagnosis and prognosis of cancer using such a methodology, initially a small volume of blood will be collected from the patient by a nurse. The nurse will insert the sample into the hand-held LOC device and the rest of the analysis will be carried out by the device and require no additional technical handling by the nurse. The information of the results will right away be sent to a computer or a smart device for further investigation by a doctor. Such an automation will not only speed up the detection but it also offers a straightforward monitoring process of patient recovery during the course of their treatment. Upon further investigation, the studies can be extended for the development of multiplexed platforms for parallel sensing of groups of miRNAs which would provide one with more complete information about the state of cancer development. As stated in our literature review, the detection of multiple miRNAs gives a better idea of the progress of the disease, and the development of multiplexed detection platforms is a crucial area to be investigated in future studies.
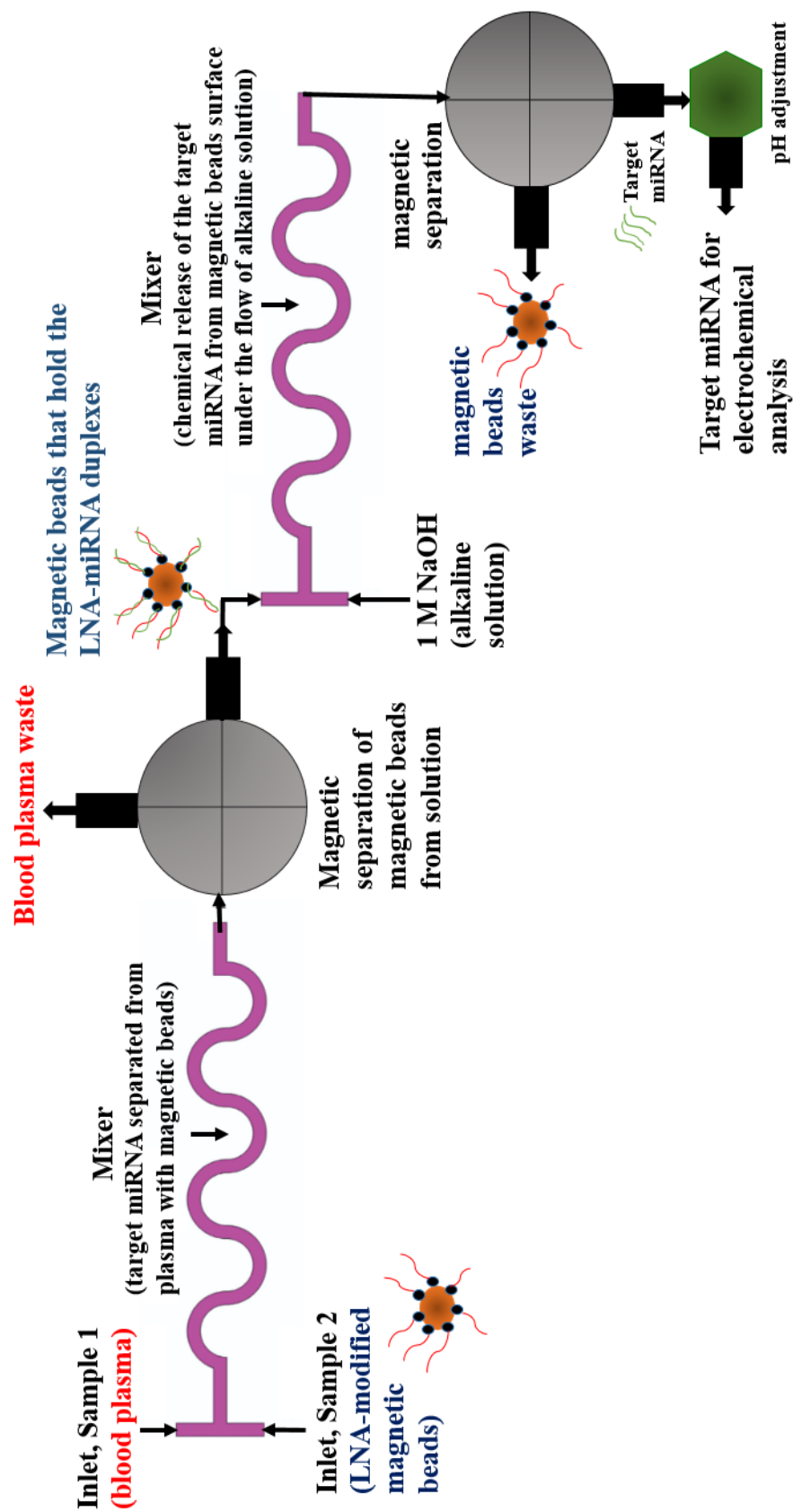
Figure 6. 1 Schematic for transferring the methodology of magnetic beads-based separation and detection of microRNAs to Lab-on-a-chip type technology.

All in all, the development of a successful oligonucleotide-based biosensor is an interdisciplinary subject and relies on a broad knowledge base in; the characterisation of bio-recognition probes with their respective analytes, the immobilisation of bio-recognition probes onto electrode surfaces, the optimisation of surface chemistry, sensor design, microfluidics and fabrication. We have exploited the probe/target methodologies for analysing the practical applications of the detection of circulating miRNAs. Our studies demonstrated the great potential of effective and low-cost oligonucleotide-based sensors upon adopting strategic approaches for the integration of functional units for the effective separation of targets, and their detection. The studies can be extended to the development of multiplexed platforms for the parallel sensing of groups of miRNAs. If developed successfully, such a device could offer the easy and fast assessment of patient's states, and the detection of cancer at early stages before any symptoms arise.

References

Alyassin, M.A. et al., 2009. Rapid automated cell quantification on HIV microfluidic devices. *Lab on a chip*, 9, pp.3364–3369.

Browne, A.W. et al., 2011. A lab-on-a-chip for rapid blood separation and quantification of hematocrit and serum analytes. *Lab on a Chip*, 11, pp.2440–2446.

Chen, A. et al., 2014. Smartphone-interfaced lab-on-a-chip devices for field-deployable enzyme-linked immunosorbent assay. *Biomicrofluidics*, 8(064101).

Crowley, T.A. & Pizziconi, V., 2005. Isolation of plasma from whole blood using planar microfilters for lab-on-a-chip applications. *Lab on a Chip*, 5, pp.922–929.

Erickson, D. et al., 2014. Smartphone technology can be transformative to the deployment of lab-on-chip diagnostics. *Lab on a Chip*, 14, pp.3159–3164.

Haeberle, S. & Zengerle, R., 2007. Microfluidic platforms for lab-on-a-chip applications. *Lab on a Chip*, 7, pp.1094–1110.

Herold, K.E. & Rasooly, A., 2009. *Lab on a chip Technology: Volume 1 Fabrication and Microfluidics*, Caister Academic Press.

Hwang, W.L., Su, F. & Chakrabarty, K., 2006. Automated design of pin-constrained digital microfluidic arrays for lab-on-a-chip applications. In *Proceedings of the 43rd Annual Design Automation Conference*. pp. 925–930.

Jolly, P. et al., 2019. A PNA-based Lab-on-PCB diagnostic platform for rapid and high sensitivity DNA quantification. *Biosensors and Bioelectronics*, 123, pp.244–250.

Kroh, E.M. et al., 2010. Analysis of circulating microRNA biomarkers in plasma and serum using quantitative reverse transcription-PCR (qRT-PCR). *Methods*, 50, pp.298–301.

Lei, K.F., 2012. Microfluidic systems for diagnostic applications : a Review. *Journal of Laboratory Automation*, 17(5), pp.330–347.

Moschou, D. & Tserepi, A., 2017. The lab-on-PCB approach : tackling the μTAS commercial upscaling bottleneck. *Lab on a Chip*, 17, pp.1388–1405.

Murray, M.J. et al., 2018. " Future-proofing " blood processing for measurement of circulating miRNAs in samples from biobanks and prospective clinical trials. *Cancer Epidemiology, Biomarkes & Prevention*, 27(2), pp.208–219.

Shen, L., Hagenb, J.A. & Papautsky, I., 2012. Point-of-care colorimetric detection with a smartphone. *Lab on a Chip*, 12, pp.4240–4243.

Stemple, C.C. et al., 2014. Smartphone-based optofluidic lab-on- a-chip for detecting pathogens from blood. *Journal of Laboratory Automation*, 19(1), pp.35–41.

Suzuki, H. & Yoneyama, R., 2003. Integrated microfluidic system with electrochemically actuated on-chip pumps and valves. *Sensors and Actuators B*, 96, pp.38–45.

Yetisen, A.K., Akram, M.S. & Lowe, C.R., 2013. Paper-based microfluidic point-of-care diagnostic devices. *Lab on a Chip*, 13, pp.2210–2251.

Appendix

Appendix I. miRNA detection in serum using EIS technique
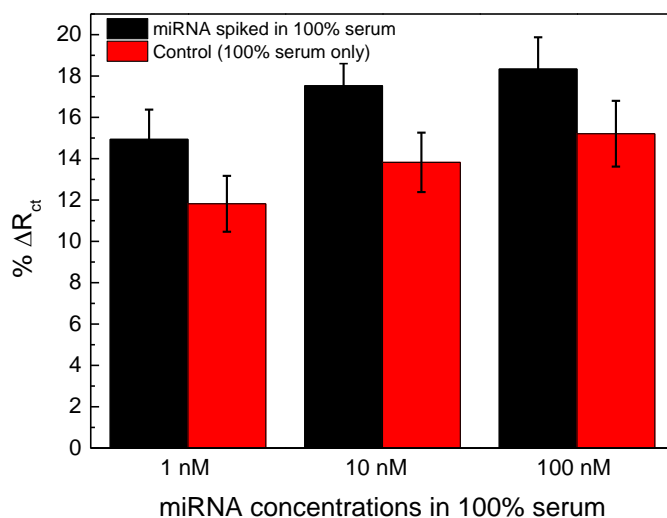

Figure I. 1 R_{ct} variations upon incubations with 100% serum only (red bars) and target miRNA concentrations spiked in 100% serum (black bars). Error bars represent the standard deviation for three separate electrodes.

Appendix II. Quartz crystal microbalance with dissipation signals (QCM-D)

Prior to assays, Q-sense analyser (Biolin Scientific, Sweden) was cleaned by using 2% Hellmanex solution (in ultrapure water). This was carried out by injecting the solution through the instrument for an hour at a flow rate of 1100 µl/min. Following that, the instrument was washed with ultrapure water for an extra hour. Prior to modification and subsequent testing, the 5 MHz gold-coated quartz crystals (Biolin Scientific, Sweden) were cleaned by immersing in freshly prepared piranha solution for 1 minute, prepared with 3:1 ratio of $H_2SO_4:H_2O_2$. Then, the crystals were rinsed with Milli-q water in order to remove any residues. After rinsing, gold-coated quartz crystals were placed separately in four sensor chambers. The chamber temperatures were set to room temperature (24°C). The quartz crystals were washed with immobilisation buffer till

stabilisation. 10 mM PB pH 7.0 was adopted for the immobilisation of PNA-probes on quartz crystal surface. 1000 µL of probe immobilisation solution was injected through the instrument at a flow rate of 1100 µl/min in order to assure the complete coverage of the crystals and the electrodes were incubated with the solution overnight.

Figure I.2 Q-Sense Analyser consisting of a flow module with pump (First picture, white module on the left) and the 4-sensor chambers (First picture, blue module on the right). The handling of the gold-coated quartz crystals and their standing in the sensor chambers is shown by the two pictures on right.

The next morning following the incubation overnight (~16hr), the crystals were washed with the immobilisation buffer until stability (~1hr). This was followed by MCH backfilling by injecting 1000 µl of 1 mM MCH prepared in measurement buffer, at a flow rate of 1100 µl /min and stopping the pump for an hour right after injection. This was done in order to make sure of the complete coverage of the crystals and allow time for the backfilling process to take place. The crystals were then washed with the measurement buffer by injecting the buffer solution at a rate of 1100 µl/min. After stabilisation with buffer, 1000 µl of the first DNA concentration was injected into system and the pump was stopped for half hour following the complete injection of the concentration. This assured the complete cover of the crystals with target DNA solution and let the hybridization process to take place for half hour. Then, the crystals were washed with measurement buffer for another half hour in order to allow

stabilisation of the response prior to next incubation. Same process was repeated for each incubation. The stabilisation could be ideally carried out by injecting the buffer for 15 minutes followed by stopping the pump for 15 minutes.
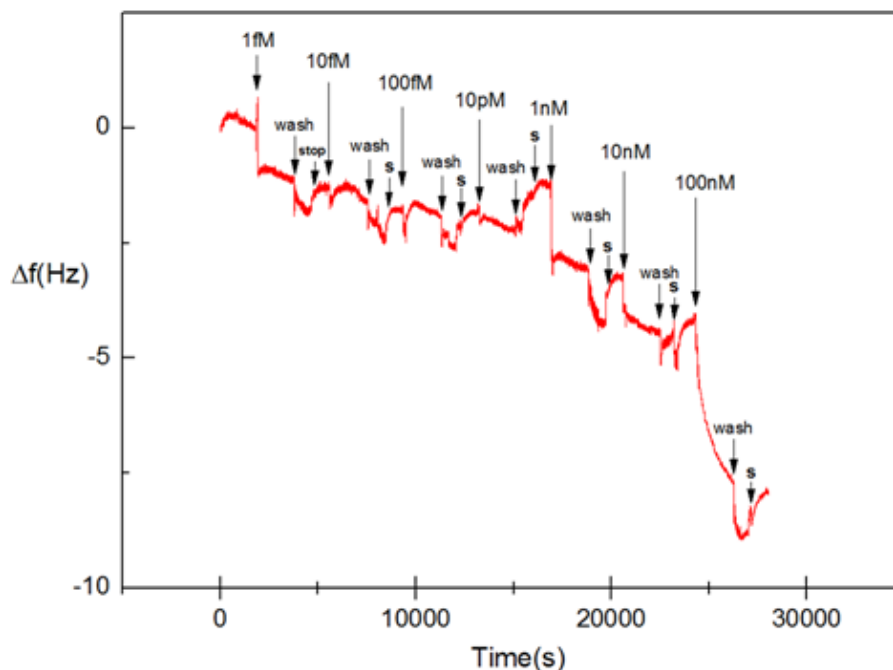

Figure I.3 Kinetic curve of frequency for the limit of detection study of gold quartz crystal immobilised with 1:4 ratio of PNA:MCH. Target DNA concentration was raised in seven steps, starting from 1 fM until 100 nM. Crystal was washed with 10 mM PB (pH 7.0) prior to each incubation.

Appendix III. Field-effect transistor-based biosensor (Bio-FET)

Biologically sensitive field-effect based transistor design was composed of two parts: (i) gold electrode where the PNA complementary sequence captures the target DNA, and (ii) the FET structure, which transduces the binding events taking place at the surface of the electrode into electrical signals. The gate of the transistor design was extended (Figure I.4), connecting the gold electrodes that are placed in a reaction cell to the n-type MOSFET, by using a metal wire. B1500A HR CMU Semiconductor Device Analyser was used on taking the MOSFET readings.
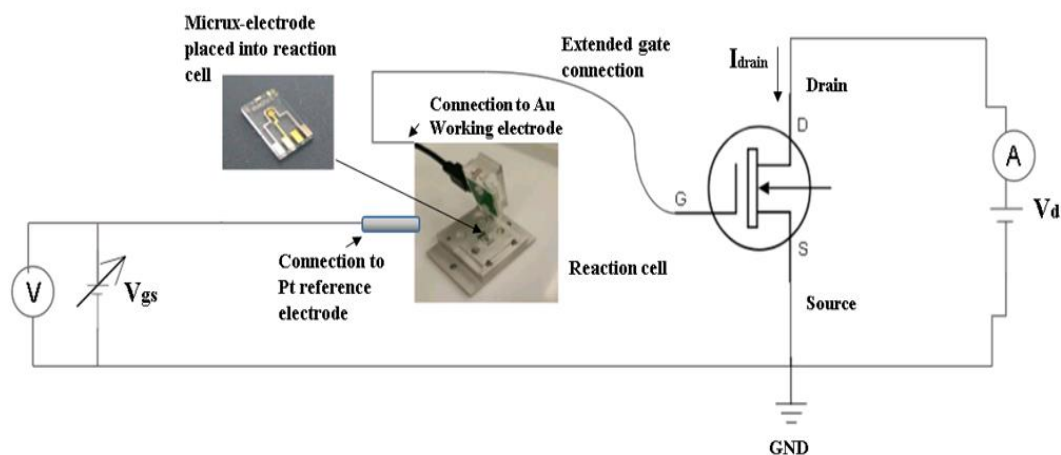
Figure I.4 Measurement circuit of the field-effect based transistor. The micro-electrodes with gold working electrode were placed in a reaction cell that is connected to the gate of a MOSFET. The gate voltage is applied through the connection to platinum reference electrode of the micro-chips.

For detection, a voltage of 50 mV was applied across the drain to source terminals and the gate-voltage was swept from $0 - 3V$. These settings limited the current to be less than 75 µA in order to avoid any changes inside the transistor due to overheating. When a voltage is applied between the drain and the source, $V_{ds} > 0$, it activates the current flow (I_d) through the induced channel under the gate dielectric. Hence, the device enters turn-on state. The conducting channel between the source and the drain is created when the applied potential is above the threshold voltage of the device ($V_{gs} > V_{th}$) (Aliakbarinodehi et al. 2017). The gate of the transistor is extended to connect to an external gold electrode which is functionalized with oligonucleotides specific to a pathogenic DNA and exposed to measurement samples. If molecular interactions take place at the gate of the transistor, such as negatively charged target ssDNA hybridizing with the complementary probe ssPNA and binding on the surface, this will in turn modulate the V_{gs} and alter I_d value. This is due to the increased negativity of the gate that leads to a raise of the minimum V_{gs} that is required to bring the n-MOSFET to the turn-on state. Hence, these variations are used to quantify the binding events taking place at the surface of the gold electrodes. The

variations are monitored in terms of shifts on the transfer characteristics (I_d *vs* V_{gs} curve) of the transistor (Chi et al. 2000; Estrela et al. 2010).
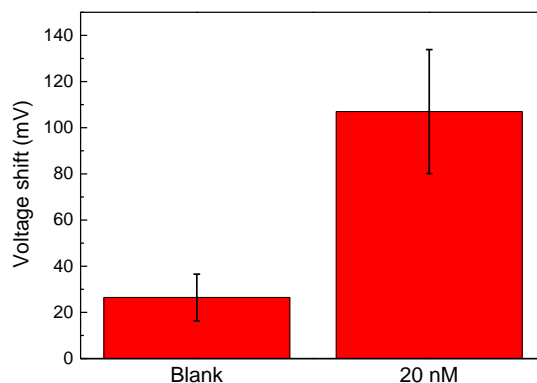

Figure I.5 V_{gs} changes vs. target DNA concentration bar graphs (Blank & 20 nM) using BioFET detection method. Error bars represent the standard deviation for three separate electrodes.

References

Aliakbarinodehi, N. et al., 2017. Aptamer-based field-effect biosensor for tenofovir detection. *Scientific Reports*, 7(44409), pp.1–10.

Chi, L. et al., 2000. Study on extended gate field effect transistor with tin oxide sensing membrane. *Materials Chemistry and Physics*, 63, pp.19–23.

Estrela, P. et al., 2010. Label-free sub-picomolar protein detection with field-effect transistors. *Analytical Chemistry*, 82(9), pp.3531–3536.